Master thesis in analytical organic chemistry

(Natural products)

Analysis of the marine sponge *Pachymatisma normani*

Lars Andreas Barka Højmark

Department of Chemistry

University of Bergen

2020

Front page: Image of *Pachymatisma normani*

Acknowledgments

List of selected abbreviations

Chemicals

MeOH	Methanol
DMSO	Dimethyl sulfoxide
EtOAc	Ethyl acetate
NH_4^+	Ammonium
CH_3CN	Acetonitril

Other

FW	Fresh weight
V	Volume
DAD	Diode array detector
HPLC	High performance liquid chromatography
Prep-HPLC	Preparative-HPLC
t_R	Retention time
LC	Liquid chromatography
MS	Mass spectrometry
ESI	Electron spray ionization
LR-MS	Low resolution Mass spectrometry
TIC	Total ion current
PIS	Product ion scan
m/z	Mass to charge ratio
NMR	Nuclear magnetic resonance
1D	One dimensional
2D	Two dimensional

Abstract

Marine sponges are evolutionary some of the oldest multicellular organisms on earth and have in the last few decades attracted an increasing amount of attention. Sponges are simple filter feeders that host symbiotic microorganisms and have proven to be a prominent source of bioactive metabolites. In this thesis extracts from the marine sponge *Pachymatisma normani* was analysed to identify any of the metabolites produced by microorganisms residing on the sponge. The sponge was collected in Norwegian waters and there are very limited amounts of research regarding the sponge.

P. normani was extracted using methanol and the crude extract was screened for compounds with UV-VIS absorption, using HPLC with a DAD-detector. Followed by choosing the most abundant compound as the primary target molecule. The UV-VIS absorbance for the target molecule was highest in the 330 nm window. Both liquid-liquid extraction and preparative-HPLC was used to purify and isolate a sample of the target molecule.

The first extract was initially purified using liquid-liquid extraction and resulted in large quantities of precipitate of a white crystalline solid in the aqueous phase. The precipitation continued as the concentrated sample was stored. HPLC analysis of the purified sample resulted in a chromatogram containing additional peaks with UV-VIS absorption in the 330 nm window, indicating that the liquid-liquid extraction interfered with the sample. Preparative-HPLC with an UV-VIS detector fixed at 330 nm was used to purify the sample further. Followed by acquiring ^{1}H-, COSY, HSQC and HMBC spectra of the sample. The target molecule was by no means isolated and the spectra contained a lot of impurities, with many overlapping peaks in the ^{1}H-NMR spectrum. But there were some peaks in the aromatic region with decent resolution. Analysing the COSY spectrum revealed that there was an aromatic system with four proton signals, one was hidden inside a cluster of overlapping peaks. Through further analysis of the HSQC and HMBC spectra it was possible to piece together an aromatic compound with four protons and an extension containing two carbonyl groups, but there were still some blind spots to the structure.

A second extraction and a new sample of the target molecule was prepared in the same fashion as before, except for liquid-liquid extraction. By not using liquid-liquid extraction to purify the sample it seemed to remain far more stable. There was significantly less of the white precipitate and no additional peaks in the HPLC analysis. A mass of 189.1 g/mol was acquired with MS,

an uneven mass is often an indication that the structure contains a nitrogen atom. ^{1}H-, COSY, HSQC, HMBC and ^{15}N-HSQC spectra were recorded of the sample. The proton spectrum had better resolution and less overlap in the aromatic region. It did however contain additional peaks in the aromatic region along with a couple of NH peaks, but there was no correlation between the NH peaks and the target molecule. The sample from the second extraction provided spectra with better resolution and confirmed the elucidation done in previous sample. HR-MS was utilised to acquire an elemental composition and combined with the knowledge from the NMR elucidation the composition would have to be $^{12}C_{10}{}^{1}H_7{}^{14}N_1{}^{16}O_3$. $^{12}C_{10}{}^{1}H_5{}^{16}O_2$ had been covered by NMR analysis, but there were several possible variables to apply $^1H_2{}^{14}N_1{}^{16}O_1$ to the structure. Product ion scan was used to fragment the target molecule in order to pinpoint the position of the remaining atoms. Leading to a fragmentation pattern of [M+H] → *m/z* 144.1 → *m/z* 116.0 → *m/z* 89.1. The heaviest fragment had a loss of 45, confirming the location of an acid group. From *m/z* 144.1 to *m/z* 116.0 there is a difference of 28 and fits the loss of second carbonyl group. From *m/z* 116.0 to *m/z* 89.1 there is a loss of 27, a loss that is typical for HCN and confirming the ring-location of the nitrogen atom. While also confirming that the target molecule would have to be kynurenic acid.

Kynurenic acid is a known metabolite that is derived from tryptophan and has shown to have a neuroprotective effect. In humans a decreased level of kynurenic acid has been linked with depression, while elevated levels can be found in patients diagnosed with schizophrenia. Other studies have shown kynurenic acid to be a prominent antidote against neurotoxins. The compound has also been isolated from a sponge cultivated microbe once before. *P. normani* is suspected to have a hostile toxicity due to its barren surroundings, while the endosymbiotic microbes in the sponge produce a known neuroprotective agent.

Table of contents

Chapter 1 - Introduction

Chapter 2 - Experimental methods

Chapter 3 - Results and discussion

Chapter 4 - Conclusion and further work

Chapter 1

Introduction

1.1 Motivation

The Ocean covers 71 % of earth's surface and is a critical component in our biosphere (Fattorusso, Gerwick et al. 2012). It offers a complex environment with immense biodiversity which is largely undiscovered. Providing natural products from the tissues of marine animals and plants, as well as natural products produced by microorganisms.

Marine sponges have since the 1960s attracted attention from natural product chemists and pharmacologist, as they have proven to be a prominent source of bioactive metabolites (Fattorusso, Gerwick et al. 2012). Covering a broad range of bioactive effects including anticancer, antiviral, antibacterial, antifungal, antiprotozoal, anthelmintic, anti-inflammatory, immunosuppressive, neurosuppressive, neuroprotective, antifouling and more (Blunt, Copp et al. 2005, Mehbub, Lei et al. 2014). Marine sponges could potentially provide novel leads against bacterial, fungal and viral diseases as infectious microorganisms continue to evolve and develop.(Mehbub, Lei et al. 2014) Sponges are also responsible for yielding highest number of novel metabolites reported per year compared to other sources of natural products in the marine environment (Fattorusso, Gerwick et al. 2012).

1.2 Marine sponges

Sponges are believed to be the sister group of all other animals, as they were the first to branch off the evolutionary tree of common ancestors for animals (Feuda, Dohrmann et al. 2017). Sponges is the most primitive group of multicellular organisms on earth (Sømme 2018). They are mostly immobile creatures that lack any tissue or internal organs. That survive by filtering water to absorb nutrients. Sponges play a key-part in deep-water and coral reef communities as they filter water and excrete high amounts ammonium (Hoffmann, Radax et al. 2009). Sponges have been proven to be fertile hosts for microorganisms, that produce nitrite and nitrate through their activity. Compounds that are essential nutrients in the marine ecosystem.

1.2.1 Body structures and classification

The water flow of a sponge can be described as chimney, water is filtered into the sponge and is ejected at the top through the osculum (Ruppert, Fox et al. 2004). Sponges are categorised into three types of structures, that offer a difference in complexity.

The simplest type of structure is called asconoids and comes in the shape of a vase or a tube (Hågvar 1998, Ruppert, Fox et al. 2004, Sømme 2018). This structure is limited by size, because the absorption of nutrients does not manage to scale with size. Only a few sponges follow the asconoid-structure and rarely manage to exceed a diameter of 1 mm.

Syconoids is a more complex version of the asconoids (Hågvar 1998, Ruppert, Fox et al. 2004, Sømme 2018). They have a similar shape to the asconoid, but the walls contain pockets that increase the absorbance nutrients. Allowing these sponges to grow up to a couple centimetres in diameter.

Both the asconoid and syconoid structures had a hollow build, while the more complex leuconoid structure have a compact build (Hågvar 1998, Ruppert, Fox et al. 2004, Sømme 2018). That is filled with a branching canal system that is more efficient at absorbing nutrients. Leuconoid sponges are often more than 1 meter in diameter.
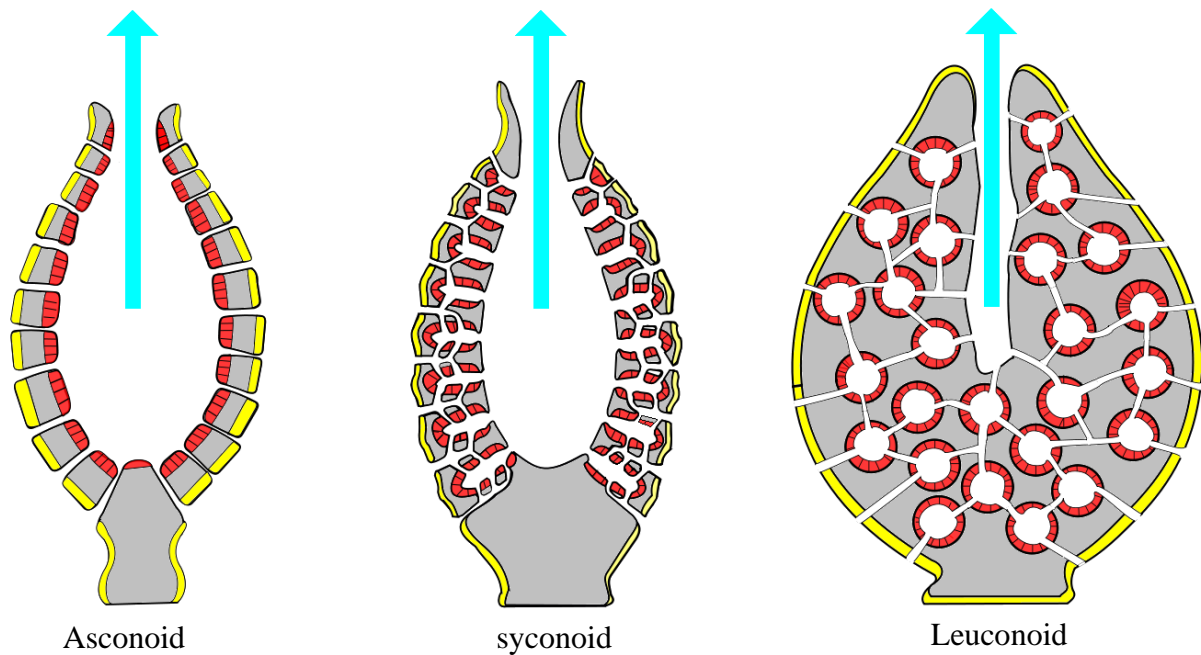
Figure 1.1 – Illustration of asconoid, syconoid and leuconoid structures. Waterflow through the osculum is visualized by the blue arrow (Ruppert, Fox et al. 2004). By Philcha - Own work, CC BY-SA 3.0, https://commons.wikimedia.org/w/index.php?curid=5100738

Marine sponges are distributed into four classifications primarily based on their skeletal composition (Hågvar 1998, Singleton 2018). These classes are calcarean, hexactinellida, demospongia and homoscleromorpha. Calcarean sponges are small and have a skeletal composition of calcite and can have asconoid-, syconoid- or leuconoid-builds. They are typically found at shallow waters throughout the world. Hexactinellida (glass-sponge) are tropical deep-sea sponges that uses silica as their skeletal composition and uses either the syconoid or leuconoid build. Around 90 % of sponges are classified as demospongia-type, which follow leuconoid structure and uses silica as their skeletal composition. Homoscleromorpha were originally classified as demospongia, but was recognized to be phylogenetically separated from demospongia (Kober and Nichols 2007, Gazave, Lapébie et al. 2012). They are characterized as small and compact sponges with a silica composition (Sømme 2018).

1.2.2 Symbiosis

Having a hollow skeletal structure that filters nutrients make sponges a suitable host for symbiotic microbes, as long as they can withstand their digestive system. (Yoo Kyung Lee 2001) These microorganisms range from archaea, bacteria, cyanobacteria to microalgae. Most of the natural products derived from marine sponges probably originates as metabolites from the microbes they host.

Up to 40 % of the sponge tissue volume might be comprised of these microbial communities. They too feed of the water filtered by the sponge, but often contribute to sponge metabolism with oxygen through photosynthesis, nitrogen fixation and nitrification (Taylor, Radax et al. 2007).

Sponges are primitive filter-feeders that in contrast with other animals lack a complex immune system (Proksch 1994, Thoms and Schupp 2007). Since they are also rendered mostly immobile, they cannot physically defend themselves. Instead they rely on chemical defence mechanisms provided by their microbial symbionts(Paul, Ritson-williams et al. 2011). Their chemical defence system is composed of bioactive components that help them to combat factors as predation, overgrowth and competition for space. Sponges living in strongly competitive habits such as coral reefs have been found to contain the highest concentrations of sponge metabolites with toxic or antioxidizing effects. It is common for sponges to emit these cytotoxins to create a buffer zone around themselves to fend off competition (Thompson, Walker et al. 1985, Becerro, Thacker et al. 2003). If the cytotoxicity is high enough, they might even create a bare zone, allowing for an easy conquest of the surrounding area. Marine sponges have managed to stand the test of time, and much of their success in the evolutionary process is due to their symbiotic relationship(Green 1977, Taylor, Radax et al. 2007).

1.2.3 Sponge sample

A sample of *Pachymatisma normani* was provided by Hans Tore Rapp for this thesis. The sponge was collected in Korsfjorden outside of Bergen (23.03.2018), where it was immediately frozen. Furthermore, the sponge was stored frozen to maintain its pristine condition. According

to Hans Tore Rapp no vegetation or "growth" is seen on this sponge, indicating a "hostile" environment with possible toxic components.

Figure 1.2 – Frozen sample of *P. normani*.

P. normani is a demospongiae that is part of the *Pachymatisma* genus in the *Geodiiade* family, (Artsdatabanken 2015). The species is not endangered and has been deemed viable. *P. normani* has previously been synonymized with its relative *Pachymatisma johnstonia* that is one of the most common type of sponge found in the north-eastern parts of the Atlantic (Crdenas, Xavier et al. 2007). *P. normani* are located along the coast of Norway and in the waters surrounding Iceland, while *P. johnstonia* has been located at the coasts of the British Isles, France, Spain and Italy.

No research has been done on *P. normani* in terms of natural products, but some have been done on *P. johnstonia* (Warabi, Zimmerman et al. 2004). In 2004 a novel glycolipid called Pachymoside A was isolated from *P. johnstonia*. Crude extracts from the sponge had earlier shown promising activities for inhibiting bacterial type III secretion.
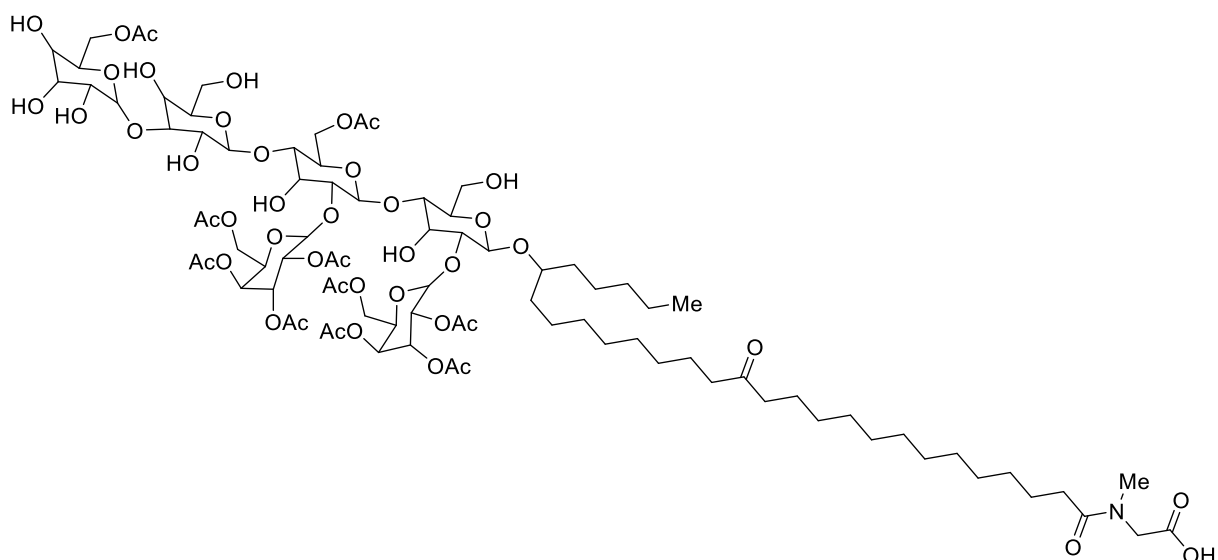
Figure 1.3 – Pachymoside A, a novel glycolipid that was isolated and identified through extraction of *P. johnstonia* (Warabi, Zimmerman et al. 2004).

1.2.4 Marine sponges as a source of natural products

Marine sponges have shown promising results in terms of novel compounds with bioactive effects, but marine sponges in the wild is a limited source (Pérez-López, Ternon et al. 2014). They have a time-consuming growth cycle and only produce small quantities of the desired compounds. Meaning large amounts of fresh material would be required to exploit these compounds. Making Marine sponges vulnerable to overexploitation, which should be avoided given the central role they might have in the aquatic ecosystem (Hoffmann, Radax et al. 2009).

One method of solving this issue could be cultivation of marine sponges (Osinga, Tramper et al. 1999). Cultivation of sponges is usually done through aquaculture or with controlled conditions. Aquaculture is cost efficient and offers a high survival but is limited by the natural growth rate of the sponges. While controlled conditions are more expensive but eliminates the environmental stress factors and manages to boost the growth rate.

A more sustainable method of exploiting the compounds would be to cultivate the symbiotic microorganisms (Uria and Piel 2009). Since they are most likely the source of the compounds of interest, and cultivating marine sponges is time consuming and yields limited quantities.

1.3 Natural products derived from marine sponges

In the last decades the discovery of new marine natural products has accelerated in cases of new compounds discovered, and it estimated that about 30 % of these are derived from marine sponges (Yong-Cheng, Sheng-Ping et al. 2011, Mehbub, Lei et al. 2014). Studies have shown that novel compounds derived from marine sponges offer a broad range of bioactive effects such as anticancer, antiviral, antibacterial, antifungal, antiprotozoal, anthelmintic, anti-inflammatory, immunosuppressive, neurosuppressive, neuroprotective, antifouling and others (Blunt, Copp et al. 2005). Since infectious microorganism are constantly evolving and developing resistance towards existing pharmaceuticals, marine sponges might provide novel leads to combat viral, bacterial and fungal diseases (Laport, C. S. Santos et al. 2009, Sagar, Kaur et al. 2010).
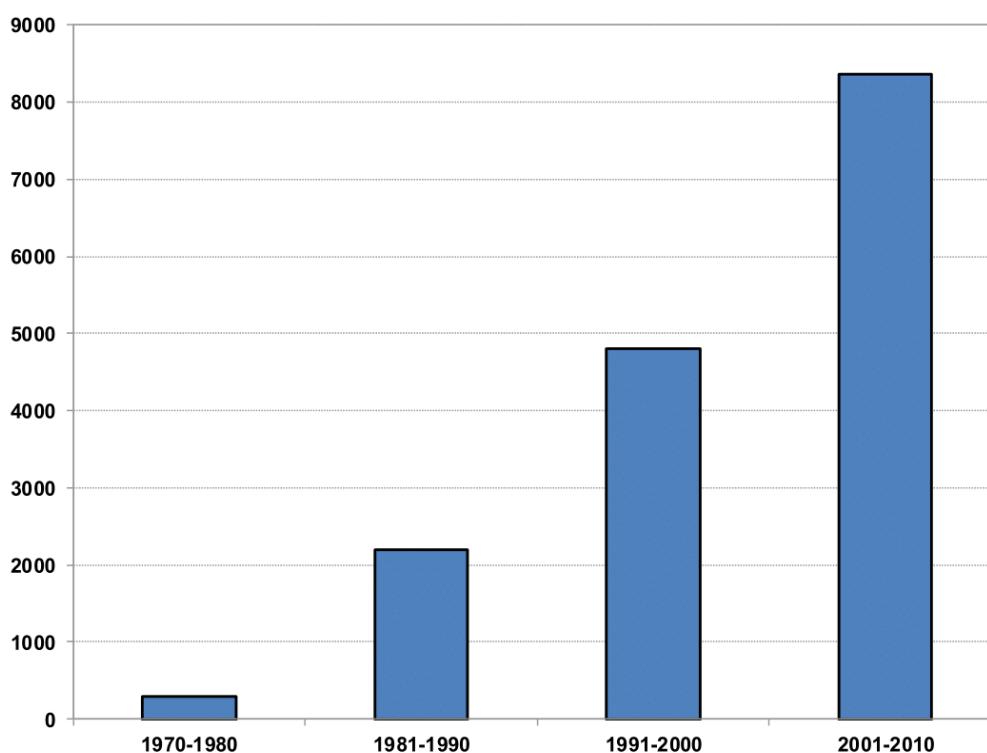

Figure 1.4 – A bar graph illustrating the ramp up of new natural products isolated from marine sources from 1970-2010 (Mehbub, Lei et al. 2014).
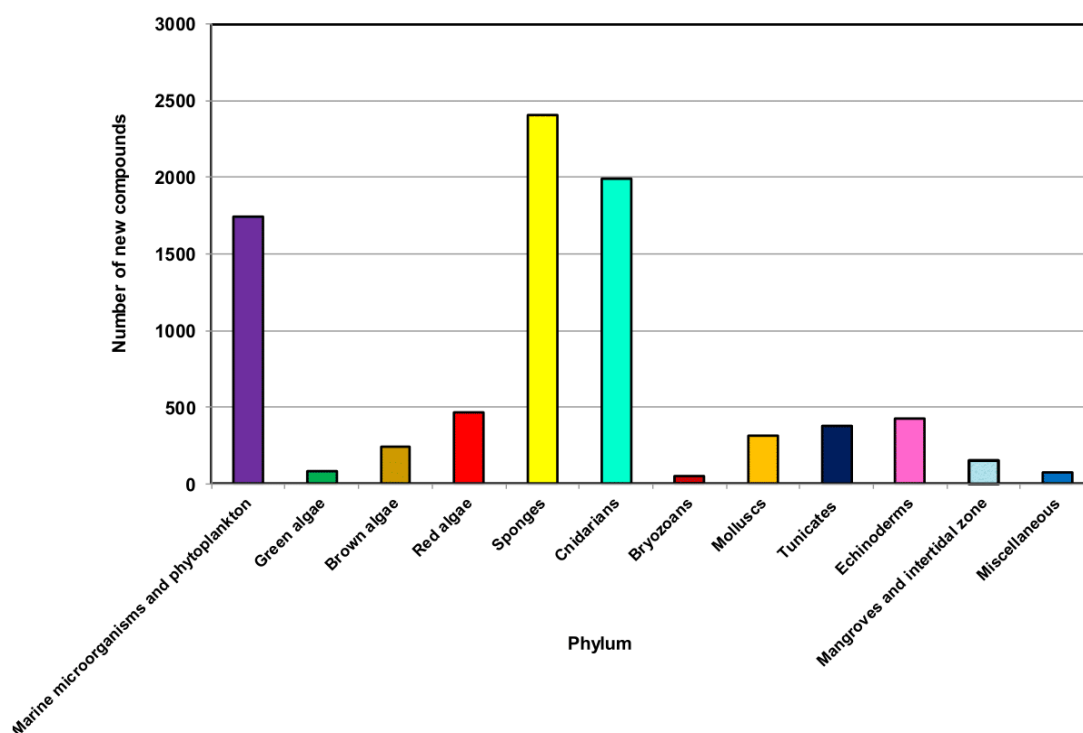
Figure 1.5 – Total number of new natural products isolated from different marine sources from 2001 – 2010 (Mehbub, Lei et al. 2014). With marine sponges representing about one third of the cases.

Natural products have been used as medicine since ancient times and have in the modern era proven to be a successful source of novel drug leads (Dias, Urban et al. 2012). The use of sponges for medicinal purposes can be traced as far back as ancient Greeks (Sipkema, Franssen et al. 2005, Voultsiadou 2007). Where sponges where often soaked in hot water, iodine, wine, urine or honey and placed on body to treat various health problems or diseases. Some modern examples of bioactive compounds derived from sponges are given in the figures 1.6-1.10 below.

Inflammation is a protective response where the body changes the blood flow to increase the permeability of blood vessels (Tan, Luscinskas et al. 1999). The cause of inflammation is often microbial infections, physical damage or chemical agents. Manoalide **(a)** is an anti-inflammatory agent that was derived from the sponge called *Luffariella variabilis (Bennett, Mong et al. 1987)*. That has shown to be a potent inhibitor of phospholipase A_2, an inflammation agent that is found in venom of animals like snakes and bees. Other studies have shown that

manoalide also have antibiotic properties (de Silva and Scheuer 1980). **(b)** Dysidotronic acid **(b)** is an example of another phospholipase A_2 inhibitor that showed a higher selectivity and potency against the inflammation enzyme than manoalide. The compound was isolated from a sponge called *Dysidea sp* (Giannini, Debitus et al. 2000).
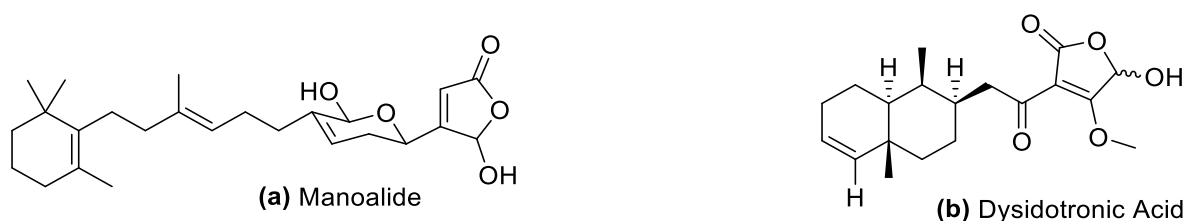

Figure 1.6 – **(a)** Manoalide is an anti-inflammatory agent that was derived from the sponge called *Luffariella variabilis (Bennett, Mong et al. 1987)*. **(b)** Dysidotronic acid is an example of another anti-inflammatory compound derived from a sponge called *Dysidea sp* (Giannini, Debitus et al. 2000).

The majority of novel compounds with bioactive effects that are isolated from marine sponges have antitumor/cytotoxic properties (Mehbub, Lei et al. 2014). Renieramycin M **(c)** was isolated from *Xestospongia sp.*, and is a sponge derived compound with anticancer activity (Halim, Chunhacha et al. 2011). Preclinical studies revealed promising results against lung cancer. Halichondrin B **(d)** is an example of a natural product with anticancer properties that was successfully developed into a drug (Paterson and Anderson 2005, NationalCancerInstitute 2009). The compound was isolated from the marine sponge *Halichondria okadai*. Due to its anticancer activities, Halichondrin B was used as a precursor to develop Eribulin (E7389). A drug used to treat patients with metastatic breast cancer.
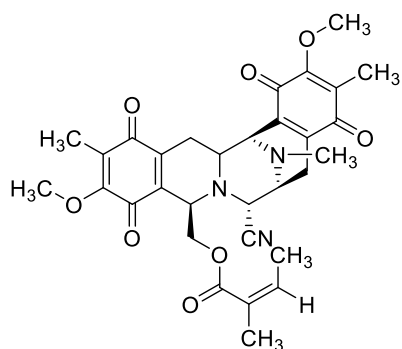
(c) Renieramycin M
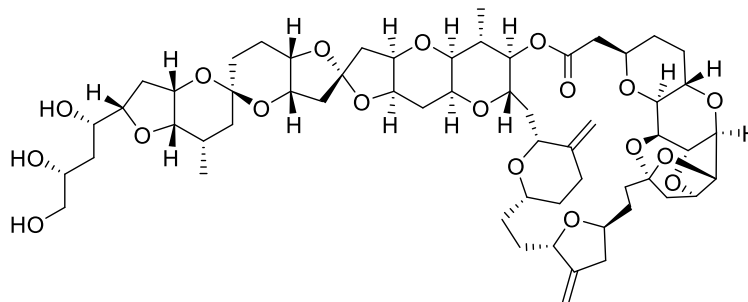
(d) Halichondrin B

Figure 1.7 – **(c)** Renieramycin M was isolated from *Xestospongia sp.* and has shown to exhibit anticancer activity (Halim, Chunhacha et al. 2011). **(d)** Halichondrin B was isolated from *Halichondria okadai* and was used as a precurses to develop the anticancer drug called Eribulin (E7389) (Paterson and Anderson 2005, NationalCancerInstitute 2009).

Immunosuppressive drugs are compounds that weaken the immune system and is often used against allergies or to prevent organ rejection after transplants (Sipkema, Franssen et al. 2005, Perdikaris, Vlachogianni et al. 2013). 4a-merhyl-5a-cholest-8-en-3-ol **(e)** and 4,5-dibromo-2-pyrrolic acid **(f)** are two immunosuppressive compounds that was isolated from the sponge *Agelas flabelliformis* (Gunasekera, Cranick et al. 1989)
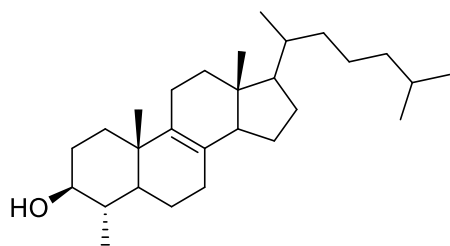
(e) 4a-merhyl-5a-cholest-8-en-3-ol
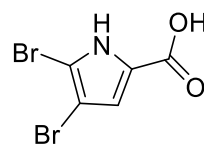
(f) 4,5-dibromo-2-pyrrolic acid

Figure 1.8 – **(f)** 4a-merhyl-5a-cholest-8-en-3-ol and **(f)** 4,5-dibromo-2-pyrrolic acid were both isolate from the sponge called *Agelas flabelliformis*, both have shown to possess immunosuppressive properties (Gunasekera, Cranick et al. 1989).

The main function of antiviral drugs is to inhibit the viral replication without damaging the host cell to much(Suwannarach, Kumla et al. 2020). The importance of antiviral drugs has become especially apparent with the ongoing Covid-19 pandemic of 2020. Laboratories all over the world are screening for possible treatments against the coronavirus. One example of an antiviral lead derived from a marine sponge is dragmacidin F **(g)**, which was isolated from *Halicortex* (Cutignano, Bifulco et al. 2000). Another is Avarol **(h)**, which was isolated from *Dysidea avara* (Sagar, Kaur et al. 2010).
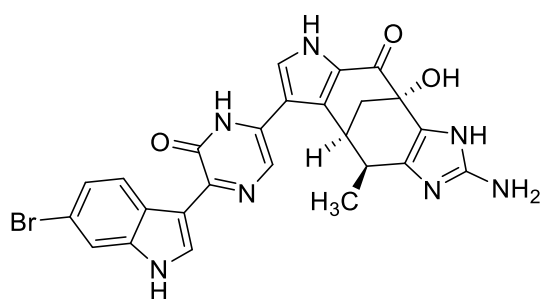

(g) Dragmacidin F
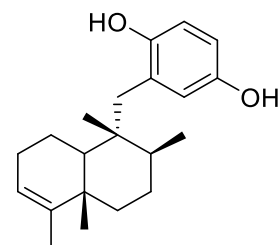
(h) Avarol

Figure 1.9 – **(g)** dragmacidin F is a compound with antiviral properties that was isolated from *Halicortex* (Cutignano, Bifulco et al. 2000). Another sponge derived compound with antiviral properties is **(h)** Avarol, which was isolated from *Dysidea avara (Sagar, Kaur et al. 2010).*

Resistance towards antibiotics is a growing concern, but derivatives isolated from marine sponges have also shown promising antimicrobial effects (Sipkema, Franssen et al. 2005). Purpunoines A **(i)** is halogenated alkaloid with antimicrobial properties that was isolated from *Iotrochota purpurea* (Shen, Liu et al. 2012).
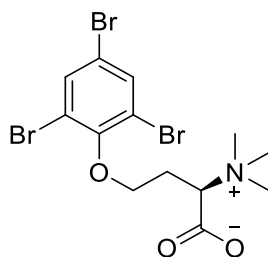
(i) Purpuroines A

Figure 1.10 – **(i)** Purpunoines A was isolated from *Iotrochota purpurea* and has shown to possess an antimicrobial effect (Shen, Liu et al. 2012).

1.3.1 Alkaloids

Numerous classes of natural products have derived from marine sponges over the years, but most of the attention has been directed towards alkaloids, peptides, and terpenoids (Ernesto Fattorusso 2012). Due to their pronounced pharmacological activities that make them interesting candidates for drug discovery.
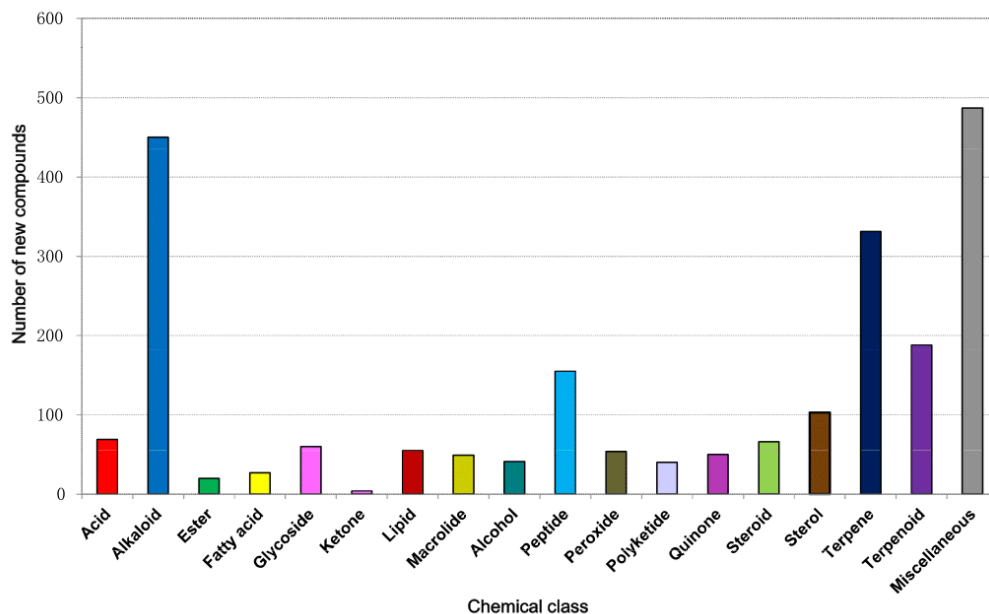
Figure 1.11 – Number of new compounds isolated from marine sponge from 2001-2010 distributed into chemical class (Mehbub, Lei et al. 2014).

Alkaloids derived from plants have provided us with drugs since ancient times (Ernesto Fattorusso 2012). The classification of alkaloids is quite broad, it is a highly diverse group of natural products. Where the main relation is a naturally occurring organic compound that contains a basic nitrogen atom (Civjan 2012). This makes alkaloids a classification with high structural diversity. Covering everything from simple structures like coniine to more complex structures like dragmacidin F (Cutignano, Bifulco et al. 2000). Many alkaloids are also precursors of amino acids, resulting in a more characteristic structure (Gutzeit and Ludwig-Müller 2014). A few examples of amino acid derived alkaloids are given in table 1.1.
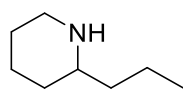
Coniine
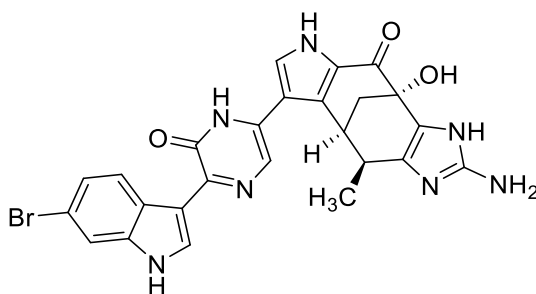
Dragmacidin F

Figure 1.12 – Coniine is isolated from poison hemlock, and is supposedly the poison Socrates chose to drink when he was sentenced to death (Koskinen 2012). Dragmacidin F is a compound a with antiviral properties that has been isolated from a marine sponge called *Halicortex (Cutignano, Bifulco et al. 2000)*.

Table 1.1 – Examples of alkaloid structures derived from amino acids.(Gutzeit and Ludwig-Müller 2014)

Basic structure	Precursor	Formula basic structure
Quinoline	tryptophan	
Quinolizidine	lysine	
Imidazole	histidine	

14

Chapter 2

Experimental methods


```
Direct solvent extraction
         │
         ▼
   Crude extract ─────────────────────────┐
         │                                 ▼
         ▼                        Liquid-liquid extraction
  Analytical HPLC                         ╱      ╲
         │                               ▼        ▼
         ▼                        Aqueous phase   EtOAc phase
  Preparative HPLC                       │
         │                               ▼
         ▼                        Analytical HPLC
        NMR                              │
         │                               ▼
         ▼                        Preparative HPLC
       LC-MS                             │
                                         ▼
                                        NMR
```
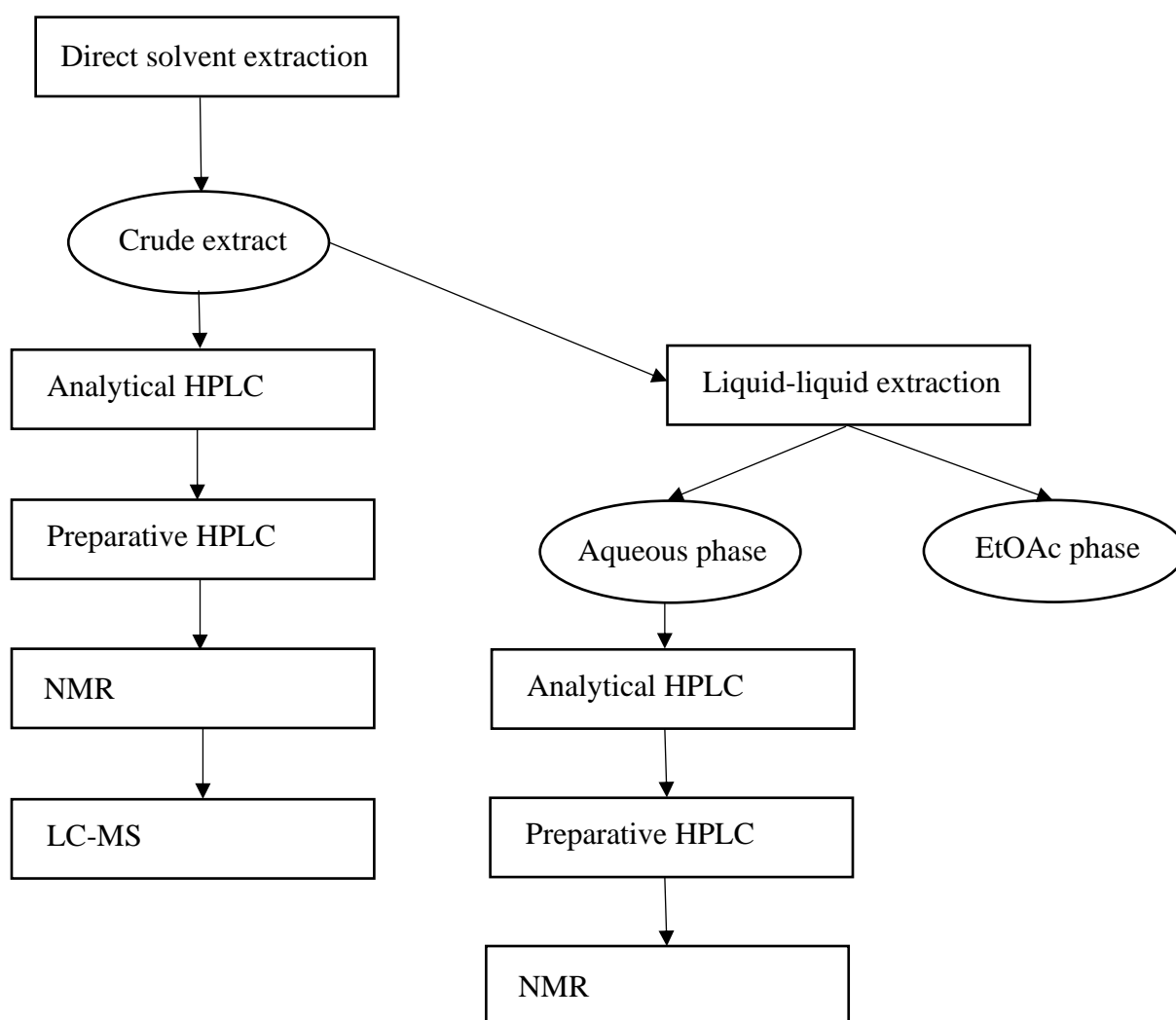
Figure 2.1 – The general scheme for the experimental work done on *P. normani*

2.1 Direct solvent extraction

P. normani was cut into small pieces and weighed in a beaker. Then it was vigorously stirred in methanol at room temperature for 24 hours. The extraction was repeated three times during this time period, table 2.1. Followed by filtering the extract to remove solid sponge particles, because most of the sponge would pulverize during extraction. Afterwards the extract was concentrated by removing the solvent under reduced pressure on a rotary evaporator with the water-bath set to 34 °C. Due to content of possible toxic components, the sponge and its extracts were always treated carefully utilizing gloves and protective glasses.

Table 2.1 – Samples (**E1-E3**) of *P. normani* were extracted three times with methanol. Given below is the fresh weight and volume used in each extraction.

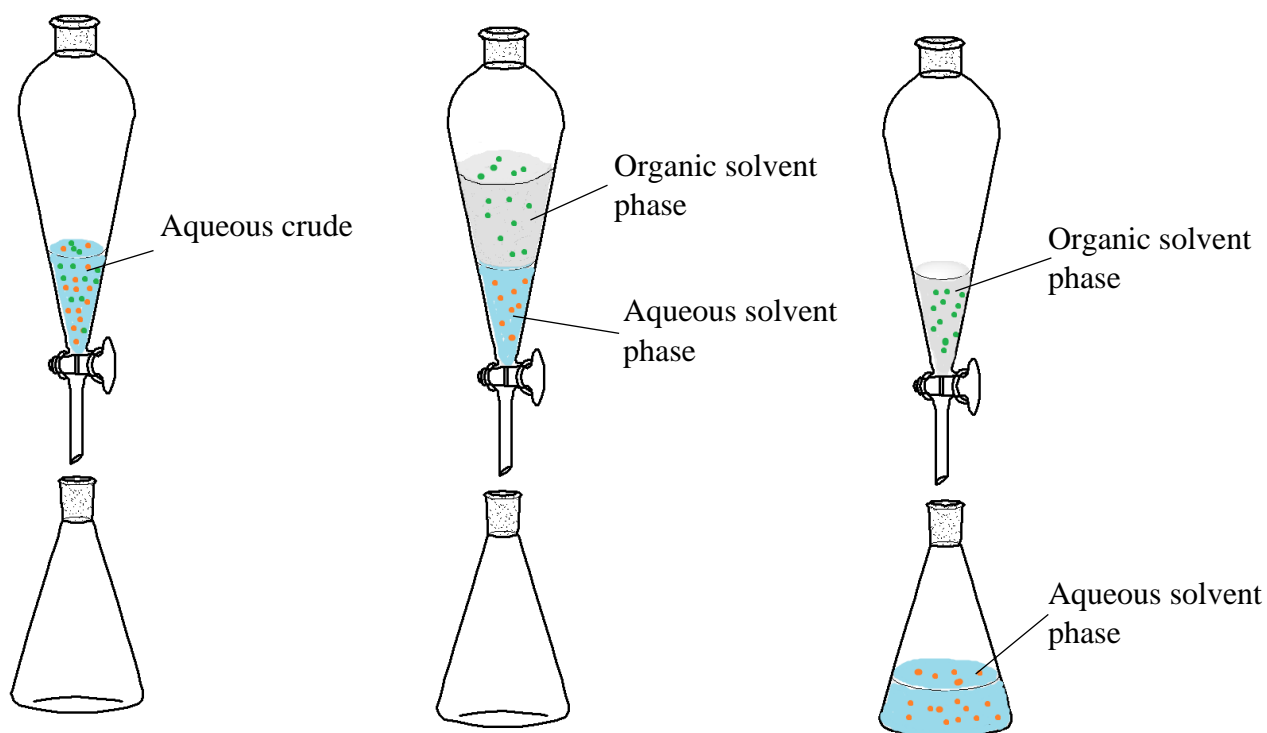| Extraction of *P. normani*	$FW_{P.\ Normani}$ [g]	$V_{extract}$ [mL]
E1	23.21	3×80
E2	23.44	3×80
E3	50.13	3×160

2.2 Purification

Crude extracts were purified using liquid-liquid extraction and preparative-HPLC

2.2.1 Liquid-liquid extraction

Purifying a sample with liquid-liquid extraction involves distribution a mixture between two solvents(Jerry R. Mohrig 2014). These solvents must be immiscible, meaning that they are insoluble with each other. Instead they form two separate layers. Water is often paired against a less polar organic solvent like diethyl ether, ethyl acetate or dichloromethane. When a mixture is mixed with the two solvents the components will distribute itself in the two layers based on polarity.

Figure 2.1 – Example of how extraction can be used to purify a crude extract (Jerry R. Mohrig 2014).

2.2.2 Liquid-liquid extraction with ethyl acetate

E1 was purified with liquid-liquid extraction against ethyl acetate. After extraction the volume of methanol was reduced using a rotary evaporator. It was then transferred to a separating funnel where it was diluted in super distilled water (300 mL). Followed by extraction against ethyl acetate (3×300 mL). When both solvents are in the funnel it is shaken for a couple of minutes before the phases are left to separate. Highly polar compounds will reside in the aqueous-phase, while less polar compounds will prefer the EtOAc-phase. Both phases were collected separately, and the EtOAc-phases where combined. Since water has the highest density of the

two solvents it will be in the lower layer of the funnel. Afterwards the phases were concentrated using a rotary evaporator.
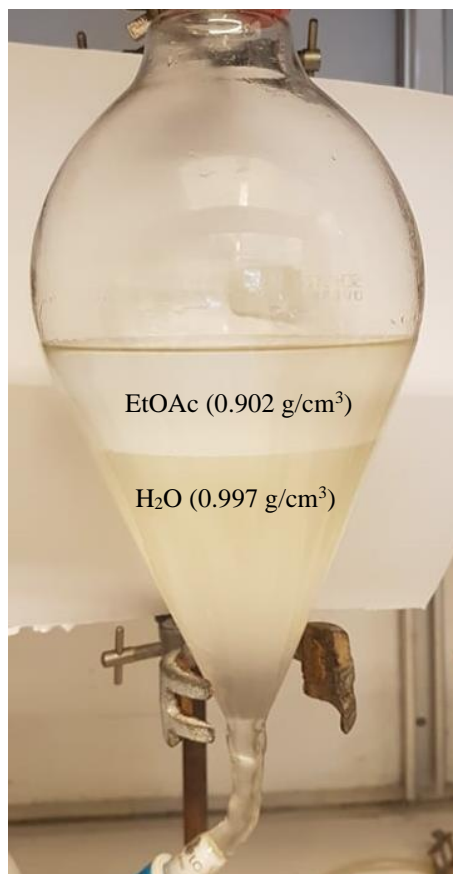

Figure 2.1 – Liquid-Liquid extraction of **E1** (Donald L. Pavia 2015).

Analysis

Several analytical methods were used to analyse the sponge: HPLC, LC-MS, HR-MS and NMR.

2.4 High performance liquid chromatography (HPLC)

Chromatography is an analytical method for separating compounds in a mixture (Harris 2016). It follows the same principles as extraction but takes place in a column with a mobile- and stationary phase. The stationary phase is placed inside the column and is usually a viscous liquid

chemically bonded to the inside of a capillary tube or onto the surface of solid particles packed within the column. The mobile phase in liquid chromatography is the solvent that moves the sample through the column. The separation of components in a sample is due to differences in physical and chemical properties, these will determine how the components interact with the phases resulting in different retention times.

HPLC is an acronym for high performance liquid chromatography, where high pressure is used to push solvent through a column that is tightly packed with small particles (Harris 2016). This results in chromatograms with high-resolution. Resolution is referring to how well the components in a sample is separated in a column.

There are primarily two methods for HPLC, normal- and reverse phase (Miller 2005). Normal phase was the original mode of operation, using a polar stationary phase and a less polar mobile phase. Reverse phase has however become the most common mode, using a nonpolar or weakly polar stationary phase against a polar mobile phase.

HPLC supports both analytical and preparative use (Miller 2005). Analytical HPLC is used to quantify and/or identify compounds in a sample. Whereas preparative HPLC is used to isolate and/or purify compounds in a mixture.
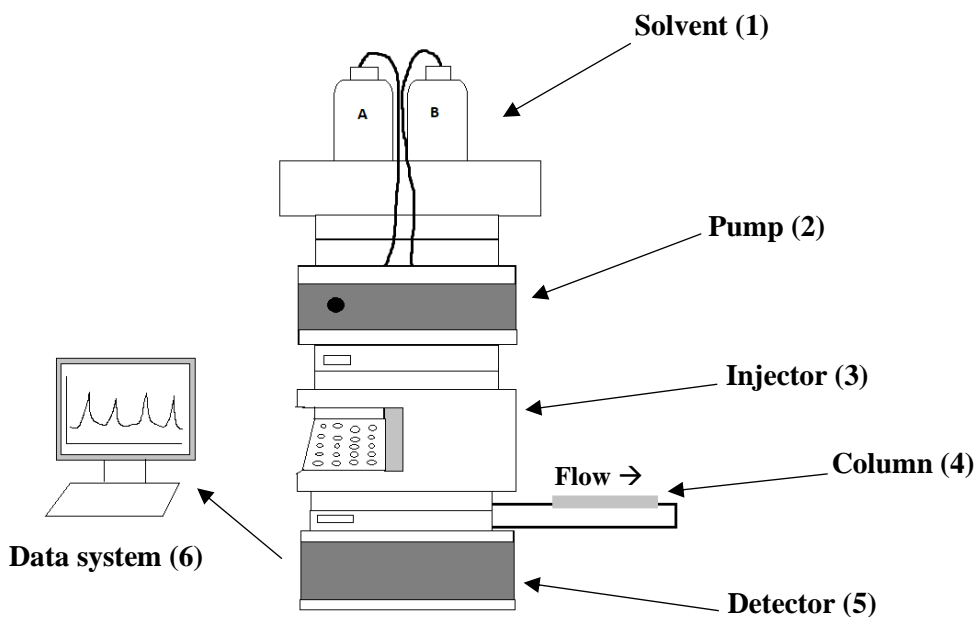
Figure 2.2 – A standard HPLC system consists of solvent reservoir (1), a pump house (2), an auto sampling injector (3), a column (4), a detector (5) and a data system (6).

2.5 Ultraviolet Spectroscopy (UV-VIS)

Most organic molecules and functional groups are transparent in the ultraviolet (UV) and visible (VIS) regions of the electromagnetic spectrum (Donald L. Pavia 2015). These regions cover the wavelengths from 190 nm to 800 mm. When a transparent material is exposed to continuous radiation, a portion of that radiation might be absorbed. If it does, the residual radiation will result in a spectrum containing gaps called absorption spectrum.

When an atom or molecule absorbs energy it passes from a low energy state (ground state) to a higher energy state (excited state), figure 2.3. (Donald L. Pavia 2015) In UV-VIS spectroscopy the source of the excitation is ultraviolet and visible light. The difference in energy during the excitation process is measured and quantified to yield a spectrum.

E(excited) _____

$\Delta E = [E(excited) - E(ground)] = h\nu$
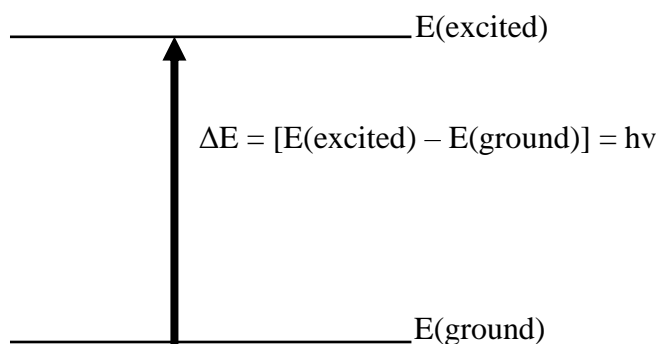
E(ground) _____

Figure 2.3 – The excitation process. (Donald L. Pavia 2015)

The diode-array spectrophotometer is a modern improvement of the spectrophotometer (Miller 2005). A diode array is composed of a series of photodiode detectors placed side by side on a silicon crystal. Where every photodiode is connected to each other and designed to record a narrow band of the spectrum. Making it possible to record the entire spectrum at once.

2.6 Mass spectrometry (MS)

Mass spectrometry is an analytical method that measures the mass of charged particles like atoms, molecules and fragments of molecules (Donald L. Pavia 2015). MS is highly sensitive method of analysis that require small amounts of sample, but the injected sample is destroyed in the process (Smith 2005). A mass spectrometer consists of five major components, figure 2.3. The sample is introduced in the sample inlet, gets ionised and/or fragmented in the ion source while the mass analyser systematically separates the ionised components by mass. The ions are counted by the detector and transferred to a data system, where the signals are converted into a digital spectrum.
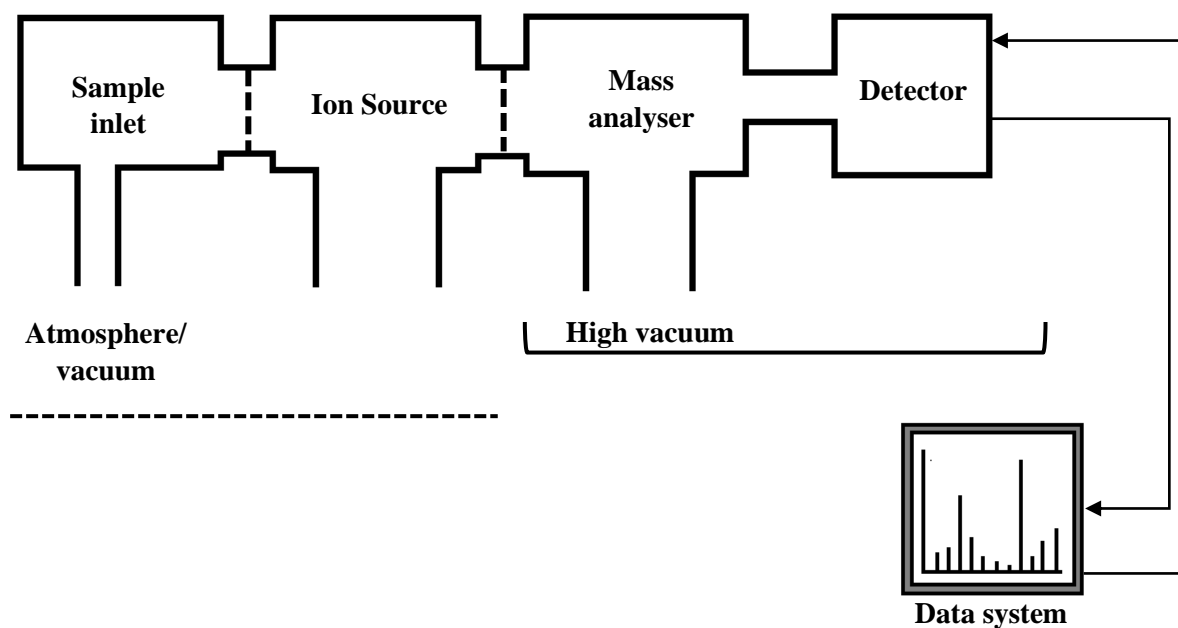
Figure 2.3 – The components of a mass spectrometer. (Donald L. Pavia 2015)

Depending on the sample inlet and desired fragmentation there is a wide variety of ion sources to choose from. Electrospray ionisation (ESI) is most commonly paired with an LC inlet, and was used in this research (Donald L. Pavia 2015). ESI uses a charged capillary to spray charged droplets of a solution containing the sample molecules into a heated chamber. In the chamber the solvent is evaporated with a nitrogen giving solvent-free sample ions in gas phase, which is then carried into the mass analyser.

The instrument used in this research had a triple quadrupole (QqQ) mass analyzer, that consists of three quadrupoles that's been linearly arranged. Quadrupoles compose of four solid rods that are aligned in parallel order to the ion beam (Donald L. Pavia 2015). By applying a direct-current (DC) voltage and a radiofrequency /RF) field to the rods they generate an oscillating electrostatic field. Once ions enter the electrostatic field, they will acquire an oscillation based on their mass and ions with the correct/selected mass reach a stable oscillation and moves through the quadrupole down to the detector. The quadrupoles in MS/MS have two separate

function, the first and third quadrupole act as independent mass to charge analyzers (Smith 2005). While the second serve as a collision activation chamber that can fragment ions. Product ion scan was as fragmentation method in this thesis. Where the first quadrupole is just to select a precursor ion that passes on to the second quadrupole where it is fragmented. Resulting in a spectrum containing all possible fragment of the precursor ion.

2.7 Nuclear Magnetic Resonance Spectroscopy (NMR)

NMR-spectroscopy is regarded as one of the most effective tools when it comes to structure elucidation of organic compounds (Donald L. Pavia 2015). Being a non-destructive analytical method that provides results with high accuracy, which is quite beneficial for natural products. As the isolation of natural products is a time-consuming process that often result in yields of limited proportions.

It is possible to study many nuclei by utilizing NMR techniques, but hydrogen and carbon are the two most commonly available (Donald L. Pavia 2015). When studying hydrogen nuclei with NMR, one can differentiate between the distinct types of hydrogen nuclei in a structure. In addition to obtaining information regarding the nature of the immediate environment of each hydrogen type. Similar information can be obtained for the carbon nuclei as well.

An atomic nucleus requires a property called spin in order to be suitable for NMR analysis (Donald L. Pavia 2015). Any atomic nucleus with an odd mass, odd atomic number, or both can be quantized by NMR. The naturally abundant isotope of hydrogen (^{1}H) has spin, making it suitable for NMR, table 2.2. The abundant carbon (^{12}C) on the other hand does not. Carbon based NMR utilizes the ^{13}C isotope instead, with a natural occurrence of 1.1 %. Making it far less sensitive compared to hydrogen with natural abundance of 99.98 %.

Table 2.2 – Spin quantum numbers of some the common nuclei (Donald L. Pavia 2015).

Element	$^{1}_{1}H$	$^{2}_{1}H$	$^{12}_{6}C$	$^{13}_{6}C$	$^{14}_{7}N$	$^{15}_{7}N$	$^{16}_{8}O$	$^{17}_{8}O$
Nuclear spin quantum number	$\frac{1}{2}$	1	0	$\frac{1}{2}$	1	$\frac{1}{2}$	0	$\frac{5}{2}$
Number of spin states	2	3	0	2	3	2	0	6

1D ^{1}H NMR
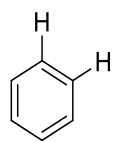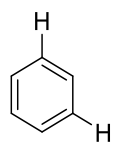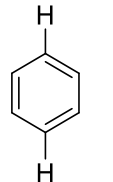
A high abundance of the ^{1}H-isotope makes one dimensional experiments of hydrogen highly sensitive (Donald L. Pavia 2015). Meaning they can rapidly produce NMR spectra, providing proton chemical shifts, spin-spin couplings (J_{HH}) and integration data. 1D proton experiments alone are usually not enough when elucidating structures. The chemical shift of proton signal describes its environment and is given in ppm. The higher electronegative an environment has, the further downfield the chemical shift will be located. The integration value can determine how many protons contribute to a signal, as protons with same chemical environment will overlap into one signal.

The multiplicity of the peaks is determined by the number of neighbouring protons (Donald L. Pavia 2015). A lone proton, or protons located in the same chemical environment will give singlet signals. One neighbouring proton gives a doublet, two neighbouring protons give a triplet and so forth. The multiplicity is given by (n+1), where n is the number of neighbouring protons.

The coupling constant for a signal is given in Hz and is the distance between the peaks in a multiplet (Donald L. Pavia 2015). In a six-membered-ring like benzene, the coupling constant depends on which position the neighbouring proton is oriented in. If protons are in ortho position to each other, they will have a chemical bond distance of three (^{3}J) and a coupling constant between 7-10 Hz. While a chemical bond distance of four (^{4}J) means that the protons are in meta position, giving a coupling constant between 1-3 Hz. See table 2.3 below.

Table 2.3 – The three different substitution possible in a six-membered ring, illustrated with hydrogen placement in chemical structure and their coupling constant (Donald L. Pavia 2015).

	Ortho	7-10 Hz	^3J
	Meta	1-3 Hz	^4J
	Para	0-1 Hz	^5J

2D Homonuclear (H,H)-Correlated NMR Spectroscopy (COSY)

The multiplicity of a signal in 1D ^1H NMR correlates to the number of neighbouring protons, but it can be difficult to assign the position of these protons. (Donald L. Pavia 2015) COSY-spectroscopy makes this task easier, as they produce cross coupling signals for neighbouring protons with a coupling distance up to $^4J_{HH}$.

2D ^{1}H-^{13}C Heteronuclear Single Quantum Correlation Spectroscopy (HSQC)

This is a two-dimensional experiment that provides direct correlation ($^1J_{H-C}$) between a carbon and a hydrogen. (Friebolin 2011) ^{15}N-isotopes can also be used with HSQC to find the $^1J_{H-N}$ correlation.

2D ^{1}H-^{13}C Heteronuclear Multiple Bond Correlation Spectroscopy (HMBC)

HMBC experiments is used to find the correlation between protons and carbons that are separated by either two or three bonds. (Friebolin 2011) $^2J_{H-C}$ and $^3J_{H-C}$ correlations are differentiated by the cross-coupling intensity, with the three-bond length producing the highest intensity. HMBC is useful to find neighbouring carbons, to assign quaternary carbons or carbons that is not attached to a proton.
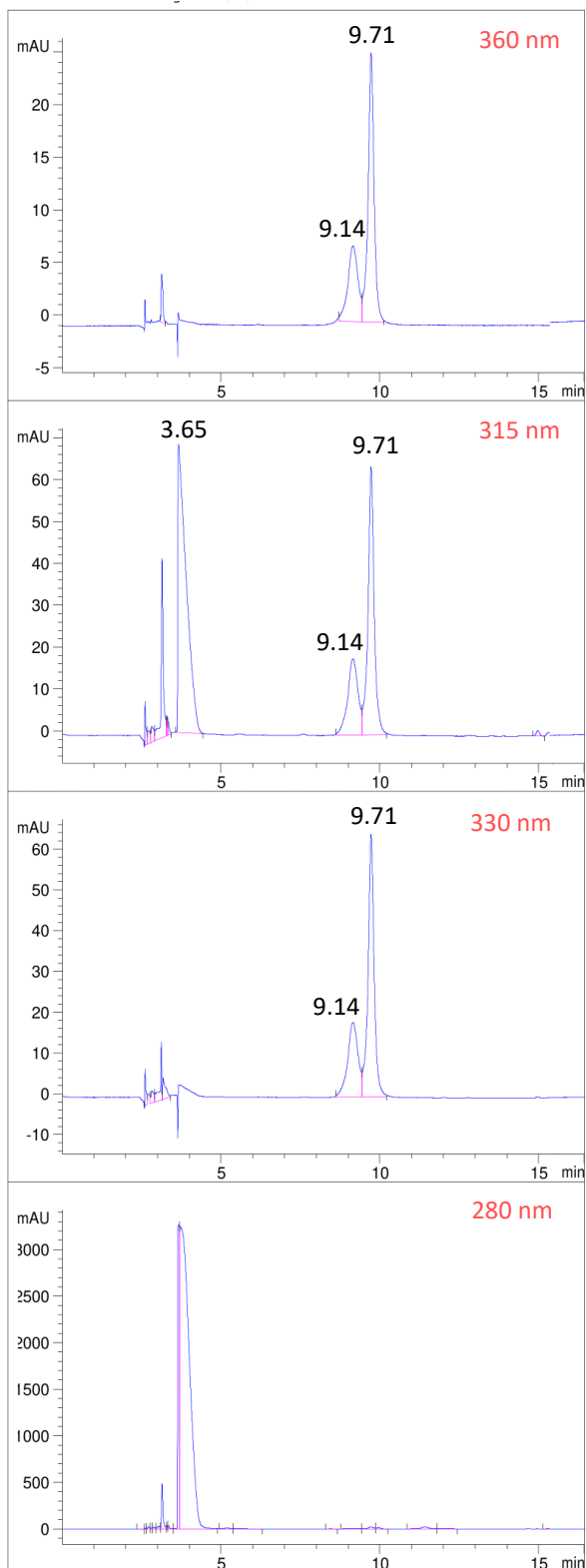
Chapter 3

Results and discussion

3.1 Initial analysis of *Pachymatisma normani* extracts

Little research has been done on *P. normani* prior to this thesis. Initially two small samples of *P. normani* was extracted, one in acetone and one in methanol. The samples were then screened using an HPLC system with a DAD-detector, figure 3.1. Revealing if the sponge contained any compounds capable of UV-VIS absorption (methods 2.5), but also to determine which solvent would be most suitable for further extractions. The DAD-detector screened for absorption in the 360 nm, 330 nm, 315 nm and 280 nm windows.

In the acetone crude there are primarily two peaks that dominate, one at 9.14 min and one at 9.71 min. They are partially overlapping and are present in the 360 nm, 330 nm and 315 nm windows. The 315 nm window also contain a third peak at 3.65 min, with a similar intensity as the peak at 9.71 min. While the methanol crude on only contained the 9.71 min signal in the 360 nm, 330 nm and 315 nm window.

Elucidating and identifying the peaks in these crudes will require purification and isolation to some extent. The signal at 9.71 min seems to dominant compound with UV-VIS absorption in both extracts. Methanol is probably the most suitable solvent for further extractions, with regards to the 9.71 min signal. As the 9.14 min and 9.71 min signals in the acetone crude might prove difficult to separate.
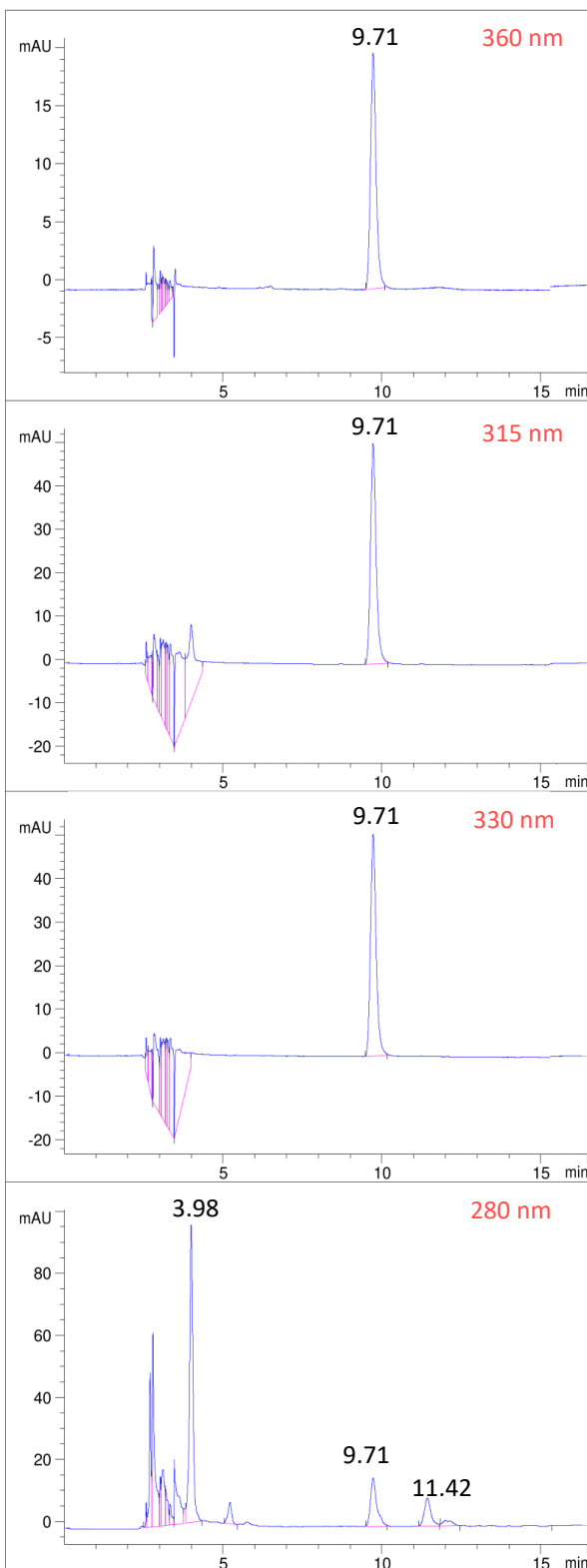
Figure 3.1 – HPLC profiles of the acetone- and methanol crude. Screened in 360 nm, 330 nm, 315 nm and 280 windows. Peaks have been assigned with retention times.

The UV-VIS spectrum for the 9.71 min peak is given in figure 3.2, and the absorption maxima is the 330 ± 20 nm range. The 330 nm window will therefore be considered the main window for HPLC-profiles. Since the compound that elutes at 9.71 min is an unknown, it will be referred to as **x**.
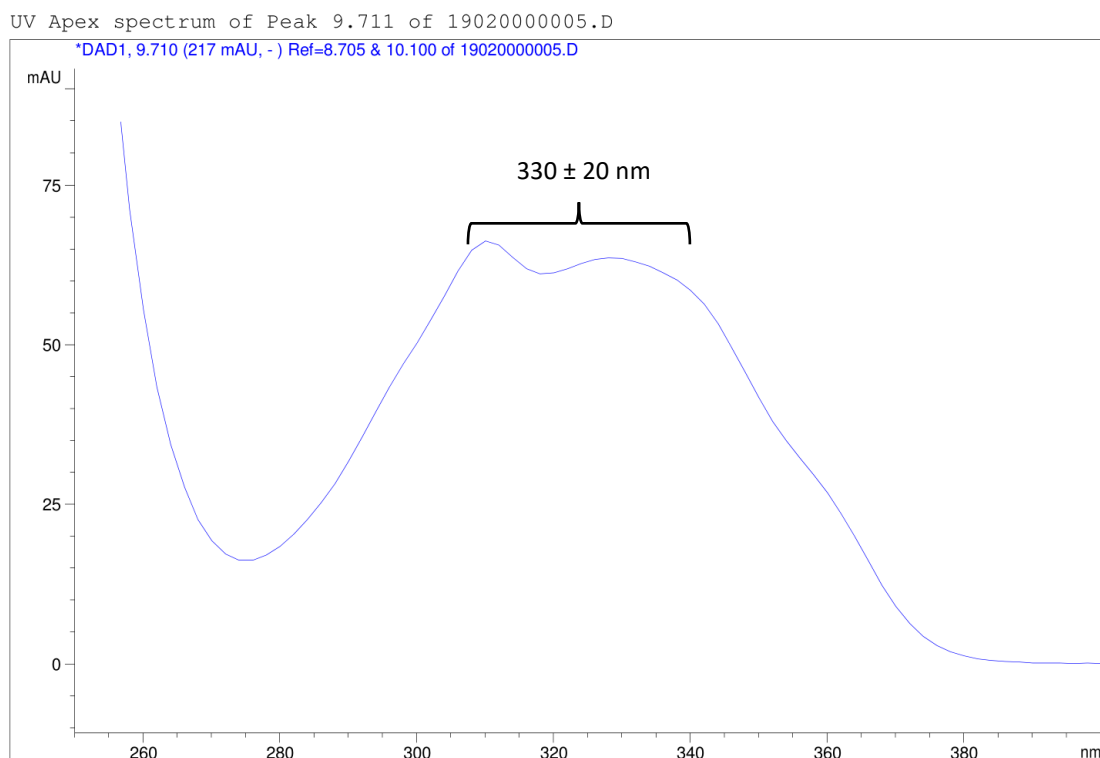
UV Apex spectrum of Peak 9.711 of 19020000005.D

Figure 3.2 – UV-VIS spectrum of the peak with $t_R = 9.71$ in the HPLC-profile of the methanol crude. The absorption maxima for this peak is in the 330 ± 20 nm range.

3.2.1 First extraction (E1) of *P. normani*

Due to conclusions based on the initial analysis of *P. normani* (results and discussion 3.1), methanol was used as extraction solvent going forward. Since the sponge was frozen the extract will also include a smaller volume of seawater, meaning that a portion of the FW of *P. normani* (23.21 g) is contributed by water. Most of the sponge tissue would pulverize by the stirring during extraction. Sponge particles made it impossible to determine the colour of the extract, but filtration revealed it to be colourless.

Filtration was followed by purification with liquid-liquid extraction with water against EtOAc. Both phases remained colourless during the extraction but gained colour when the solvents were evaporated, and the extracts were concentrated. Once concentrated the aqueous phase turned brown and yielded a mass of 0.940 g. Large amounts of a white crystalline solid would also precipitate when the aqueous phase was concentrated. A solid which did not dissolve methanol but was easily dissolvable in water. Precipitation would continue as the concentrated aqueous phase was stored. Concentrating the EtOAc phase yielded a mass of 56 mg and resulted in a green extract. Traces of the white precipitate was also present in the EtOAc phase.

Table 3.1 – The mass and colour of the aqueous- and EtOAc phase once they were concentrated.

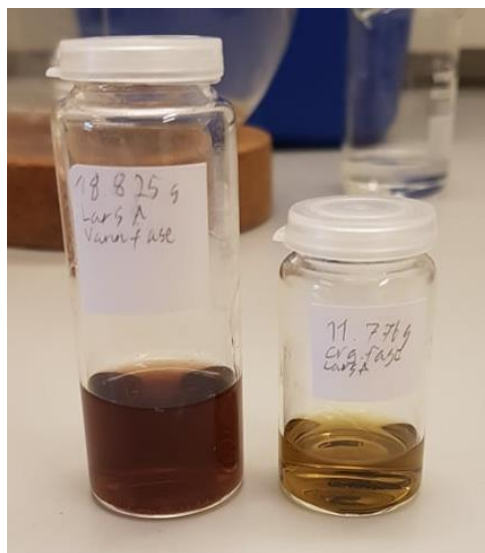|	Mass [g]	Colour
Aqueous	0.940	Brown
EtOAc	0.056	Green

Figure 3.3 – The brown concentrate of the aqueous phase to the left, and the green concentrate of the EtOAc phase to the right.

3.2.2 HPLC analysis of E1

The initial analysis and the analysis of **E1** was done on two different HPLC-systems, resulting in different retention times. HPLC-profile of **E1** recorded on the new system is given in figure 3.4, giving **x** a retention time of 16.73 min.
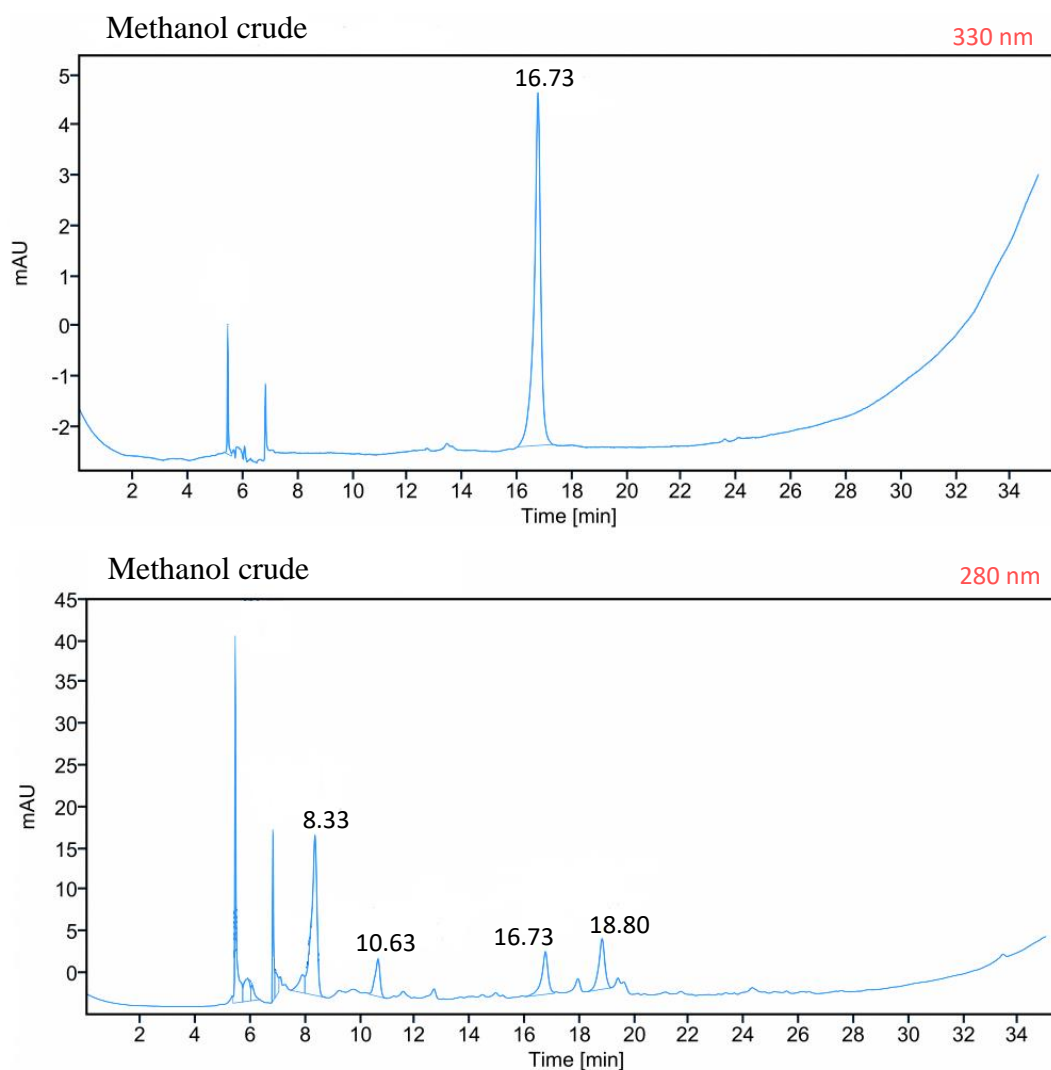

Figure 3.3 – HPLC-profile for **E1**. The retention time of compound **x** is 16.73 min in this HPLC-system.
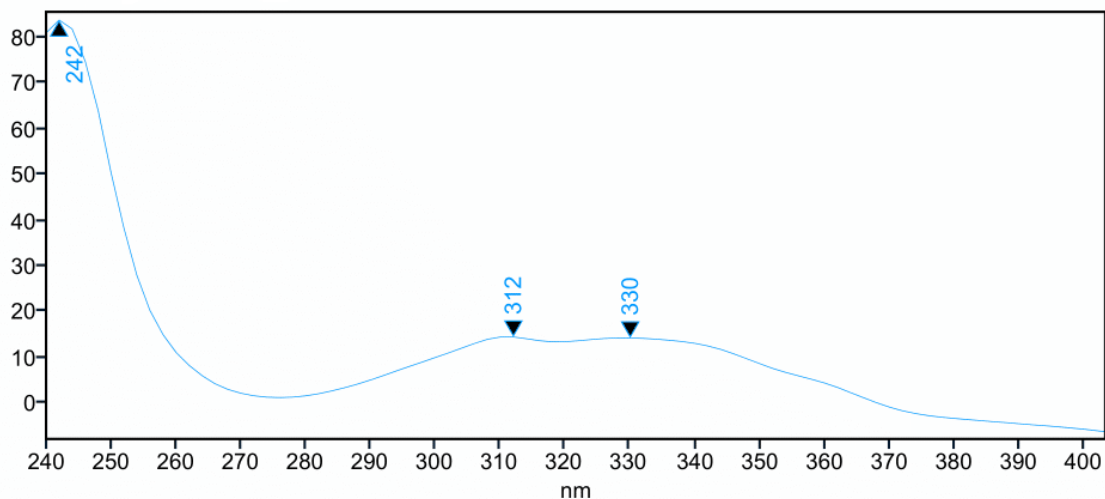
E1 crude, t_R = 16.73

Figure 3.4 – UV-VIS spectrum of **x** with t_R = 16.73. Peak **x** has an absorption maximum at 242 nm with secondary absorption peak around 320 nm.

After the aqueous phase had been concentrated it was analysed with HPLC, figure 3.4. Peak **x** was still present in the aqueous phase, but there was also an additional peak in the 330 nm window at 21.78 min. This might be due to unstable compounds in the extract that decompose during storage. The additional peak could also be a result of the liquid-liquid extraction interfering with the sample. An additional peak could also be found in the EtOAc phase at 14.15 min, with a nearly identical absorption pattern to **x**.
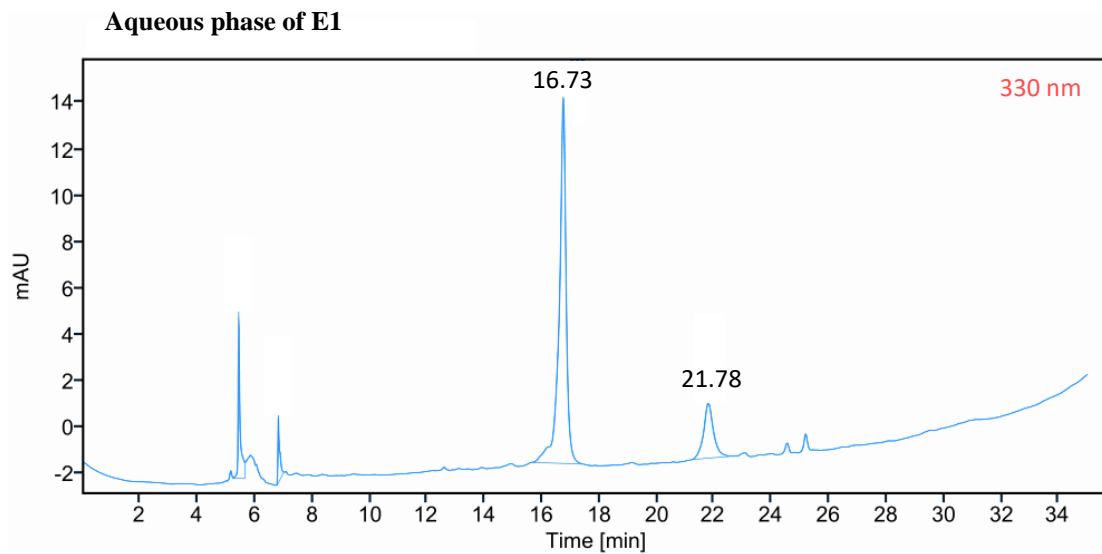
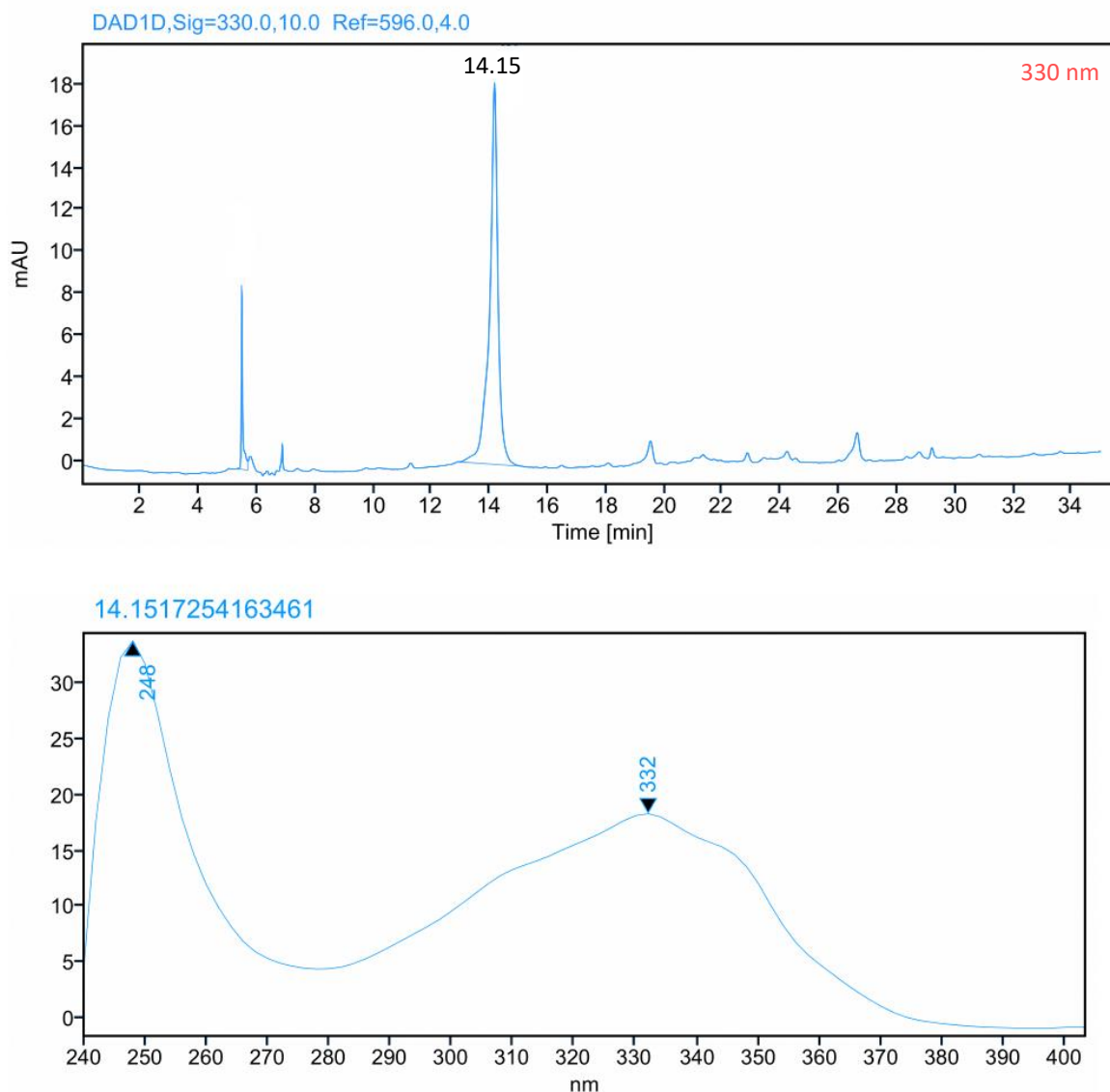Figure 3.4 – The 330 nm window of the **aqueous phase**.

Figure 3.6 – The 330 nm window of the EtOAc phase, including the UV-VIS spectrum of the peak at 14.15 min.

Following the liquid-liquid extraction the aqueous phase was injected into a preparative-HPLC in order to purify and isolate **x** further. The prep-HPLC was set to a fixed wavelength and produces signals as compounds with set UV-VIS absorption elutes. Making it possible to collect them separately. Due to **x** having UV-VIS absorption in the 330 ± 20 nm range, the prep-HPLC was fixed to 320 nm. When injecting the aqueous phase, it was dissolved in 2 mL of methanol and was filtered to remove the white precipitate. The injection needle was at 1 mL, requiring two runs.
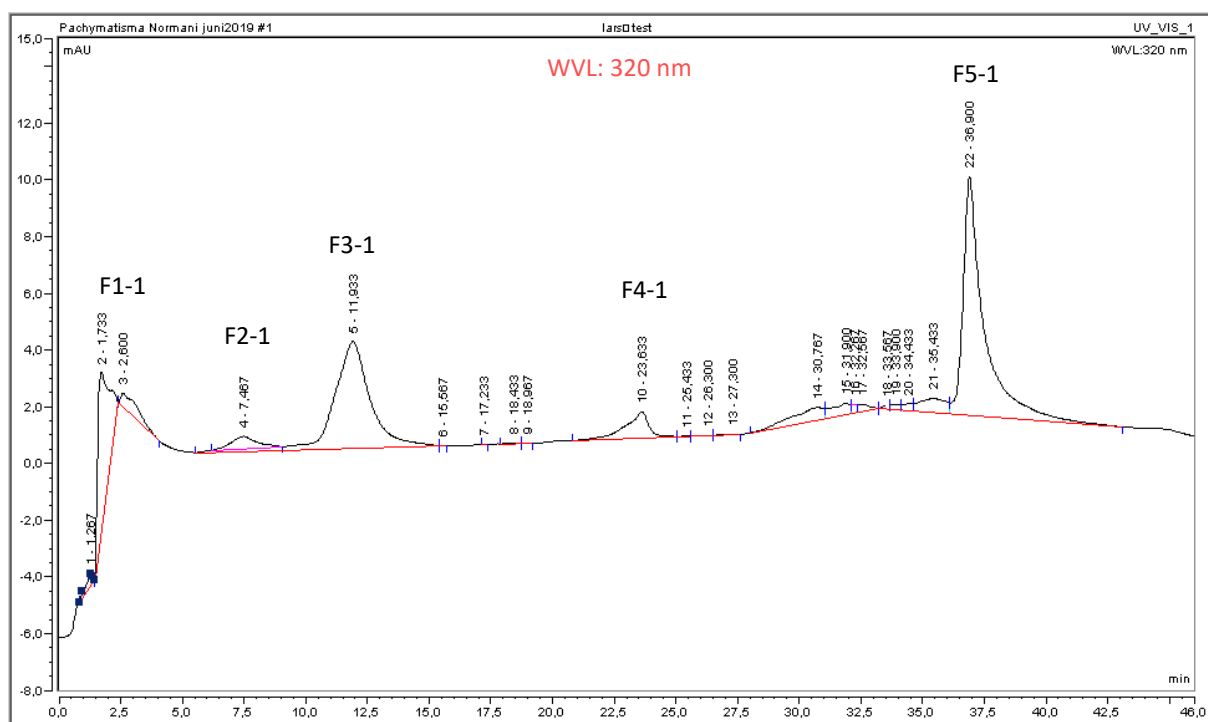
Figure 3.7 – Preparative HPLC chromatogram of the **aqueous phase** of **E1**.

Preparative-HPLC of the aqueous phase with the wavelength fixed at 320 nm resulted in five signals. Each peak was collected separately as fractions of the aqueous phase and was labelled **F1-1** to **F5-1**. Fraction **F1-1** seems to consist two partially overlapping signals, while fractions **F2-1** and **F4-1** are of a relatively low intensity compared to the other signals. **F5-1** have the highest intensity and is followed by **F3-1**. Determining which fraction contains **x** requires analysing the fractions with HPLC. The fractions where concentrated and weighed, table 3.2. Once again there was a change of colour. The aqueous phase was brown while all the fractions were orange when concentrated.

Table 3.3 – The mass and colour of the fractions **F1-1** to **F5-1** when concentrated.

Fraction	Mass [mg]	Colour
F1-1	303	Orange
F2-1	1.26	Orange
F3-1	1.95	Orange
F4-1	1.73	Orange
F5-1	4.42	Orange

After concentrating the fractions given by the prep-HPLC, they were analysed with HPLC to determine which fraction contained **x**. The HPLC-profiles of the fractions in the 330 nm window is given in figure 3.7. Fraction **F1-1** has the largest mass and contains two peaks eluting at 5.31 min and 6.59 min. Peak **x** with is in **F3-1**, while the peak at 21.90 min is in **F4-1**. Both **F2-1** and **F5-1** are contain only traces of peaks in the 330 nm window. Despite **F5-1** being of a relatively high intensity in the prep-HPLC. It does however have a rather high retention time and might require a longer runtime to be analysed with the HPLC.
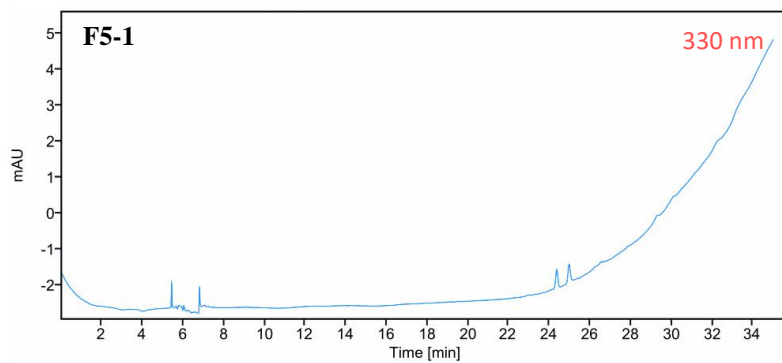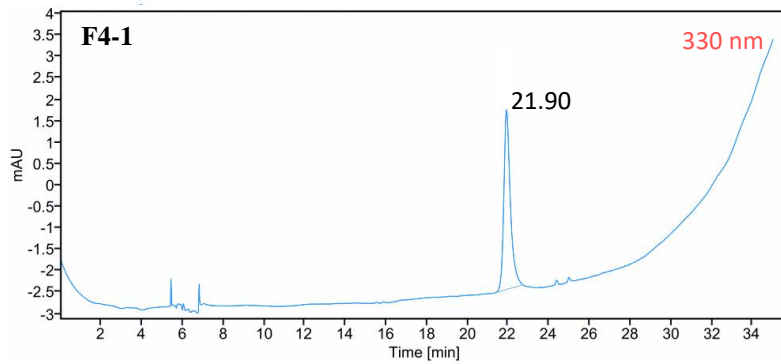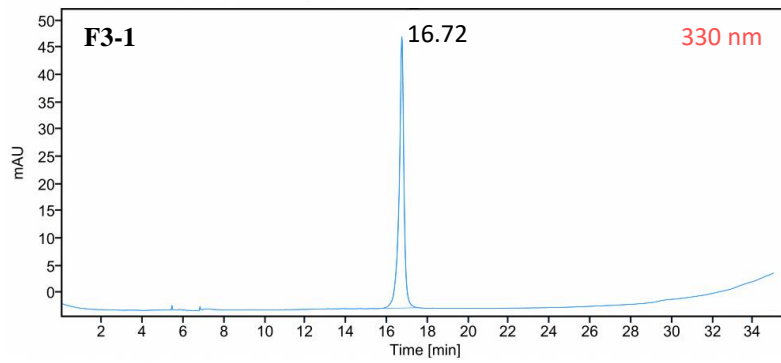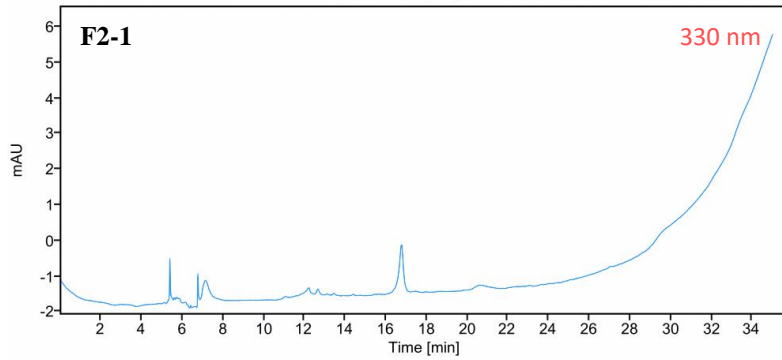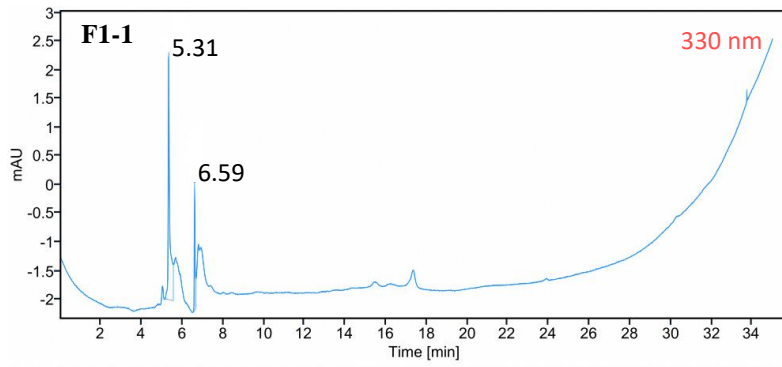
Figure 3.8 – HPLC-profiles for **F1-1** to **F5-1** in the 330 nm window.

36

3.2.3 NMR of E1

Following the prep-HPLC, fractions **F1-1**, **F3-1**, **F4-1** and **F5-1** was analysed with NMR.
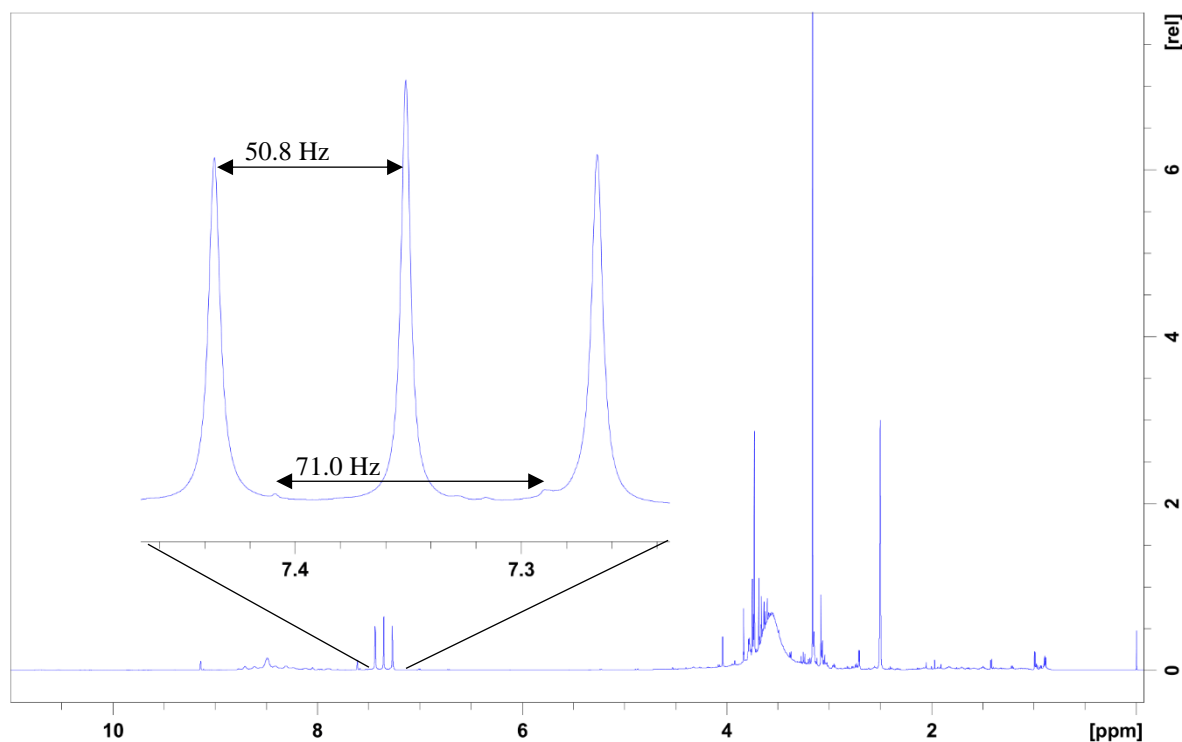
3.2.3a NMR of F1-1

Figure 3.9 – 600 MHz ^{1}H NMR spectrum of **F1-1**, dissolved in DMSO-d_6 and recorded at 298K. Emphasising on the peculiar triplet in the aromatic region. (Donald L. Pavia 2015) The triplet has couplings at 50.8 Hz and 71.0 Hz.

Fraction **F1-1** had the highest mass of the fractions at 303 mg and consists of polar compounds that elutes early. The ^{1}H NMR spectrum in figure 3.8 contain a peculiar triplet in the aromatic region, but the coupling constants of 50.8 Hz and 71.0 Hz is too large for an aromatic structure (Donald L. Pavia 2015). The shape of the triplet and coupling constants does however fit with ammonium (Lab 2019). It is likely that ammonium would be present in the sample, as sponges excrete high amounts of it (1.2 Marine sponges).

3.2.3b NMR of F3-1

^{1}H-, COSY-, HSQC- and HMBC-spectra was recorded of fraction **F3-1** of the aqueous phase.
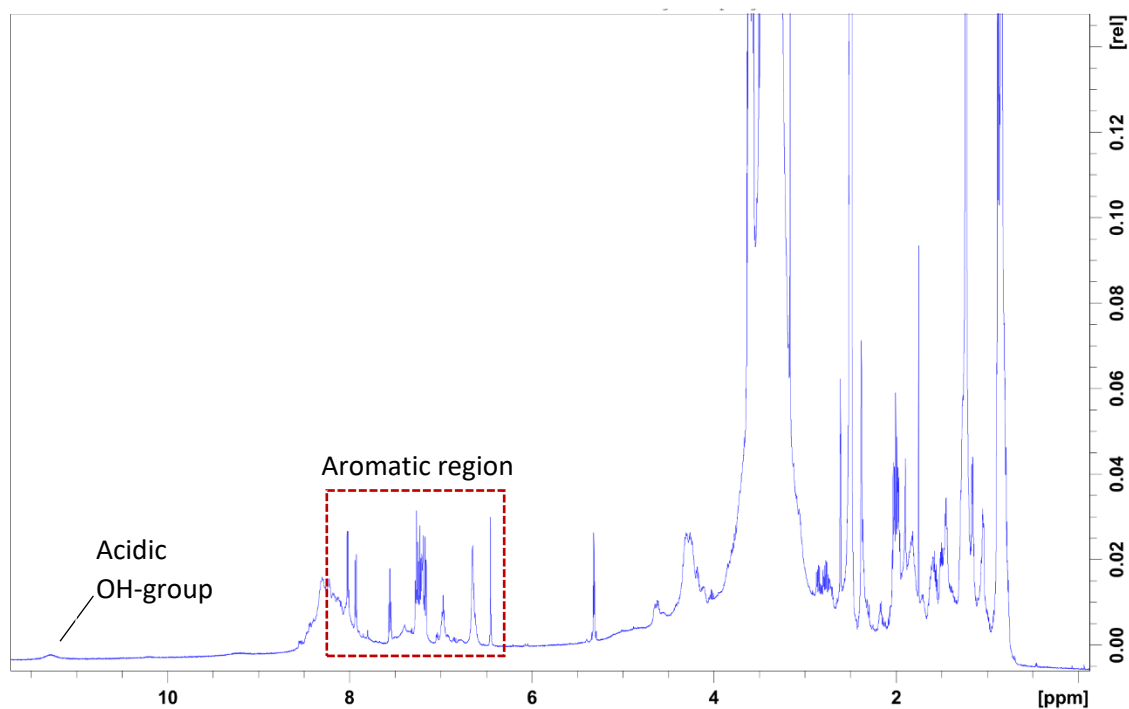

Figure 3.10 – 600 MHz ^{1}H NMR spectrum of **F3-1**, dissolved in DMSO-d$_6$ and recorded at 298K. Judging from the spectrum, the **F3-1** sample is quite impure. There are however some peaks in between the 8-6 ppm range with decent resolution. The spectrum also contain a small broad peak at 11.3 ppm, indicating that there is an acidic OH-group in the sample (Donald L. Pavia 2015).
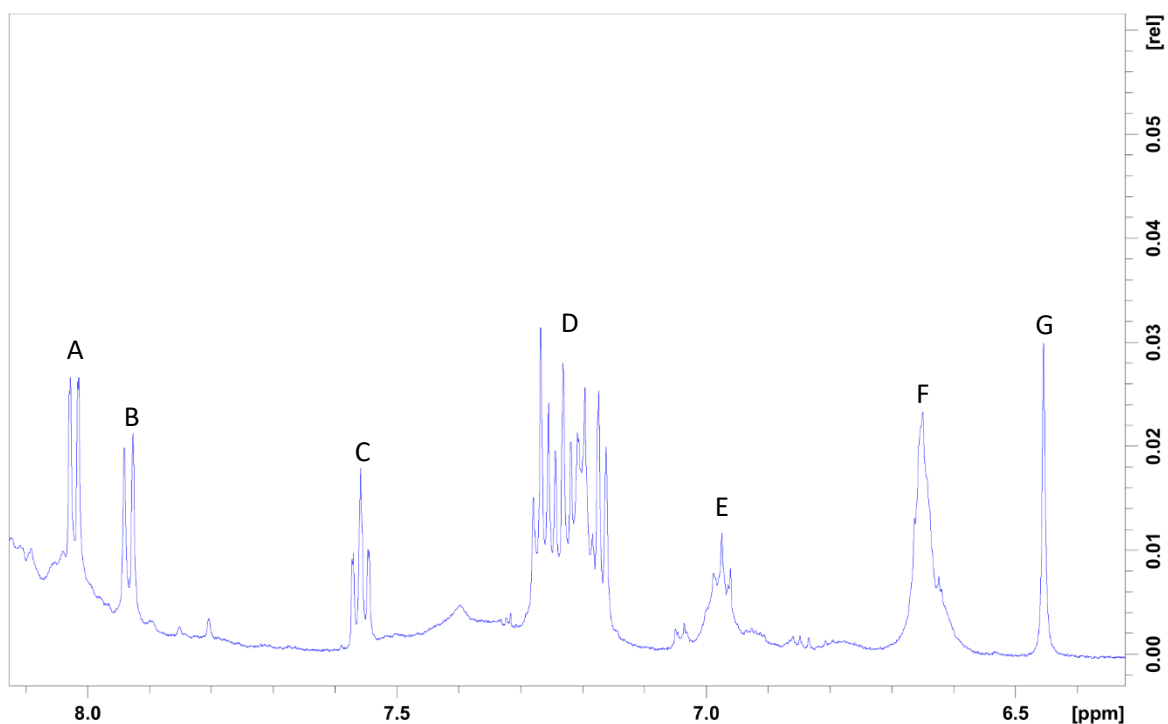
Figure 3.11 - The ^{1}H NMR-spectrum from figure 3.10 focusing on the region from 8.1 to 6.3 ppm. The peaks in this area has been labelled **A-G**.

Table 3.4 – Assigned peaks in the ^{1}H NMR spectra of **F3-1**

Peak	Chemical shift [ppm]	Multiplicity	Environment
A	8.02	Doublet of doublets	Aromatic
B	7.93	Doublet	Aromatic
C	7.56	Triplet	Aromatic
D	7.26 – 7.17	Higher order	Aromatic
E	6.97		
F	6.65		
G	6.46	Singlet	

The aromatic region for protons is in the chemical shift range between 8.0 – 6.5 ppm (Donald L. Pavia 2015). A range that cover peaks **A-F**, while **G** is just below. Peak **A** at 8.02 ppm is a doublet of doublets with coupling constants of 1.15 Hz and 8.1 Hz, which is typical for meta and ortho couplings (2.7 NMR spectroscopy). **B** at 7.93 ppm is also a doublet with a coupling constant at 8.3 Hz, while **C** at 7.56 ppm is a triplet with 1.3 Hz and 7.69 Hz as coupling constants. Since peaks **A** and **B** are doublets, they have one neighbouring proton compared a triplet like **C** that has two neighbouring protons. **D** is a cluster of overlapping peaks between 7.26 – 7.17 ppm, making it impossible to determine any splitting pattern. Both **E** and **F** are broad peaks, which could be a sign of partially overlapping peaks. Peak **G** at 6.46 ppm is a singlet, meaning it has no neighbouring protons.
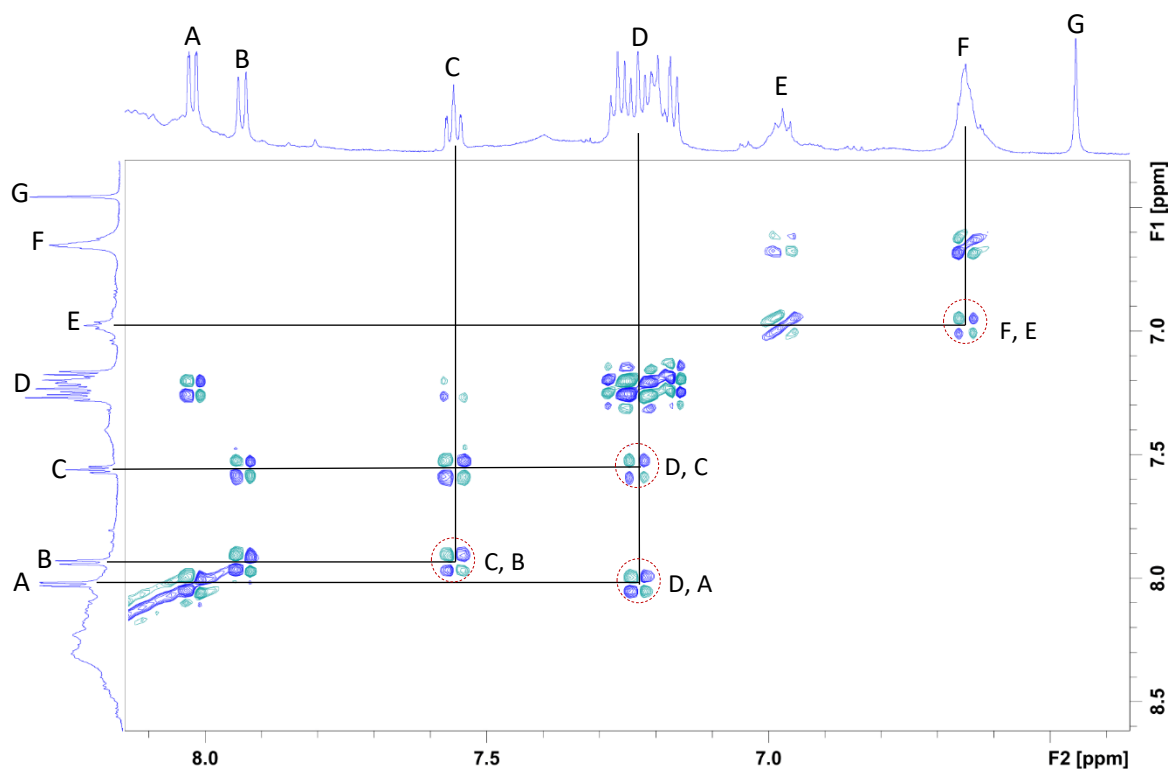
Figure 3.12 – 600 MHz COSY-spectrum of F3-1, dissolved in DMSO-d$_6$ and recorded at 298K. Showing the chemical shifts between 9.00 to 6.40 ppm, containing ^{1}H NMR-spectrum from figure 3.10 in both the y- and x-axis. Peaks **D** and **C** couple to each other, while **D** also couple to **A** and **C** also couple to **B**. **E** and **F** is also coupled together. Cross coupling peaks means that they are neighbouring protons (2.7 NMR Spectroscopy).

The Cosy-spectrum of **F3-1** given in figure 3.12 show that peaks **A**, **B**, **C** and **D** are interlinked. Neighbouring peaks within a ^4J distance give cross coupling signals. Doublet **A** have one neighbouring proton which is **D**, and so does doublet **B** which couple to **C**. Since **C** is a triplet it has two neighbouring protons, which **D** and **B**. Peak **D** is also cross coupled to two peaks, meaning the **D** signal within the cluster should be a triplet. If the peaks where assigned in position compared to **A**, would **D** in the ortho position, **C** in meta position and **B** in para position. Illustrated in figure 3.13 below. Peaks **E** and **F** also couple to each other. Since **G** is a singlet and lack any neighbouring protons it does not have any cross coupling either.
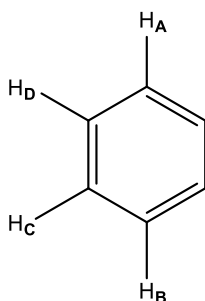

Figure 3.13 – Illustration of how peaks **A-D** could be assigned on a six-membered ring, based on the ^{1}H NMR-spectrum and COSY-spectrum in figures 3.11 and 3.12.
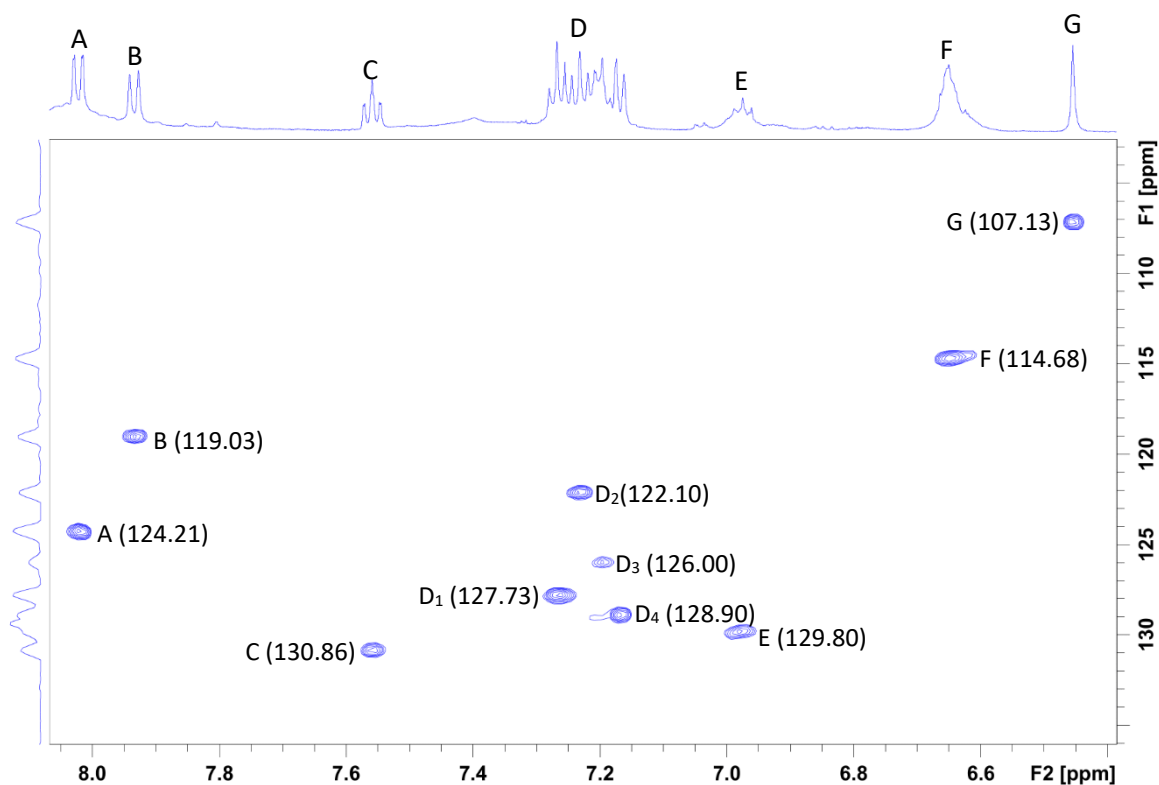
Figure 3.14 – 600 MHz HSQC-spectrum of F3-1 dissolved in DMSO-d_6 and recorded at 298K. The x-axis contains the ^{1}H NMR-spectrum from figure 3.10, showing the area between 8.1-6.4 ppm. The y-axis contains the ^{13}C NMR shift, showing the area between 100-140 ppm. HSQC shows the chemical shift for the carbon each proton is directly coupled to (2.7 NMR spectroscopy).

Table 3.5 – ^{1}H- and ^{13}C chemical shifts of peaks **A-G** given in the HSQC-spectrum in figure 3.14.

Peak	^{1}H chemical shift [ppm]	^{13}C chemical shift [ppm]
A	8.02	124.21
B	7.93	119.03
C	7.56	130.86
D_1	7.26	127.73
D_2	7.23	122.10
D_3	7.20	126.00
D_4	7.17	128.90
E	6.97	129.80
F	6.65	114.68
G	6.46	107.13

The HSQC-spectrum of **F3-1** in figure 3.14 assigns peaks **A-F** with aromatic carbons, see table 3.3 for chemical shifts. Aromatic carbons usually appear in the chemical shift range of 110-175 ppm (Donald L. Pavia 2015). **G** might be coupled to a double bond, which usually appear in the 100 – 150 ppm shift range and have the ^{1}H shift between 4.5-6.5 ppm (Donald L. Pavia 2015). While aromatic protons usually occur in the 6.5-8.0 ppm range. The HSQC-spectrum also reveal that the cluster peak **D** consists of four proton coupled carbons, **D_1-D_4**.
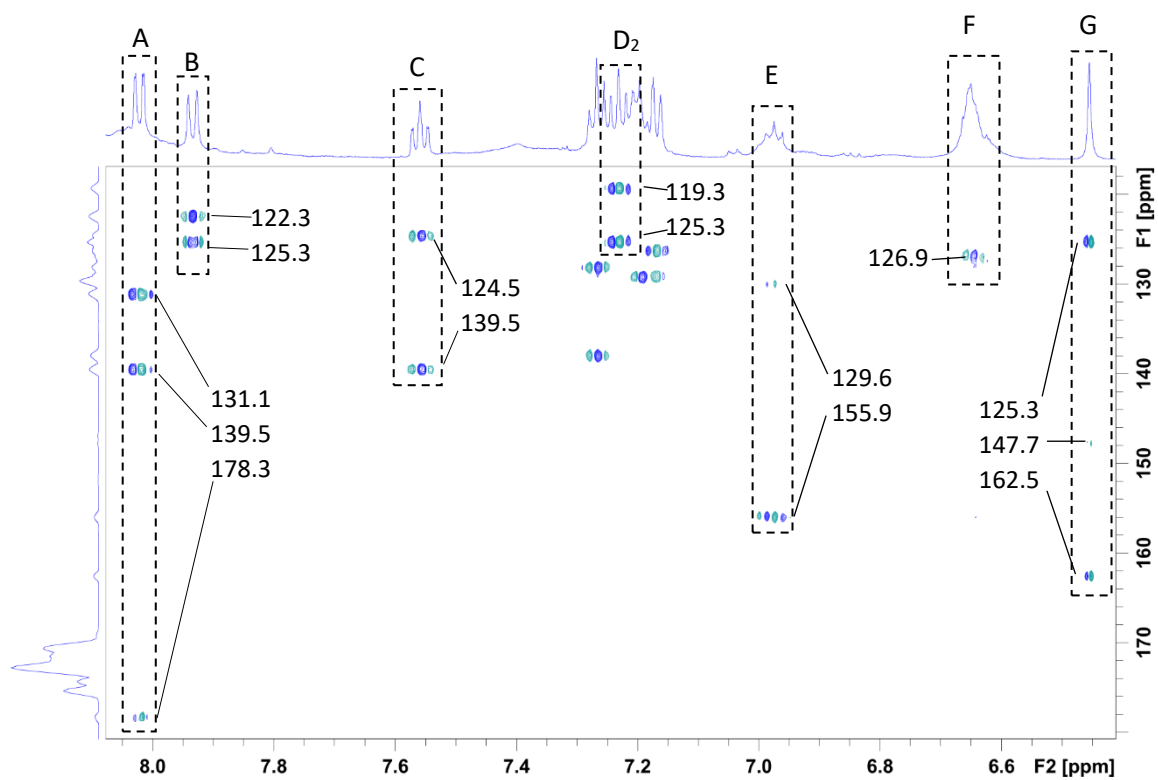
Figure 3.15 – 600 MHz HMBC-spectrum of **F3-1**, dissolved in DMSO-d$_6$ and recorded at 298K. Showing the ^{1}H chemical shift between 8.1-6.4 ppm in the x-axis, and the ^{13}C chemical shift between 110-180 ppm in the y-axis. Signals are produced by carbons that have a ^3J coupling to a proton (2.7 NMR spectroscopy).

Table 3.6 – ^{1}H- and ^{13}C chemical shifts of peaks **A-G** given in the HMBC-spectrum in figure 3.15

Peak	^{1}H chemical shift [ppm]	^{13}C chemical shift [ppm]
A	8.02	131.1
		139.5
		178.3
B	7.93	122.3
		125.3
C	7.56	124.5
		139.5
D_1	7.26	128.1
		137.9
D_2	7.23	119.3
		125.3
D_3	7.20	129.2
D_4	7.17	129.2
		126.3
E	6.97	126.9
F	6.65	155.9
		126.9
G	6.46	162.5
		147.7
		125.3

The HMBC-spectrum shows that peak **A** couples to three carbons. The carbon at 131.1 is directly coupled to proton **C**, while the carbon at 139.5 is not coupled to a proton and is most likely a quaternary aromatic carbon. Carbonyl carbon like acids, ester, amides and anhydrides are typically located in the chemical shift between 155-185 ppm (Donald L. Pavia 2015). The third carbon at 178.3 ppm that **A** couples to is probably a carbonyl. Peak **C** also couples to the quaternary carbon at 139.5 ppm as **A**, and to the carbon at 124.5 which is directly coupled to

A. Peak **D** was revealed to be an overlap four different signals in the HSQC, while the HMBC reveal that peak **D₂** is connected with **A**, **B** and **C**. **D₂** couples to **B** at 119.0 ppm and to a quaternary carbon at 125.3 ppm, which is also shared with **B**. This carbon is also shared with **G,** which couples to another carbonyl at 162.5 ppm. **G** also have a weak signal to a carbon 147.7 ppm. So far it seems like peaks **A**, **B**, **C**, **D** and **G** belong to the same structure, consisting of a six membered ring with an extension containing two carbonyl-groups.
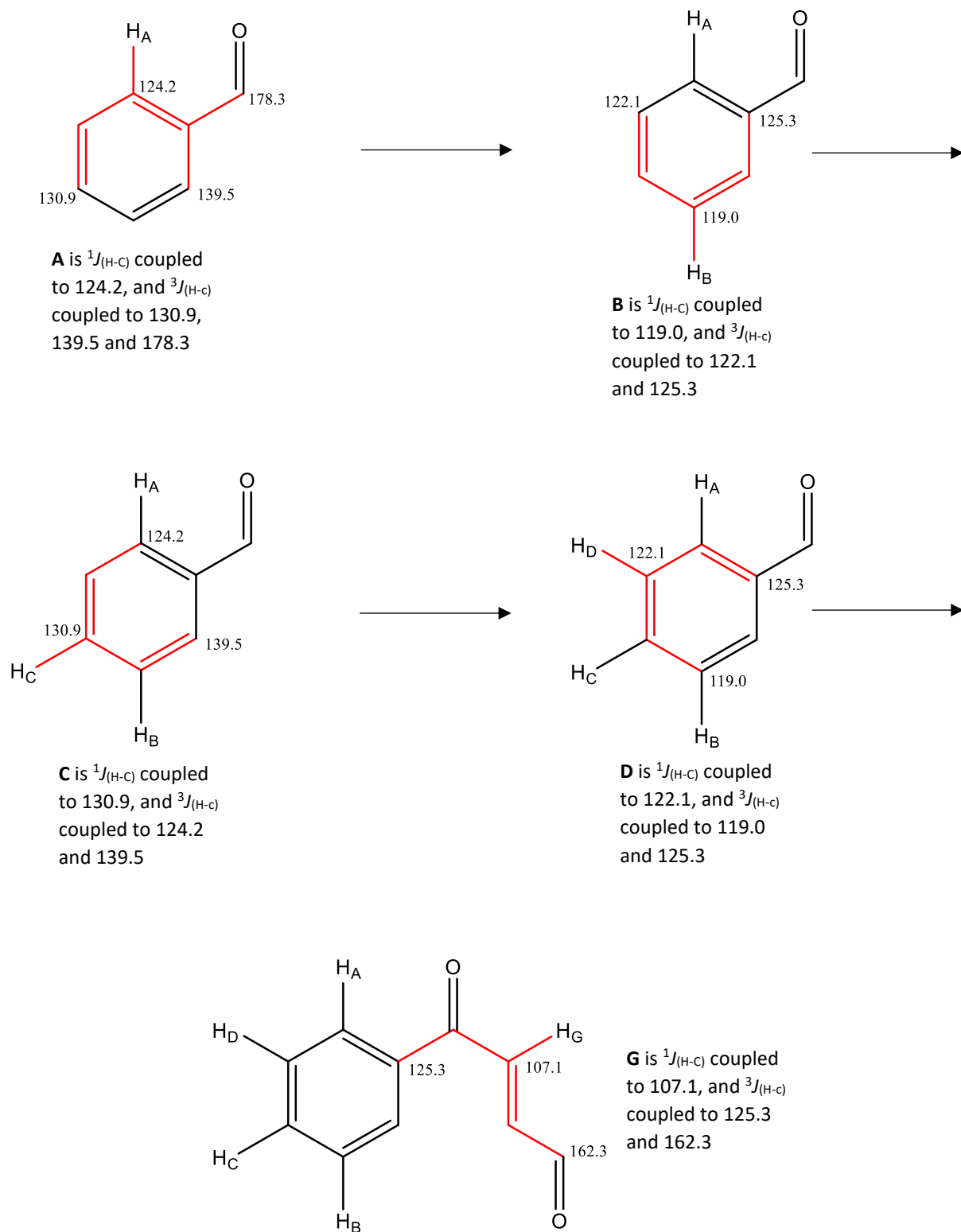
A is $^1J_{(H-C)}$ coupled to 124.2, and $^3J_{(H-c)}$ coupled to 130.9, 139.5 and 178.3

B is $^1J_{(H-C)}$ coupled to 119.0, and $^3J_{(H-c)}$ coupled to 122.1 and 125.3

C is $^1J_{(H-C)}$ coupled to 130.9, and $^3J_{(H-c)}$ coupled to 124.2 and 139.5

D is $^1J_{(H-C)}$ coupled to 122.1, and $^3J_{(H-c)}$ coupled to 119.0 and 125.3

G is $^1J_{(H-C)}$ coupled to 107.1, and $^3J_{(H-c)}$ coupled to 125.3 and 162.3

Figure 3.16 – Elucidation of **x** so far.

3.2.3c NMR of F4-1 and F5-1

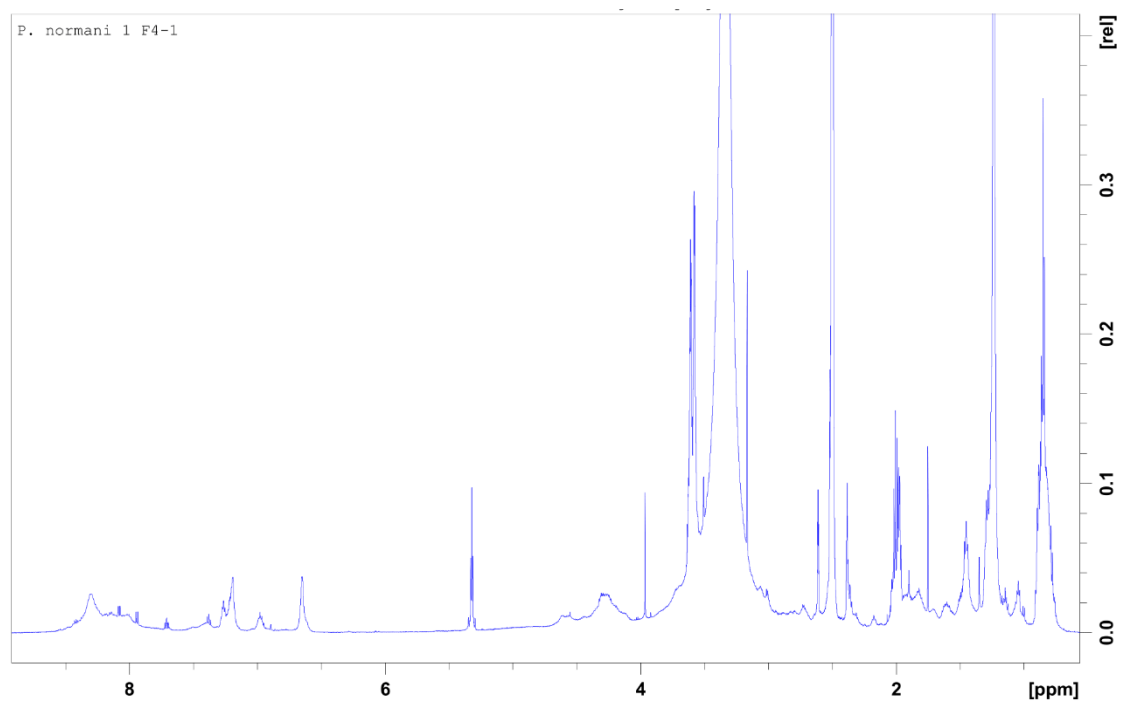^{1}H-, COSY, HSQC and HMBC spectra was recorded of samples **F4-1** and **F5-1**.

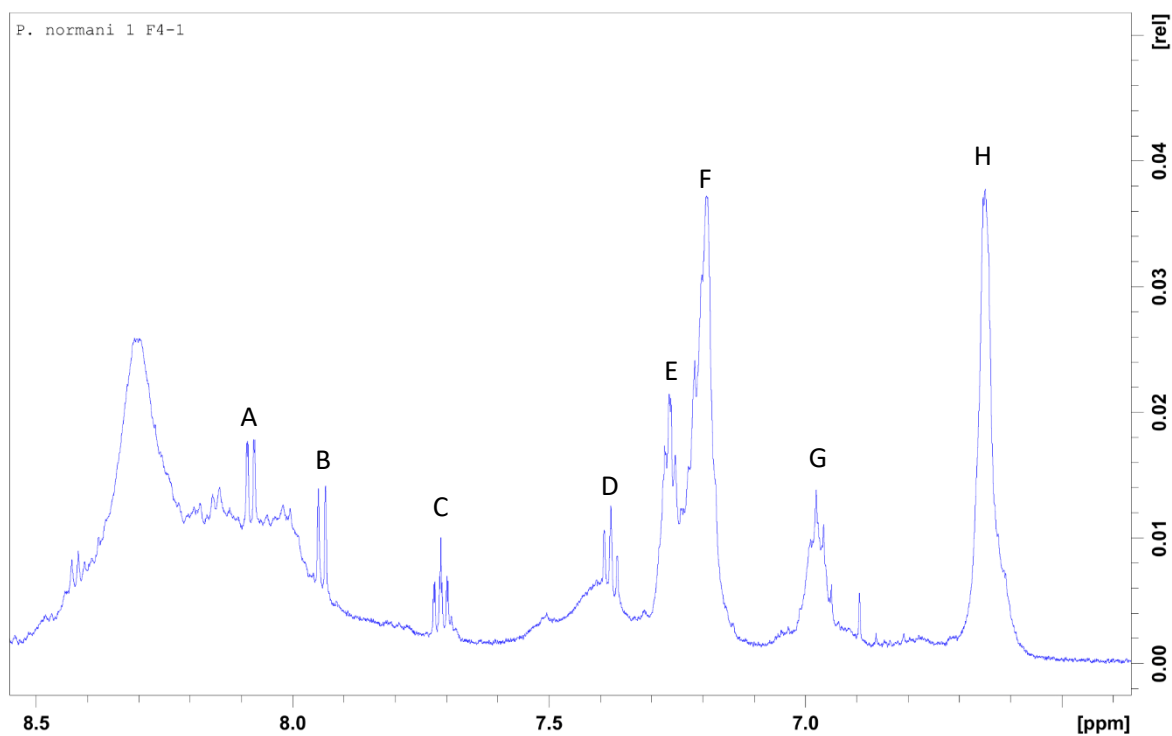Figure 3.17 – 600 MHz ^{1}H NMR spectrum of **F4-1**, dissolved in DMSO-d$_6$ and recorded at 298K.

Figure 3.18 – The aromatic region of the ^{1}H NMR spectrum of **F4-1**, figure 3.17.

The aromatic signals in **F4-1** are like those found in **F3-1**, see table 3.7 for chemical shifts. The chemical shifts and multiplicity order of peaks **A**-**D** are nearly identical to those of **A**-**D** in **F3-1** and is probably due to a breakdown product or traces of compound **x**. While peaks **E**-**F** seem to be identical to peaks **D$_1$, D$_3$, E** and **F** in **F3-1**. Chemical shifts are listed in table 3.7.
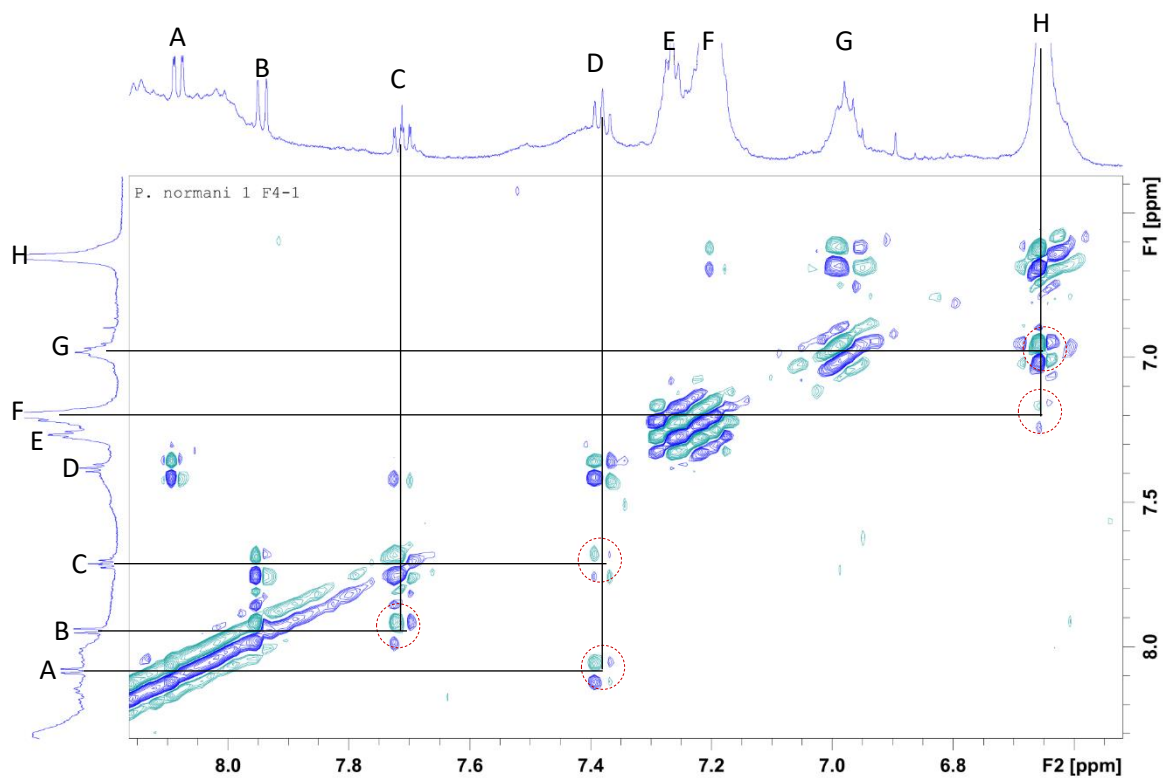
Figure 3.19 – 600 MHz COSY-spectrum of F3-1, dissolved in DMSO-d$_6$ and recorded at 298K. Showing the chemical shifts between 9.00 to 6.40 ppm, containing ^{1}H NMR-spectrum from figure 3.17 in both the y- and x-axis. Cross coupling has been highlighted with red circles.

The COSY spectrum of **F4-1** in figure 3.19 is also similar to the COSY spectrum of **F3-1** in figure 3.12. It contains the same cross coupling signals as in **F3-1**, but also has an additional weak signal between **H** and **F**.
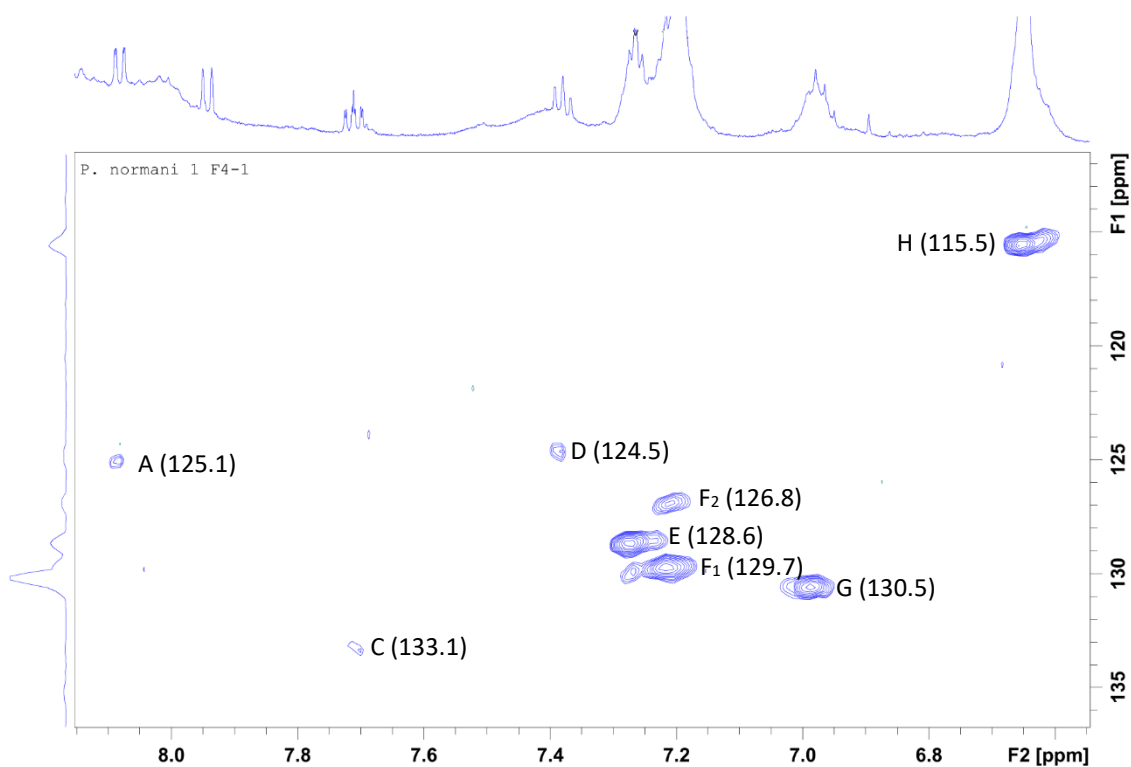
Figure 3.20 – 600 MHz HSQC-spectrum of F3-1 dissolved in DMSO-d_6 and recorded at 298K. The x-axis contains the ^{1}H NMR-spectrum from figure 3.17, showing the area between 8.1-6.4 ppm. The y-axis contains the ^{13}C NMR shift, showing the area between 100-140 ppm. Chemical shifts are listed in table 3.7.

HSQC of **F4-1** in figure 3.20 show that the carbon signals of **A**, **C** and **D** are weak compared to **E-H** and that there is no signal correlated to **B**. Peak **F** is an overlap of proton signals from two different carbons, where F_2 is of a lower intensity. The rest is similar to the HSQC spectrum of **F3-1** in figure 3.14.
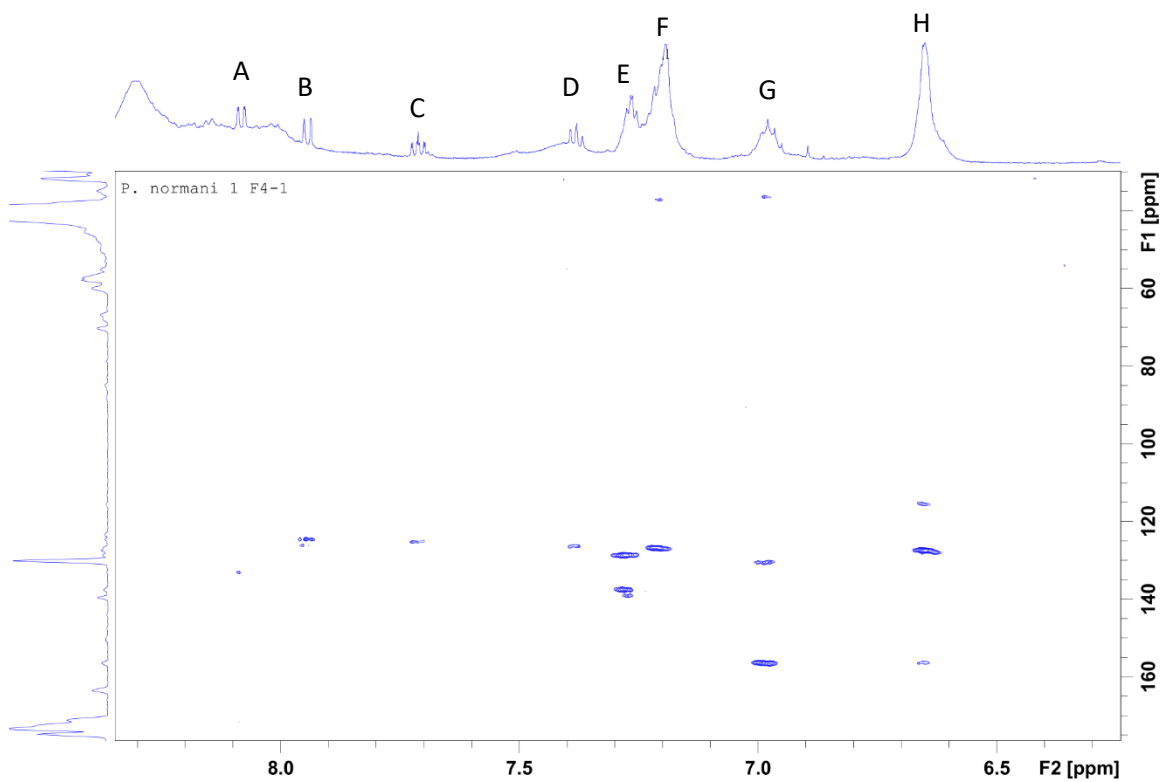
Figure 3.21 – 600 MHz HMBC-spectrum of **F4-1**, dissolved in DMSO-d$_6$ and recorded at 298K. Showing the ^{1}H chemical shift between 8.3-6.2 ppm in the x-axis, and the ^{13}C chemical shift between 110-180 ppm in the y-axis. Chemical shifts are listed in table 3.7.

Table 3.7 - Chemical shifts for peaks **A-H**.

Peak	¹H NMR [ppm]	HSQC [ppm]	HMBC [ppm]
A	8.08	125.1	133.1
B	7.94		124.5
			126.3
C	7.71	133.1	125.1
D	7.38	124.5	126.3
E	7.26	128.6	128.6
			137.3
F	7.19	129.7	126.7
			37.2
G	6.98	130.5	130.5
			156.7
			36.2
H	6.65	115.3	115.3
			127.4
			156.7

There are few carbon signals for peaks **A-D**, making it the data unsuitable for any elucidation. Peaks **E-H** also lack multiplicity and cross signals can only be found between **H** and **G**. The same signals of peaks **E-H** can be found in the NMR spectra of **F5-1** as well. The NMR spectra of **F5-1** is listed in the appendix.

3.3.1 Second extraction (E2) of *P. normani*

A second batch of *P. normani* (23.44 g) was extracted in (3 × 80 mL). **E1** was purified with liquid-liquid extraction against EtOAc, which lead to additional peaks in the 330 nm window. Since it is possible that the liquid-liquid extraction caused degradation of compounds in the sample, it might not be an ideal method to purify the sample. Therefore, purification with liquid-liquid extraction was excluded in **E2**. The extract was instead immediately concentrated after filtration, yielding an orange crude (0.523 g). There was also a significantly less of the white precipitate compared to **E1**.

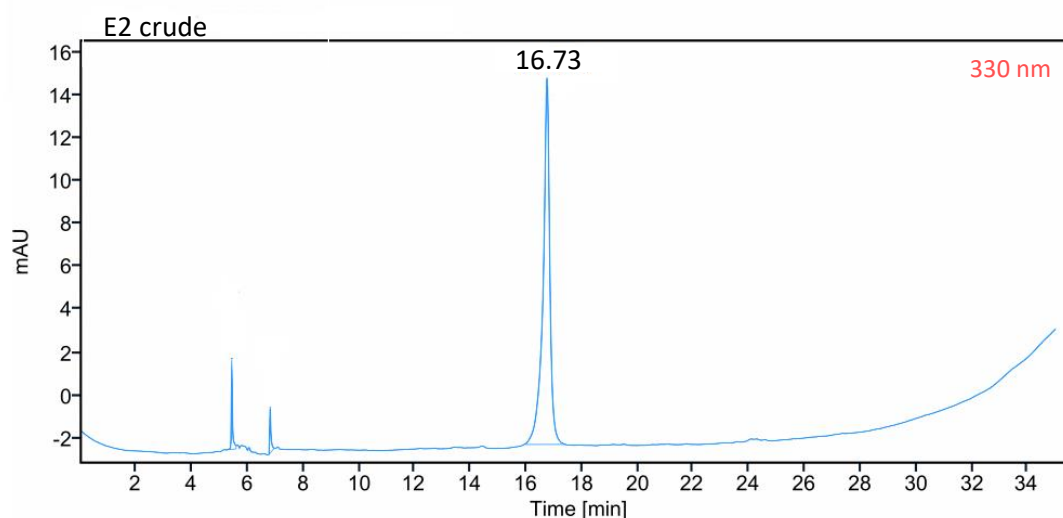Figure 3.22 – The orange crude of **E2**, dissolved in methanol.

Figure 3.23 – HPLC-profile of the crude of in **E2**, compound **x** elutes at 16.73 min.

After the extract of **E2** had been concentrated it was directly injected into the prep-HPLC, using the same conditions as in **E1**. Running the crude of **E2** with prep-HPLC yielded three fractions with UV-VIS absorption at 320 nm, **F1-2**, **F3-2** and **F5-2** (figure 3.24). They have been named based on retention time, to match their counterparts in **E1.** Fraction **F3-2** have the highest intensity and should contain compound **x**. When fraction **F3-2** was concentrated it was orange and yielded 5.87 mg.
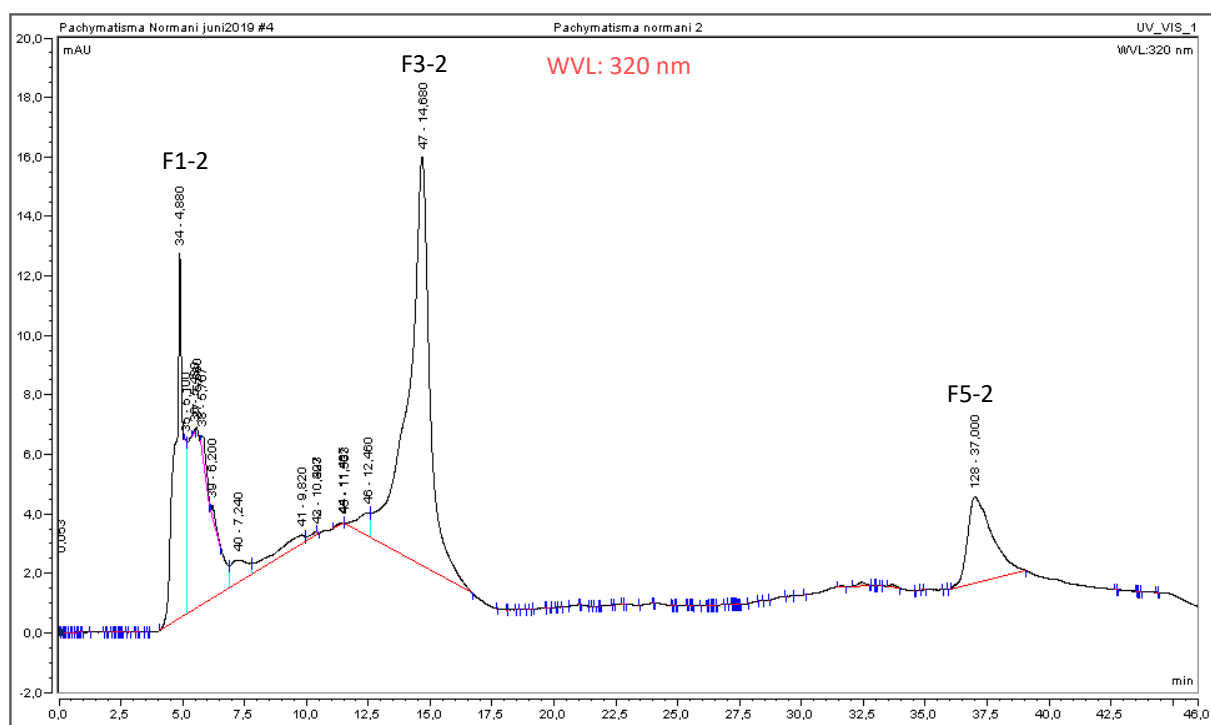

Figure 3.24 – Preparative HPLC chromatogram of the crude in **E2**.
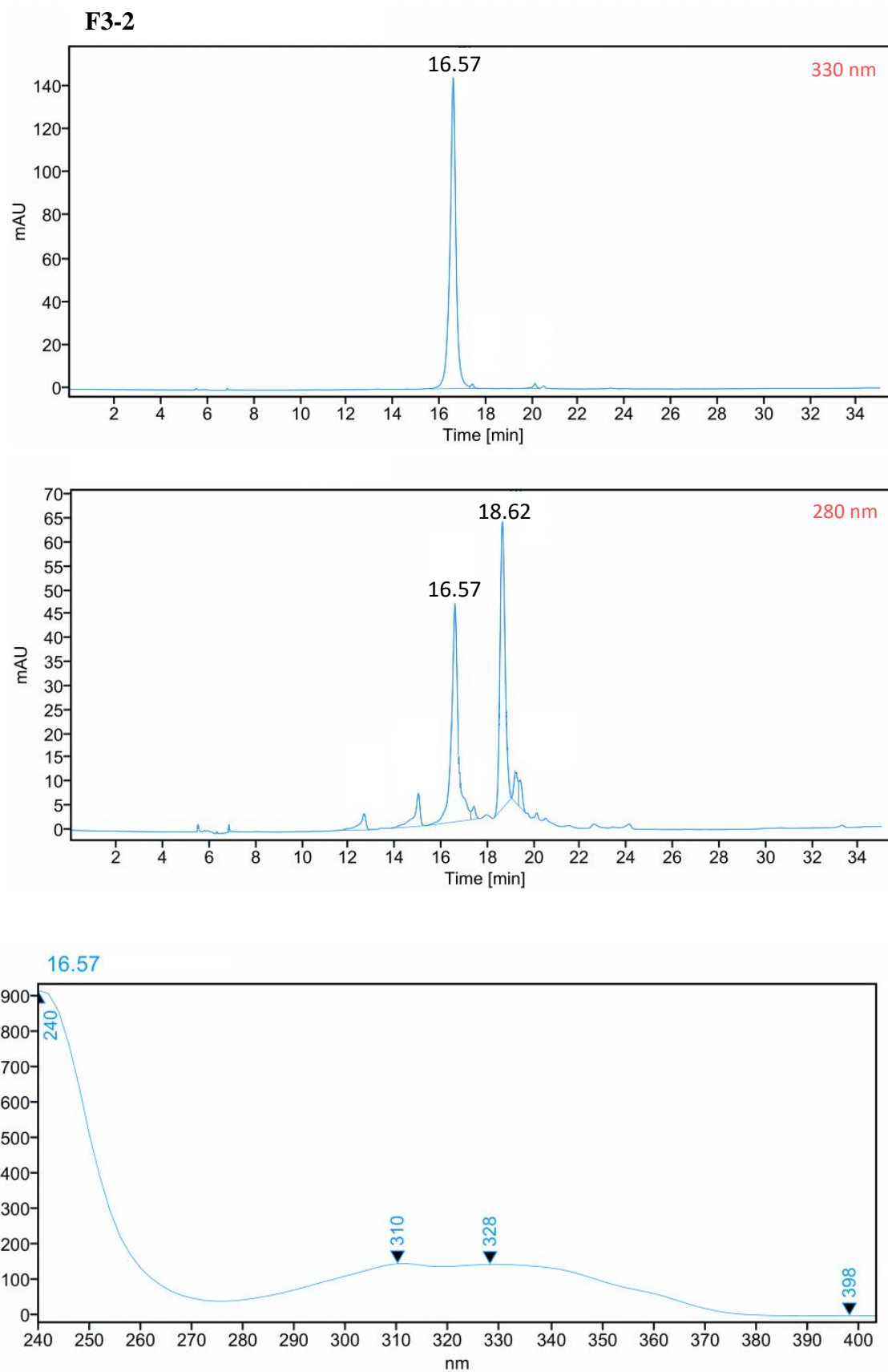
F3-2

Figure 3.25 - HPLC-profile for fraction **F3-2** from **E1.** UV-VIS spectrum of **x** with t_R = 16.57 min.

HPLC analysis of **F3-2** confirms that **x** is in the sample, eluting at 16.67 min. The 280 nm window of **F3-2** also contain an additional peak at 18.62 min. Even though **E2** yielded 5.87 mg of **F3-2** compared to **E1** with 1.95 mg of **F3-1**, does not necessarily mean there is more of **x** in **F3-2** compared to **F3-1**.

3.3.2 Mass spectrometry

After drying an isolating fraction **F3-2** it was analysed with mass spectroscopy. It was analysed with a LR-LC-MS system with positive ESI as ionization mode. The total ion current (TIC) chromatogram is given in figure 3.26. There is a lot of noise in the baseline (red line) and no peaks with good resolution. UV-VIS absorption in the 330 nm area was also included in the analysis and is also shown in figure 3.26 as the green line. The absorption maxima were at 10.245 min and the UV-VIS spectrum is given in figure 3.27, and has similar absorption pattern as the UV-VIS spectrums of **x**. With absorption peaks around the 240 nm and 330 nm area.
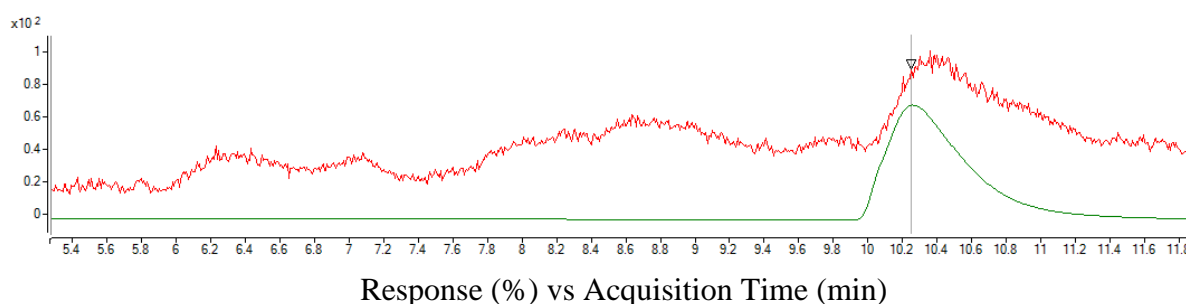

Response (%) vs Acquisition Time (min)

Figure 3.26 – LR-LC-MS of **F3-2** with positive ESI as ionisation mode. TIC scan is given by the red line, the green line is the UV-VIS absorption at 330 nm. The absorption maximum is at 10.245 min.
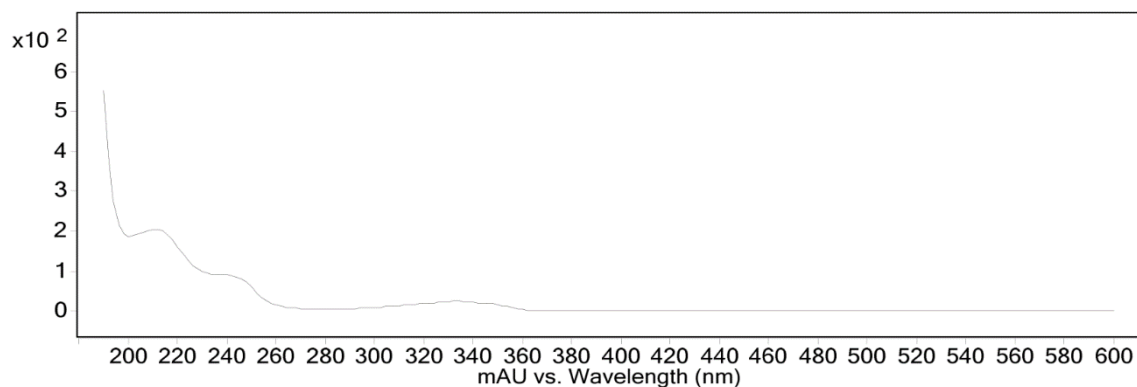
Figure 3.27 – UV-Vis spectrum of the compound with absorption maxima at 10.245 min in 330 nm window.

The mass-to-charge ratio at 10.245 min is given in figure 3.28. At 10.245 min the dominating mass-to-charge ratio is *m/z* 190.1. Since the MS was run in positive ESI mode the mass contains an additional proton, giving the dominant compound a mass of 189.1 g/mol. An uneven mass could be an indication that the compound contains a nitrogen atom.
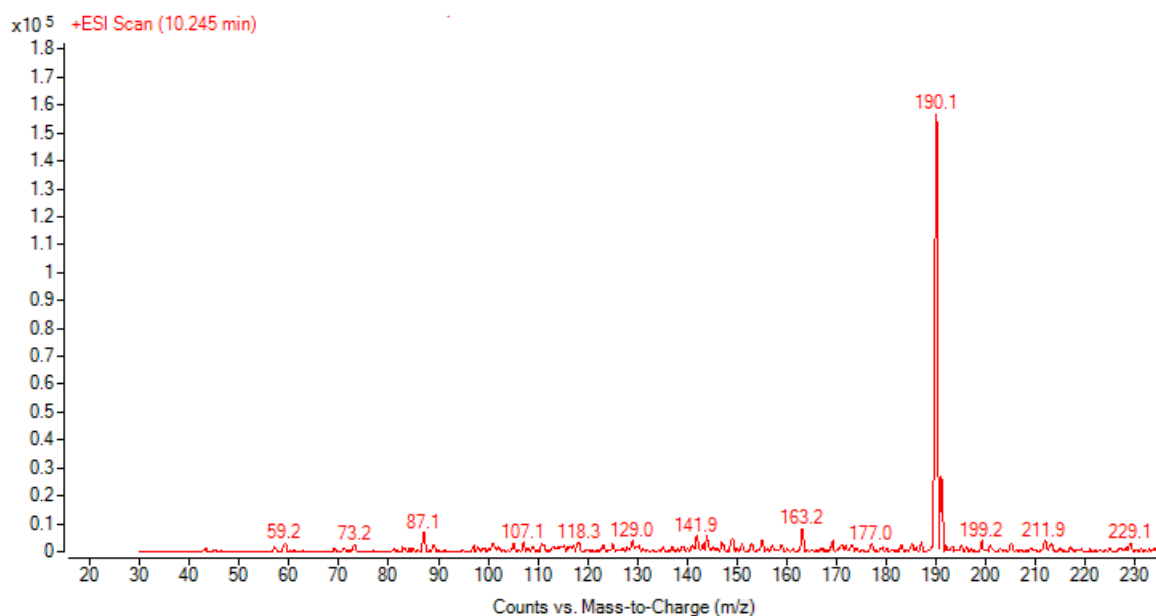

Figure 3.28 – The mass spectrum of **F3-2** at the 330 nm absorption maximum at 10.245 min, which have a mass to charge ratio of 190.1.

3.3.3 NMR from the Second extraction

^{1}H-, COSY-, HSQC-, HMBC- and ^{15}N-HSQC-spectra were recorded of **F3-2**.
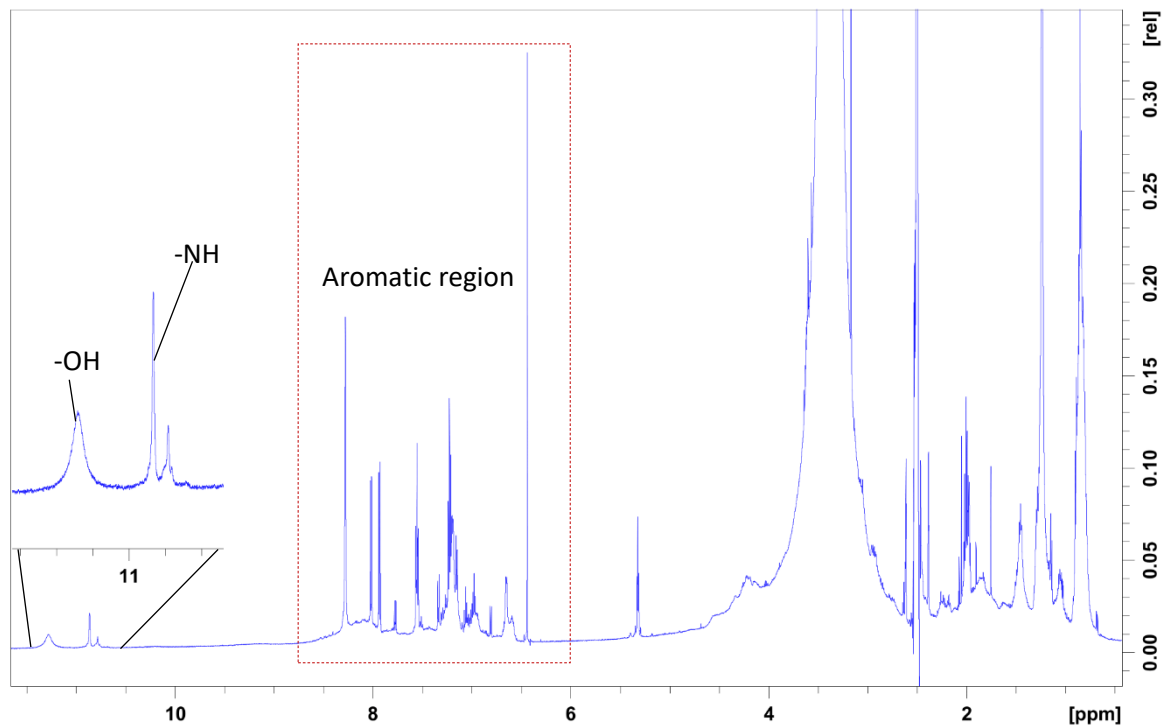

Figure 3.29 – 600 MHz ^{1}H NMR spectrum of **F3-2** from **E2,** dissolved in DMSO-d$_6$ and recorded at 298K. There are some differences between the proton spectrum of **F3-1** (figure 3.10) and the spectrum of **F3-2**. Most notable are the additional peaks in the aromatic region and a possible N-H peak around 11 ppm (Donald L. Pavia 2015). The acidic OH-group is also present at 11.3 ppm.
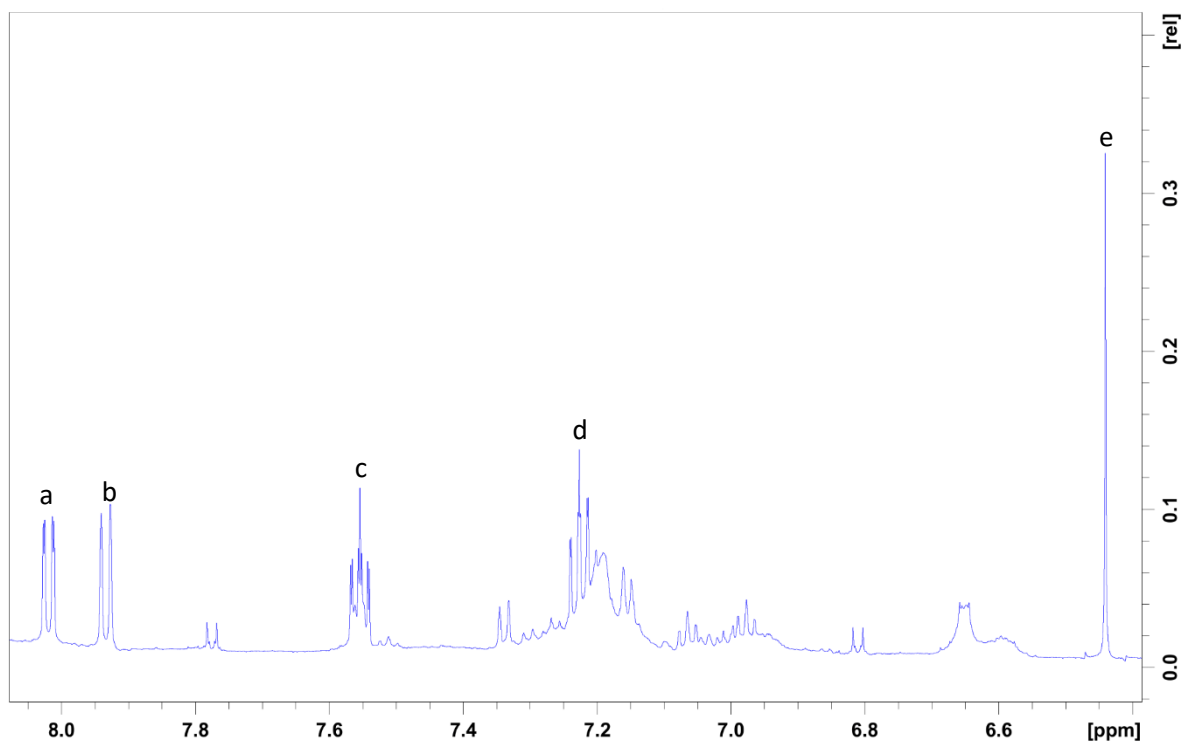
Figure 3.30 – The ^{1}H NMR-spectrum from figure 3.29 showing the region from 8.1 to 6.4 ppm. Peaks **A**, **B**, **C**, **D** and **G** from the proton spectrum of **F3-1** (figure 3.11) have been named **a-e** in the proton spectrum of **F3-2** (figure 3.30). Peak **d** is no longer a cluster of overlapping peaks as it was in figure 3.11, it is instead a triplet since it has two neighbouring protons. There are also traces of other aromatic compounds producing doublets and triplets of weaker intensities. One seems to be overlapping with **c**.
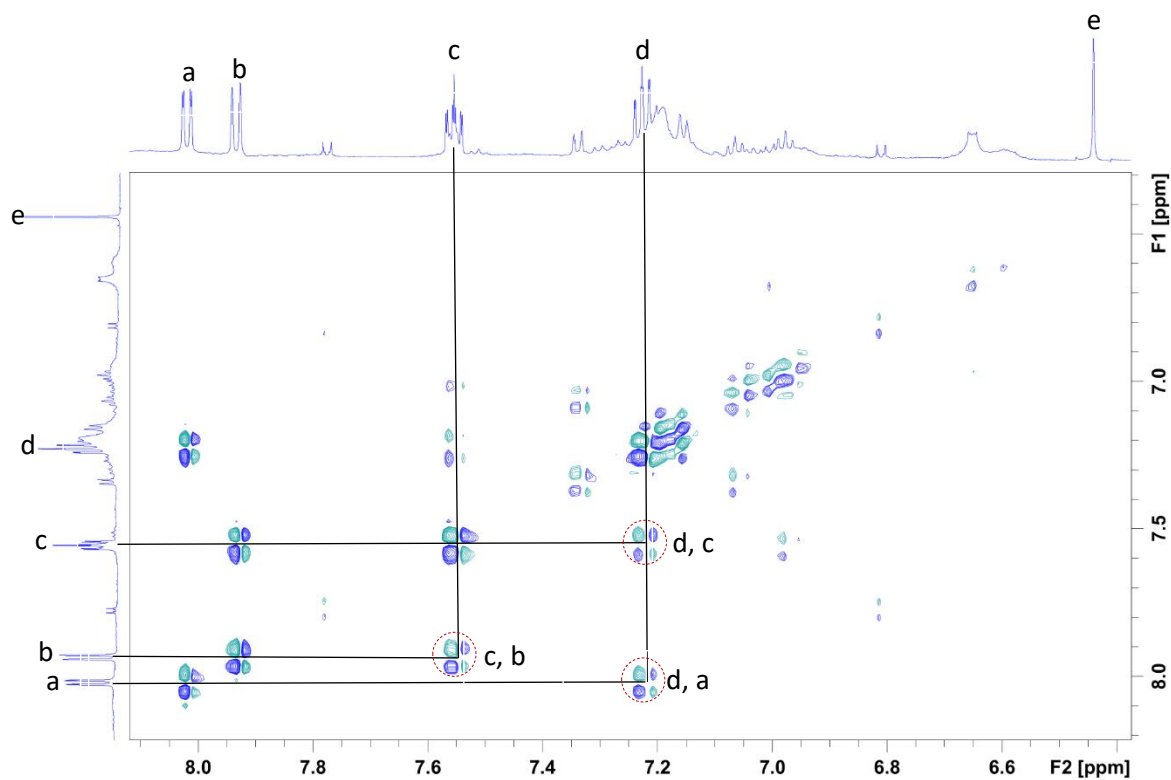
Figure 3.31 – 600 MHz COSY-spectrum of F3-1, dissolved in DMSO-d$_6$ and recorded at 298K. Showing the chemical shift between 8.2 to 6.4 ppm, containing ^{1}H NMR-spectrum from figure 3.29 in both the y- and x-axis. Regarding peaks **a-e** the COSY spectrum of **F3-2** is the same as of **F3-1** (figure 3.12). There are some additional weak signals for the other impurities in the sample.
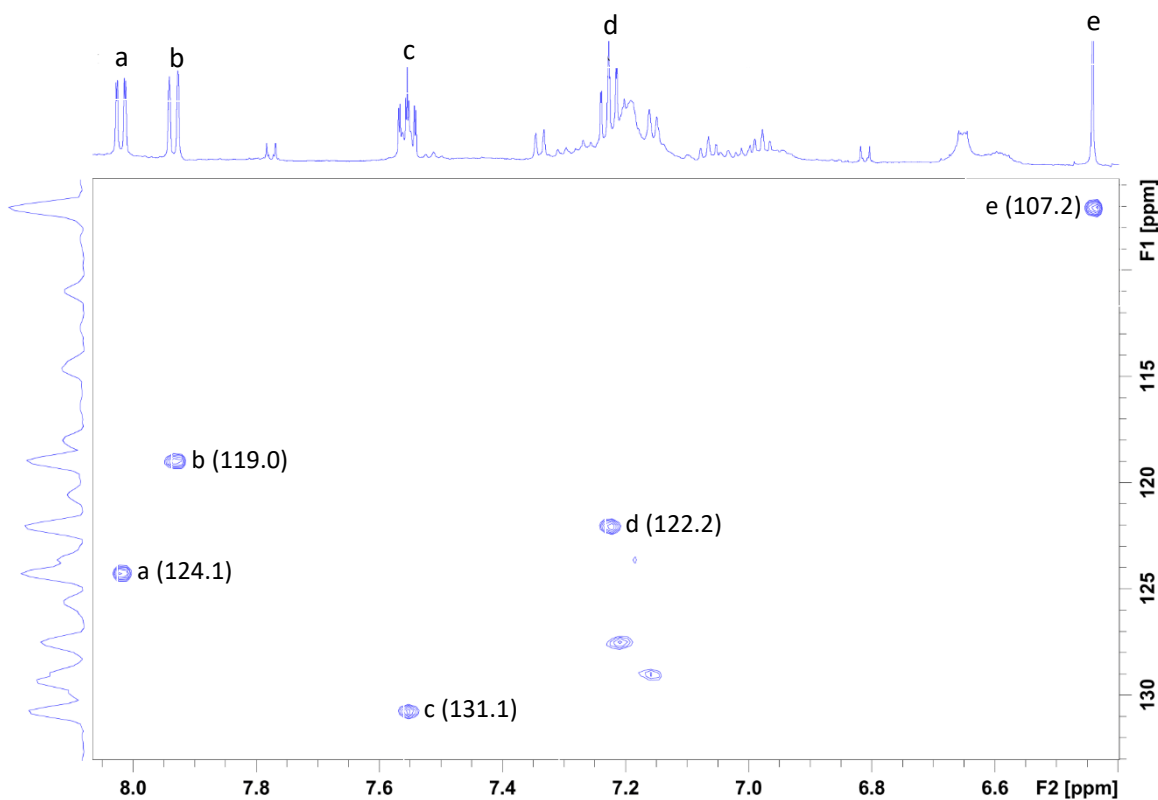
Figure 3.32– 600 MHz HSQC-spectrum of **F3-2** from **E2**, dissolved in DMSO-d$_6$ and recorded at 298K. The x-axis contains the ^{1}H NMR-spectrum from figure 3.30, showing the area between 8.5-6.0 ppm. The y-axis contains the ^{13}C NMR shift, showing the area between 90-145 ppm. HSQC is direct coupling correlation between proton and carbon.
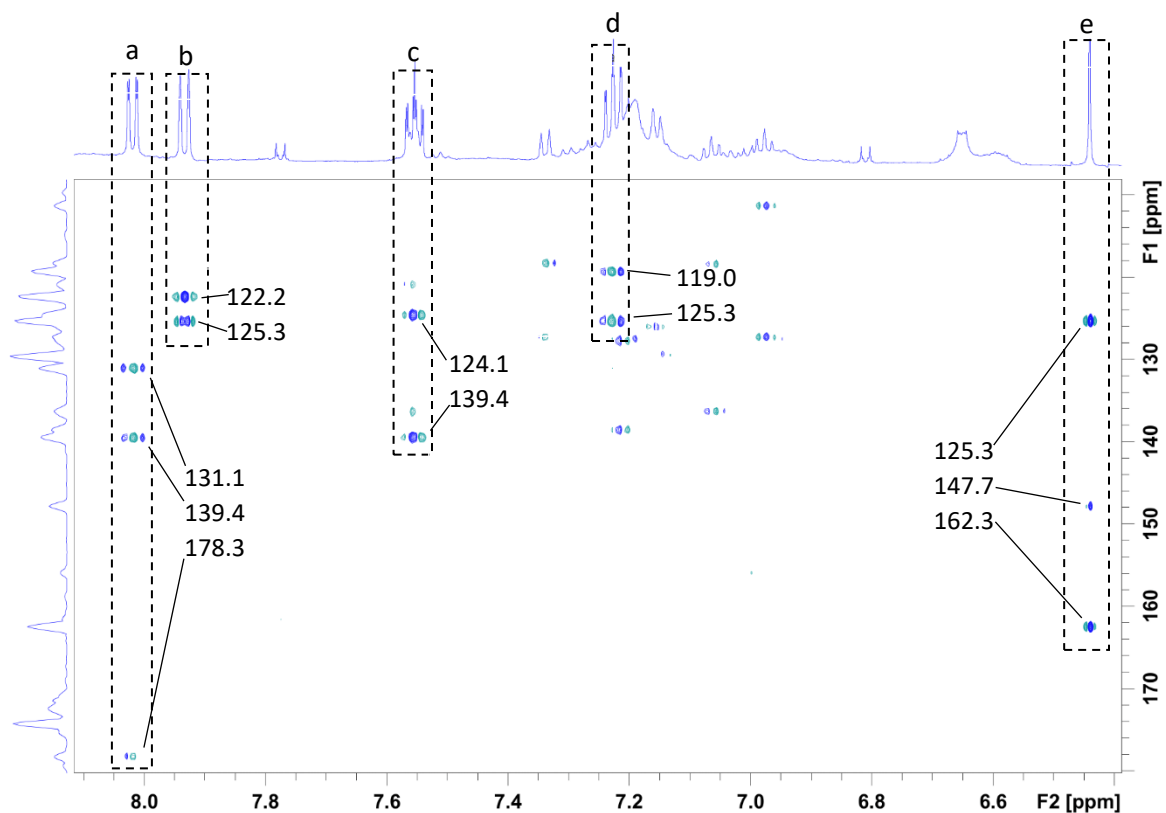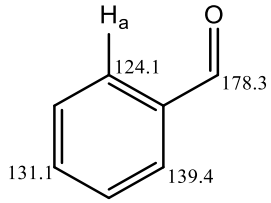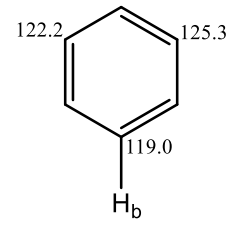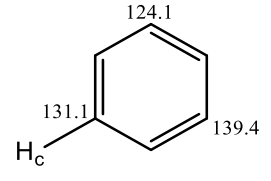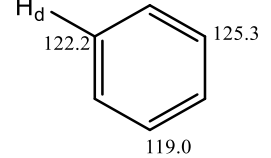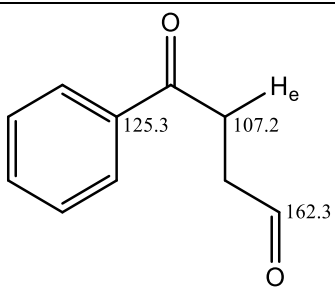
Figure 3.33 – 600 MHz HMBC-spectrum of **F3-2** from **E2,** dissolved in DMSO-d$_6$ and recorded at 298K. Showing the ^{1}H chemical shift between 8.4-6.2 ppm in the x-axis, and the ^{13}C chemical shift between 100-190 ppm in the y-axis. Signals are produced by carbons that have a ^3J coupling to proton (2.7 NMR spectroscopy).

Table 3.8 – Chemical shifts of peaks **a-e**.

Peak	[^1]H NMR [ppm]	HSQC [ppm]	HMBC [ppm]	Chemical shifts assigned to structure
a	8.00	124.1	131.1 139.4 178.3	
b	7.93	119.0	122.2 125.3	
c	7.56	131.1	124.1 139.4	
d	7.23	122.2	119.0 125.3	
e	6.44	107.2	125.3 147.7 162.3	

LC-LR-MS analysis of **F3-2** gave a mass of 189.1 g/mol for the compound with absorption maxima in the 330 nm window. An uneven mass means that the structure most likely contain nitrogen (Donald L. Pavia 2015). The [^1]H NMR-spectrum of **F3-2** from **E2** provides a spectrum with higher resolution. Providing better multiplets for peaks **a-d** than the spectrum of **F3-1** did, figure 3.10. With peak **d** being a triplet instead of a cluster of four proton coupled carbons. Peaks **d** and **c** are triplets since they have two neighbouring protons, while **a** and **b** are doublets

since they have one neighbouring proton (2.7 NMR spectroscopy). The protons spectrum in figure 3.29 also contain an acid peak at 11.28 ppm and nitrogen coupled peaks at 10.87 ppm (Donald L. Pavia 2015). The spectrum also contains other aromatic systems of lower intensity.

An aromatic system with four protons, where the multiplets are two doublets and two triplets leave two R-groups in the ortho positions to each other. Proton **a** is directly coupled to the carbon at 124.1 ppm. The HMBC reveal that **a** couples to a carbon at 131.1 ppm, which is directly coupled to proton **c**. Protons **a** and **c** also couple to a carbon at 139.4 ppm, which is a quaternary carbon. Proton **a** also have a third ^3J coupling to a carbon at 178.3 ppm, a chemical shift that is typical for carbonyls (Donald L. Pavia 2015). HSQC show that **b** is coupled to the carbon at 119.0 ppm and couples to the carbon attached to **d** at 122.2 ppm. The HMBC show that protons **b** and **d** couple to a carbon at 125.3 ppm. Proton **e** is a singlet, is directly coupled to a carbon at 107.2 ppm. A chemical shift that is typical for double bonded carbons. It also has the same integration value as protons **a-d**, suggesting it consists of one proton despite its relative high intensity. HMBC show that it also couples to the carbon at 125.3 ppm along with **d** and **b**, placing next to carbonyl at 178.3 ppm. Proton **e** also have a ^3J coupling to another carbonyl at 162.3 ppm and have a weak signal to a carbon at 147.7 ppm.

NMR analysis of both **F3-1** and **F3-2** have provided a structural foundation of **x**, which might contain an acidic OH-group or a NH-group. The MS analysis of **F3-2** indicates that **x** has a mass of 189.1 g/mol, an uneven mass suggests the possibility of nitrogen being present in the compound. There are several possible compounds that meet these requirements, some are given figure 3.34 below. When compounds **1,3** and **4** in figure 3.34 are generated in Chemdraw they produce ^{13}C chemical shifts that are like those of **x**, with compound **1** being most similar. Structure **1** is a known natural product that is called Kynurenic Acid or Transtorine (Suleiman Al-Khalil 1998). Kynurenic acid is a keto-enol tautomer, where compound **1** is the keto form and compound **2** is the enol form (Pogoda, Janczak et al. 2019).
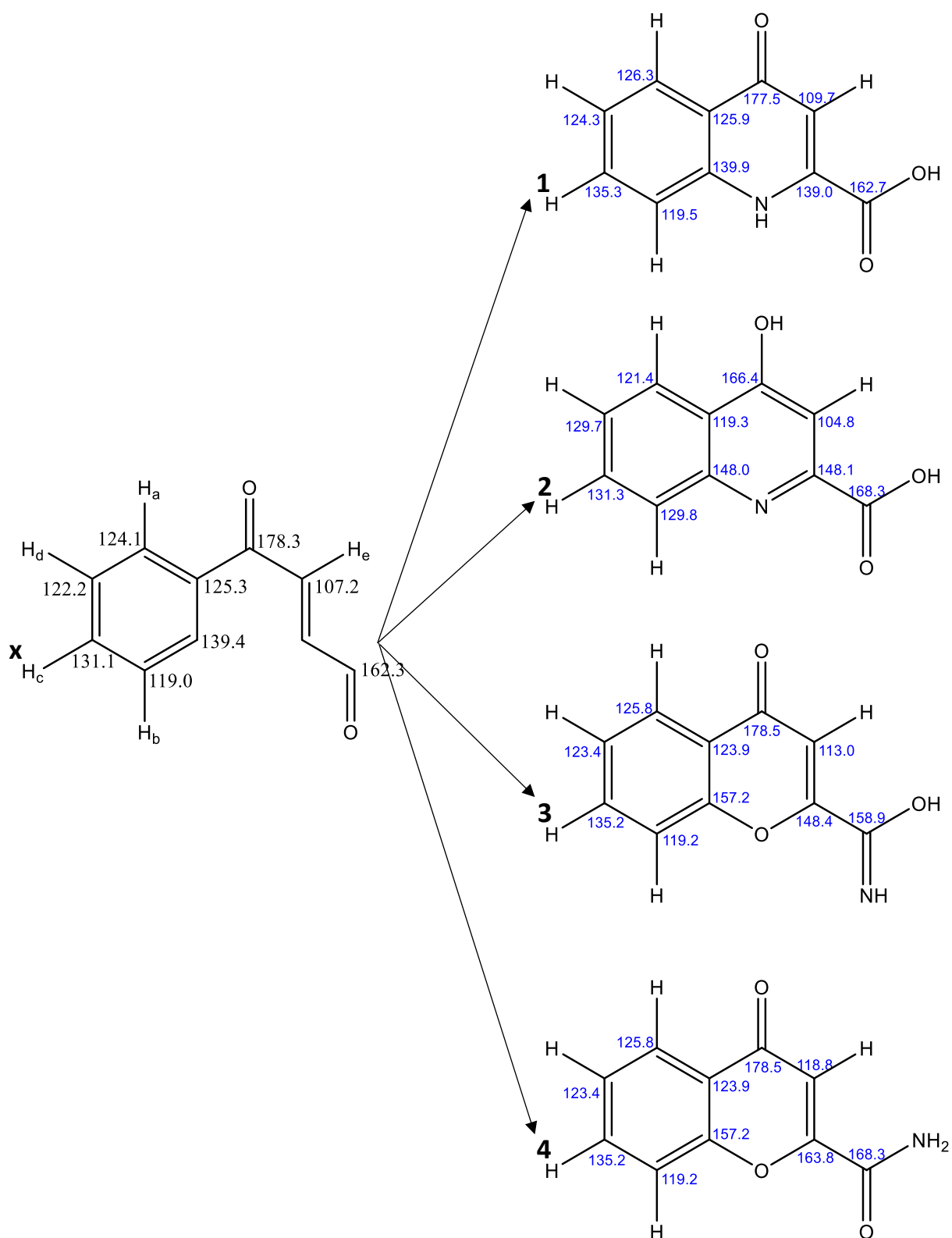
Figure 3.34 – Structural suggestions for **x**, compounds **1-4** all have a mass of 189.17 g/mol. The ^{13}C chemical shifts have been generated by Chemdraw.

The next step in elucidating compound **x** is to fill in the gaps and verify the placement and presence of any OH- or NH-groups. Therefore, a ^{15}N HSQC-spectrum was acquired of **F3-2**, figure 3.35. The spectrum provided three H-N signals at 10.87, 7.20 and 6.66 ppm. Both signals at 7.20 ppm and 6.66 ppm had was coupled to nitrogen atoms with chemical shifts at 108.6 ppm, two N-H signals with the same chemical shift could be an indication of a NH_2-group. A ^{15}N chemical shift of 108.6 ppm does most likely belong to an amine, while a chemical shift of 131.2 ppm is more likely to belong to an amide (Lab 2019).
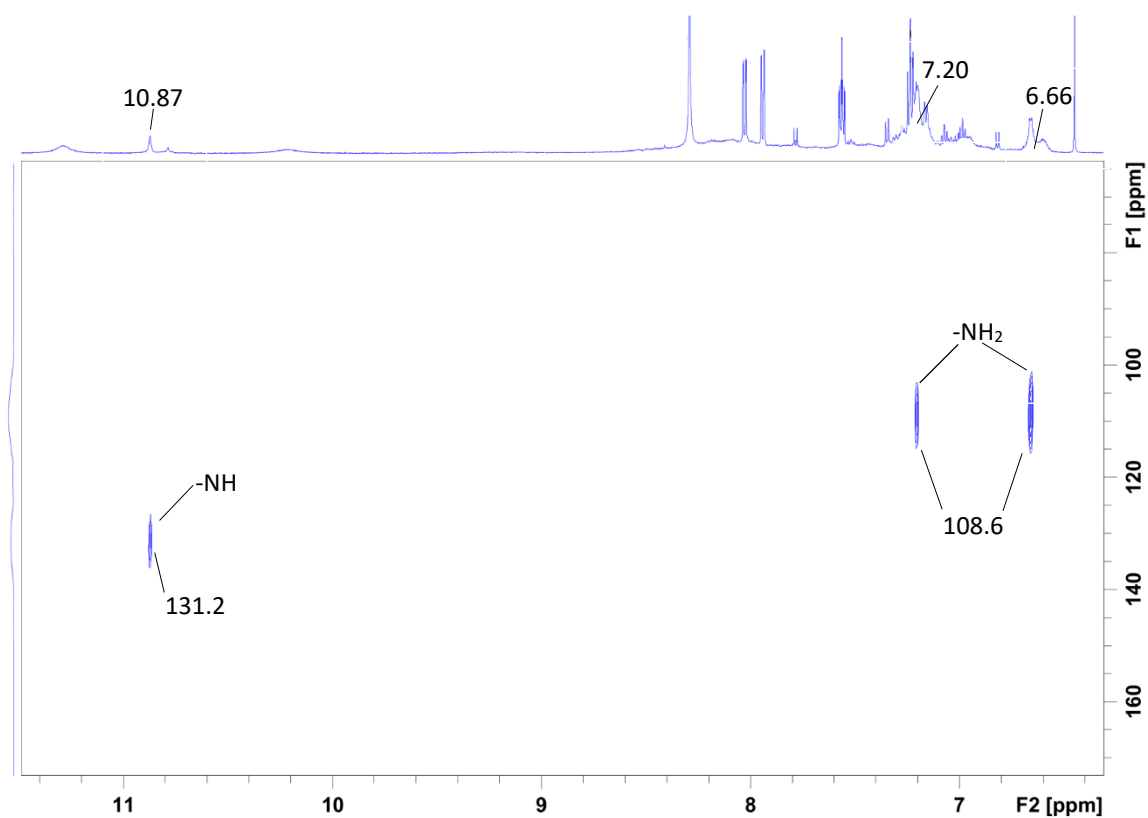
Figure 3.35 – ^{15}N HSQC of **F3-2** from **E2**, dissolved in DMSO-d$_6$ and recorded at 298K.

The HMBC-spectrum of **F3-2** is given in figure 3.36. The H-N peak at 10.87 ppm have ^3J couplings to two carbons at 109.7 ppm and 127.3 ppm. None of these matches the signals that has been linked to **x**, they seem to connect with another low intensity aromatic system in the sample.
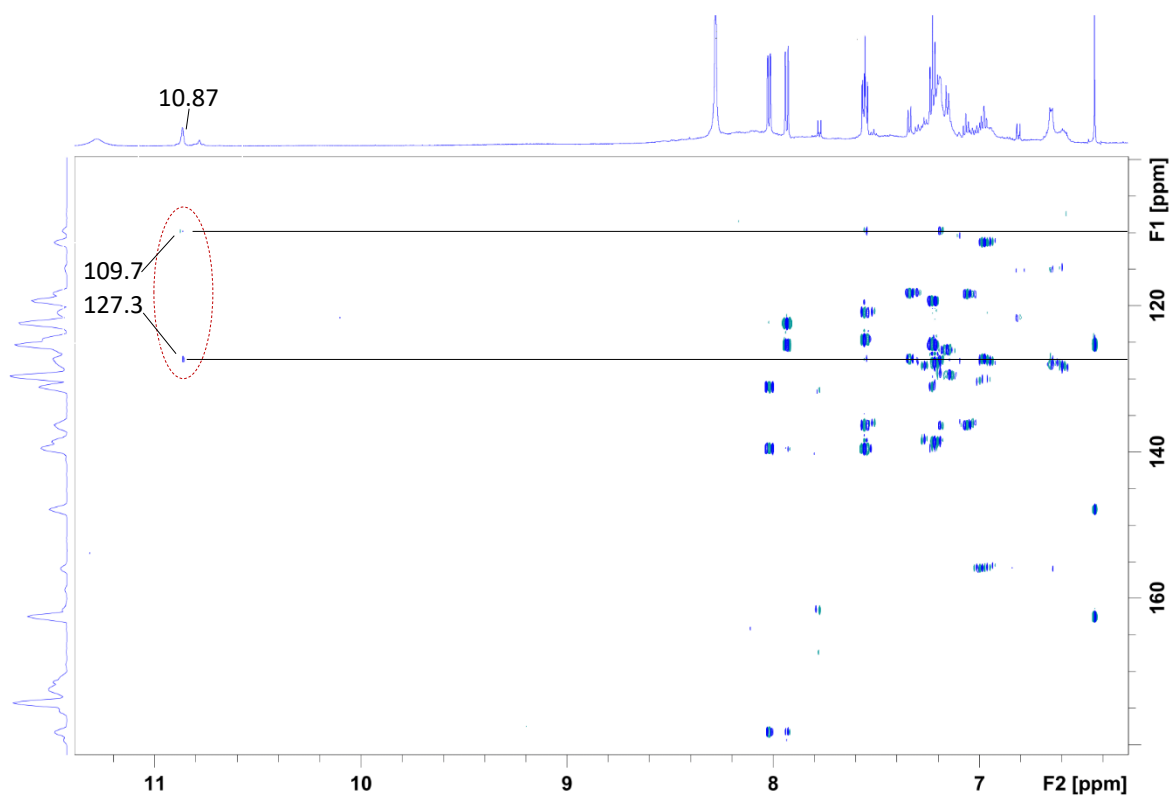
Figure 3.36 – HMBC-spectrum of **F3-2** of **E2**. Emphasising on the ^3J couplings to the H-N signal at 10.87 ppm.

3.3.4 HR-MS and LR-MS Fragmentation

Analysing **F3-2** with low resolution MS suggested a mass of 189.1 g/mol for **x**. since this mass only contains one decimal there is room for uncertainty regarding the chemical composition, as there is a wide range of possible combinations. This problem can be solved with high resolution MS, since it can more accurately depict a mass with four decimals. Analysing **F3-2** with HR-MS resulted in a mass of *m/z* 190.05277, figure 3.37. The top four suggestions are $^{12}C_{13}{}^{1}H_6{}^{14}N_2$, $^{12}C_1{}^{1}H_{10}{}^{14}N_4{}^{16}O_7$, $^{12}C_{10}{}^{1}H_8{}^{14}N_1{}^{16}O_3$ and $^{12}C_3{}^{1}H_{12}{}^{14}N_1{}^{16}O_8$. Based on the NMR analysis there should be at least 10 carbons, this eliminates $^{12}C_3{}^{1}H_{12}{}^{14}N_1{}^{16}O_8$ and $^{12}C_1{}^{1}H_{10}{}^{14}N_4{}^{16}O_7$. Compound **x** also contain two carbonyl groups, ruling out $^{12}C_{13}{}^{1}H_6{}^{14}N_2$ due to a lack of oxygen atoms and leaving $^{12}C_{10}{}^{1}H_8{}^{14}N_1{}^{16}O_3$ to be the most viable suggestion. This chemical formula matches the suggested structures of compound **1-4** in figure 3.34.

Mass	Intensity	Calc. Mass	Mass Difference (ppm)	Possible Formula	^{12}C	^{1}H	^{14}N	^{16}O	Unsaturation Number
190.05277	14731.79	190.05310	-1.72	$^{12}C_{13}{}^{1}H_6{}^{14}N_2$	13	6	2		12.0
		190.05495	-11.45	$^{12}C_1{}^{1}H_{10}{}^{14}N_4{}^{16}O_7$	1	10	4	7	-1.0
		190.05042	12.38	$^{12}C_{10}{}^{1}H_8{}^{14}N_1{}^{16}O_3$	10	8	1	3	7.5
		190.05629	-18.52	$^{12}C_3{}^{1}H_{12}{}^{14}N_1{}^{16}O_8$	3	12	1	8	-1.5
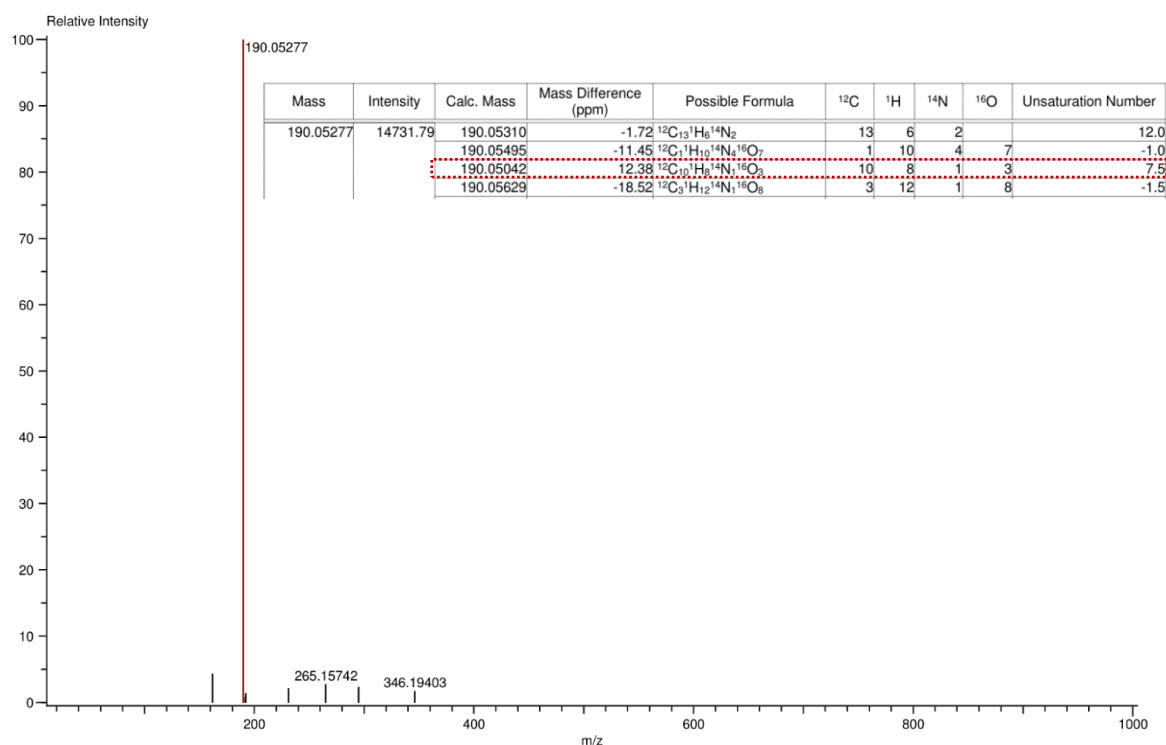
Figure 3.37 – High resolution mass spectrum of the *m/z* 190 peak with UV-VIS absorbance in the 330 nm window. With table of estimated elemental compositions for the compound with mass to charge ratio 190.05277, and the most fitting composition has been highlighted in red.
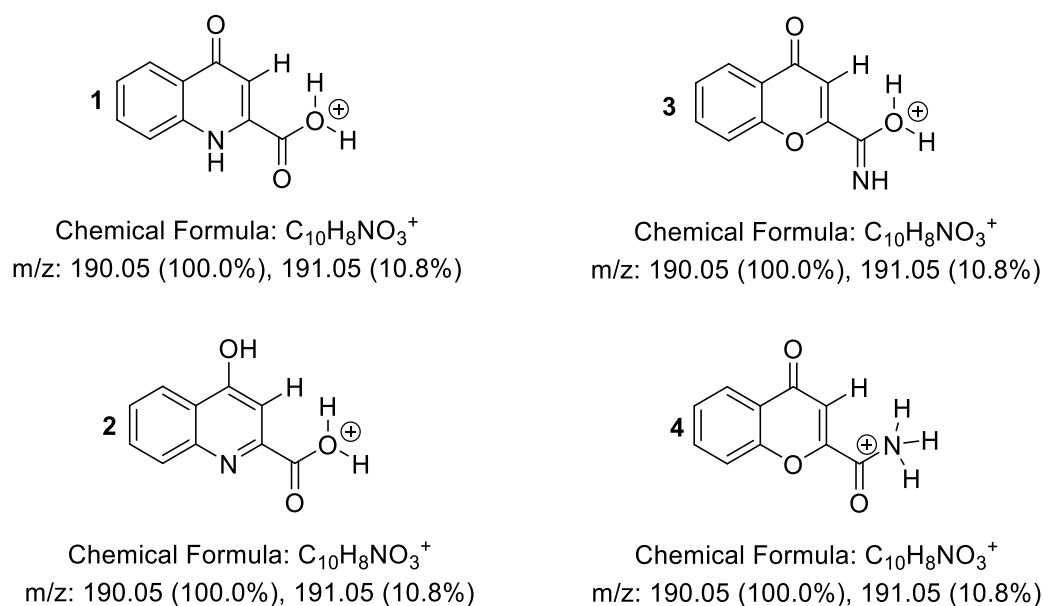
Figure 3.38 – Possible structures with elemental composition $^{12}C_{10}{}^{1}H_8{}^{14}N_1{}^{16}O_3$, including mass to charge ratio.

The HR-MS suggested that $^{12}C_{10}{}^{1}H_8{}^{14}N_1{}^{16}O_3$ is chemical formula for compound **x**, which also matches the suggested structures compound **1-4**. The analysis done so far has not yet been able to pinpoint the position of the nitrogen atom. Given the possible heterocyclic structure of **x**, it should be possible to use fragmentation to break off either an acid group or amide group. If an acidic group is fragmented from the product ion it would result in a loss of *m/z* 45, and the nitrogen would be a part of the heterocyclic system. If the nitrogen is part of an amide or imidic acid, it would result in a loss of *m/z* 44.
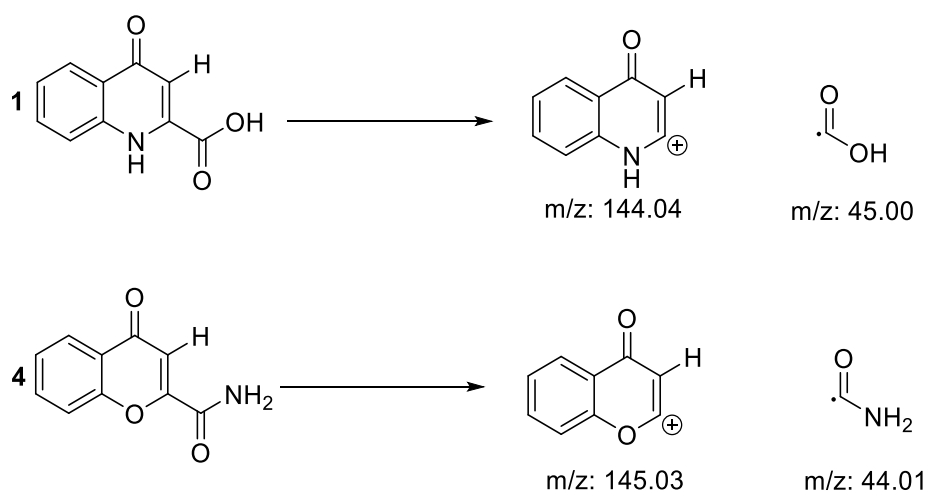
Figure 3.39 – Possible fragmentations of compounds **1** and **4** with loss of an acid or an amine.

The fragmentation of **F3-2** was done with LR-LC-MS. First, a TIC of the sample was acquired, followed by selecting *m/z* 190 as product ion. The TIC had a noisy baseline with no defined peaks, but the product ion gave a strong signal.
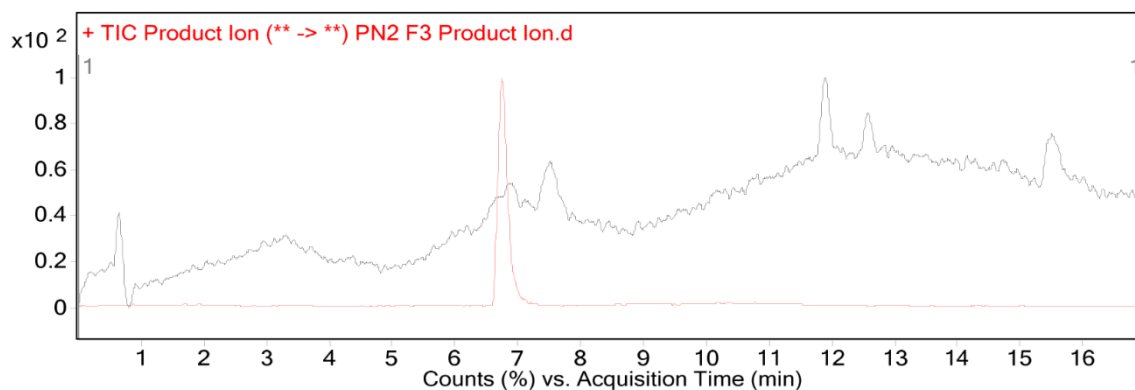
Figure 3.40 – TIC scan (black line) of **F3-2** overlaid with product ion (red line) of *m/z* 190.

Product ion scan (PIS) was used to fragment the *m/z* 190 precursor ion by applying a charge of 35 eV in the collision activation chamber. Resulting in the product ion spectrum in figure 3.42, containing fragments *m/z* 144.1, *m/z* 116.0 and *m/z* 89.1. The heaviest fragment is *m/z* 144.1 and is a loss of *m/z* 45, which supports the NMR observation that compound **x** contains an acid group. Between the *m/z* 144.1 and *m/z* 116.1 fragments there is a mass difference of 28, a loss

that characteristic for CO and indicates that the cyclic keto group is cleaved off. From *m/z* 116.0 down to *m/z* 89.1 there is a difference of 27, a loss that is typical for HCN. The loss of HCN confirms that position of the nitrogen atom.

$-H_2O/-18$
$-CO/-28$ $-CO/-28$ $-HCN/-27$

[M+H] $\longrightarrow$ *m/z* 144.1 $\longrightarrow$ *m/z* 116.0 $\longrightarrow$ *m/z* 89.1
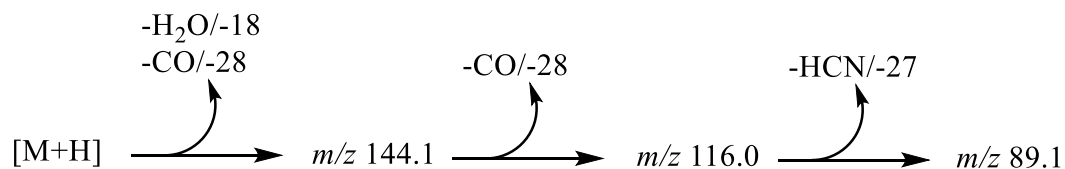
Figure 3.41 – The mass loss scheme from product ion to fragments.
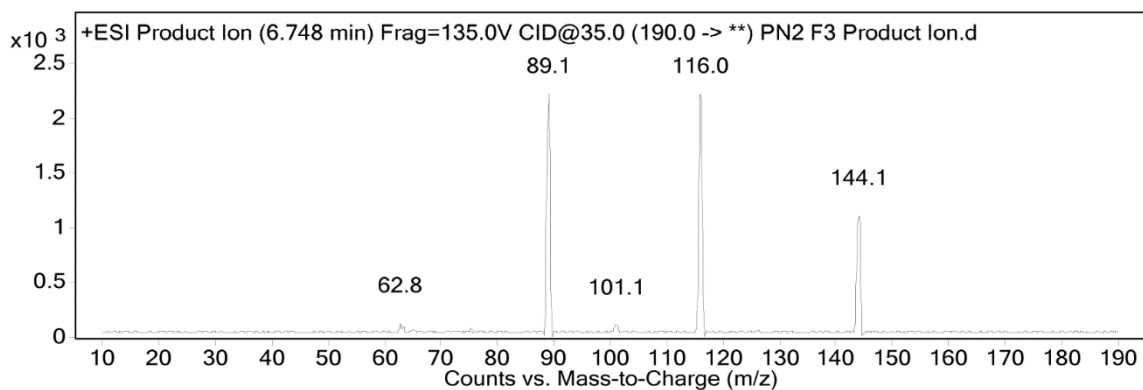
Figure 3.42 – Fragmentation of the *m/z* 190 product ion.
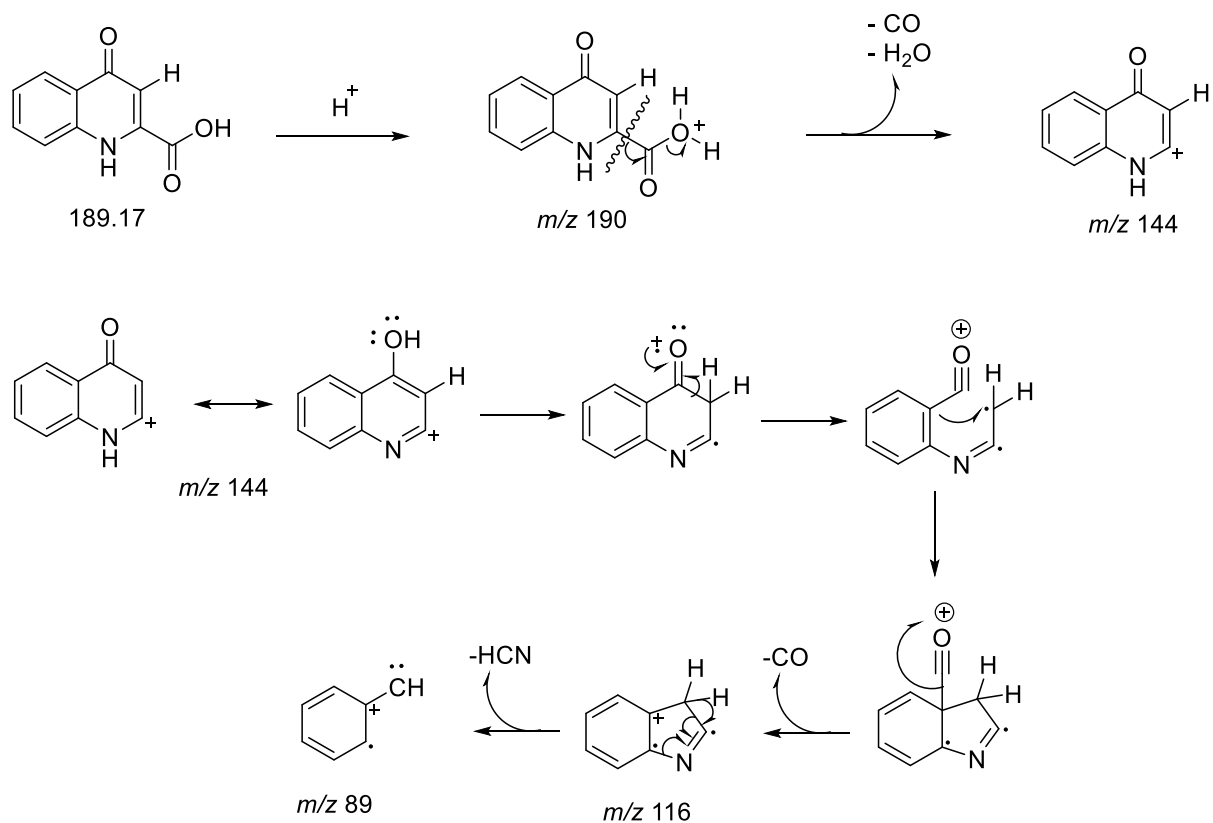
Figure 3.43 – Suggested fragmentation mechanism of the *m/z* 190 product ion. For this mechanism to work the *m/z* 144 ion would have to be in the enol-form, and the charge would have to redistribute to the oxygen atom.

UV-VIS spectroscopy was applied to the PIS mode to verify that the selected ion was compound **x**. The UV-VIS spectrum for the selected ion in the 330 nm window is given in figure 3.44. Containing a weak but identical absorption pattern to those recorded of compound **x** in HPLC analysis, figures 3.4 and 3.20.
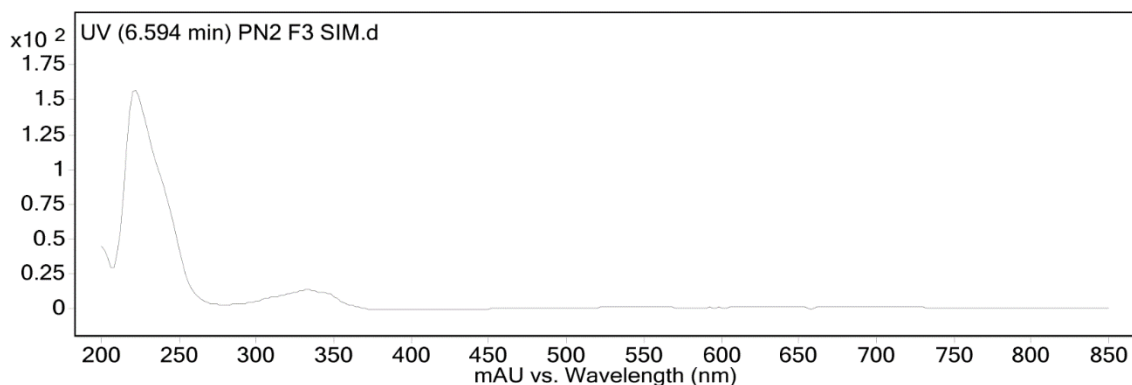
Figure 3.44 – UV-VIS spectrum in the 330 nm window of the *m/z* 190 ion.

The fragmentation pattern confirms that compound **x** is kynurenic acid. The known natural product is a keto-enol tautomer, meaning it exist in a chemical equilibrium between the keto form (ketone or aldehyde) and enol form (alcohol) (Pogoda, Janczak et al. 2019). Most of the research seems to be done on the enol form. Where both an absorption peak around 330 nm and the fragments *m/z* 144.1, *m/z* 116.0 and *m/z* 89.1 has been reported (Chan and Cai 2008, Zelentsova, Sherin et al. 2013).
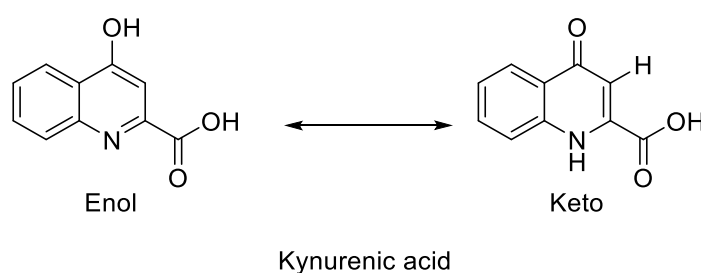
Figure 3.43 – Kynurenic acid in enol form and keto form.

Chapter 4

Conclusion and further work

4.1 Kynurenic acid

Elucidation of compound **x** with NMR and MS it suggests that **x** is kynurenic acid. Kynurenic acid is a quinolone alkaloid which is derived from tryptophan and can be found in animals and plants, in humans kynurenic acid is part of the kynurenine pathway (Suleiman Al-Khalil 1998, Liu, Ding et al. 2018). Studies suggest that kynurenic acid have a neuroprotective function in our body, and there seem to be a correlation between having depression and a low concentration of kynurenic acid in the body. Meaning it could potentially be used as a biomarker for diagnosing depression. Other studies suggest that the compound could also be used as a biomarker against schizophrenia, as elevated levels of kynurenic acid have been reported in patients diagnosed with schizophrenia (Plitman, Iwata et al. 2017, Friendshuh, Pocivavsek et al. 2020). Another study featuring mice that was injected with neurotoxic extract from poisonous mussels, kynurenic acid proved to be a powerful antidote (Pinsky, Giavim et al. 1989). The compound is most likely produced by the symbiotic microorganisms that resides in the sponge and has been isolated in other sponge associated microorganisms before (Ibrahim, Attia et al. 2018). Kynurenic acid was isolated from the bacteria *Nocardiopsis* sp. that had been cultivated from the sponge *Callyspongia* sp. This was the first time kynurenic acid had been isolated from microbial origins, and as far as we know the current isolation and identification might be the second one derived from sponges. Other compounds that can be linked kynurenine pathway has also been isolated from marine sponges (Feng, Bowden et al. 2012). Ianthellamide A was isolated from the sponge called e *Ianthella quadrangulate*, a selective inhibitor of kynurenine-3-hydroxylase. By inhibiting one of the pathways in the kynurenine pathway it would in turn increase the production of kynurenic acid. It is safe to assume that the symbiotic microbes that resides on *P. normani* produce kynurenic acid as a protective agent, possibly against the sponge itself. Since it has been described to have barren surroundings with no

growth, a possible indication that it is a sponge that promotes a "hostile" environment. Or it could be to protect themselves and the host sponge against neurotoxins from competing species.

4.2 – Further work

Before the experimental part of this thesis was stunted by the Covid-19 lockdown the process of isolating other compounds with UV-VIS absorption was in motion. Targeting the peaks at 8.33 min, 10.63 min and 18.80 in the 280 nm window, figure 3.3. The NMR spectra of **F3-2** also contained traces of another aromatic compound containing nitrogen atoms, and the peak at 18.80 min was also present in HPLC chromatogram of **F3-2**. Meaning there could be a possible correlation between the two. Several of the HMBC spectra also contain coupling signals between aliphatic hydrogens and carbonyl related carbons, possibly belonging to some fatty acids.

There are also some unanswered questions regarding the composition of the white crystalline precipitate that occurred after the liquid-liquid extraction. Another possible lead is figuring out what compound or compounds is responsible for the orange colour. Experimenting with other extraction solvents is also an option, we already know that extracting with acetone instead of methanol yielded different results.

References

Artsdatabanken. (2015). "Pachymatisma Normani sollas, 1880." Retrieved 18.02, 2020, from https://artsdatabanken.no/Taxon/Pachymatisma%20normani/120418.

Becerro, M. A., R. W. Thacker, X. Turon, M. J. Uriz and V. J. Paul (2003). "Biogeography of sponge chemical ecology: comparisons of tropical and temperate defenses." Oecologia **135**(1): 91-101.

Bennett, C. F., S. Mong, M. A. Clarke, L. I. Kruse and S. T. Crooke (1987). "Differential effects of manoalide on secreted and intracellular phospholipases." Biochemical Pharmacology **36**(5): 733-740.

Blunt, J. W., B. R. Copp, M. H. G. Munro, P. T. Northcote and M. R. Prinsep (2005). "Marine natural products." Natural Product Reports **22**(1): 15-61.

Chan, W. and Z. Cai (2008). "Aristolochic acid induced changes in the metabolic profile of rat urine." Journal of Pharmaceutical and Biomedical Analysis **46**(4): 757-762.

Civjan, N. (2012). Alkaloids. Hoboken, NJ, USA, Hoboken, NJ, USA: John Wiley & Sons, Inc.**:** 209-237.

Crdenas, P., J. Xavier, O. S. Tendal, C. Schander and H. T. Rapp (2007). "Redescription and resurrection of Pachymatisma normani (Demospongiae: Geodiidae), with remarks on the genus Pachymatisma." J. Mar. Biol. Ass. **87**(6): 1511-1525.

Cutignano, A., G. Bifulco, I. Bruno, A. Casapullo, L. Gomez-Paloma and R. Riccio (2000). "Dragmacidin F: A New Antiviral Bromoindole Alkaloid from the Mediterranean Sponge Halicortex sp." Tetrahedron **56**(23): 3743-3748.

de Silva, E. D. and P. J. Scheuer (1980). "Manoalide, an antibiotic sesterterpenoid from the marine sponge [formula omitted] (polejaeff)." Tetrahedron Letters **21**(17): 1611-1614.

Dias, D. A., S. Urban and U. Roessner (2012). "A historical overview of natural products in drug discovery." Metabolites **2**(2): 303.

Donald L. Pavia, G. M. L., George S. Kriz and James R. Vyvyan (2015). Introduction To Spectroscopy. Standford, Cengage Learning.

Donald L. Pavia, G. M. L., George S. Kriz and James R. Vyvyan (2015). Introduction To Spectroscopy. Standford, Cengage Learning.

Donald L. Pavia, G. M. L., George S. Kriz and James R. Vyvyan (2015). Introduction To Spectroscopy. Standford, Cengage Learning.

Ernesto Fattorusso, W. H. G. a. O. T.-S. (2012). Handbook of Marine Natural Products. Dordrecht, Heidelberg, New york, London, Springer Science + Buisness Media.

Fattorusso, E., W. H. Gerwick and O. Taglialatela-Scafati (2012). Handbook of Marine Natural Products. Dordrecht, Heidelberg, New york, London, Springer Science + Buisness Media.

Feng, Y., B. F. Bowden and V. Kapoor (2012). "Ianthellamide A, a selective kynurenine-3-hydroxylase inhibitor from the Australian marine sponge Ianthella quadrangulata." Bioorg Med Chem Lett **22**(10): 3398-3401.

Feuda, R., M. Dohrmann, W. Pett, H. Philippe, O. Rota-Stabelli, N. Lartillot, G. Worheide and D. Pisani (2017). "Improved Modeling of Compositional Heterogeneity Supports Sponges as Sister to All Other Animals." Curr Biol **27**(24): 3864-3870 e3864.

Friebolin, H. (2011). Basic One- and Two-dimensional NMR Spectroscopy. Darmstadt, Wiley-VCH.

Friendshuh, C. R., A. Pocivavsek, H. Demyonovich, K. M. Rodriguez, D. Cihakova, M. V. Talor, C. M. Richardson, G. Vyas, H. A. Adams, A. B. Baratta, A. Fasano, N. Cascella, S. Feldman, F. Liu, M. Sayer, M. M. Powell, H. J. Wehring, R. W. Buchanan, W. T. Carpenter, W. W. Eaton and D. L. Kelly (2020). "The Effects of a Gluten-Free Diet on Immune Markers and Kynurenic Acid Pathway Metabolites in Patients With Schizophrenia Positive for Antigliadin Antibodies Immunoglobulin G." Journal of clinical psychopharmacology **40**(3): 317.

Gazave, E., P. Lapébie, A. Ereskovsky, J. Vacelet, E. Renard, P. Cárdenas and C. Borchiellini (2012). "No longer Demospongiae: Homoscleromorpha formal nomination as a fourth class of Porifera." The International Journal of Aquatic Sciences **687**(1): 3-10.

Giannini, C., C. Debitus, I. Posadas, M. Payá and M. V. D'auria (2000). "Dysidotronic acid, a new and selective human phospholipase A 2 inhibitor from the sponge Dysidea sp." Tetrahedron Letters **41**(17): 3257-3260.

Green, G. (1977). "Ecology of toxicity in marine sponges." International Journal on Life in Oceans and Coastal Waters **40**(3): 207-215.

Gunasekera, S. P., S. Cranick and R. E. Longley (1989). "Immunosuppressive compounds from a deep water marine sponge, Agelas flabelliformis." Journal of natural products **52**(4): 757.

Gutzeit, H. O. and J. Ludwig-Müller (2014). Plant natural products : synthesis, biological functions and practical applications. Weinheim, Germany, Wiley-VCH**:** 13-16.

Halim, H., P. Chunhacha, K. Suwanborirux and P. Chanvorachote (2011). "Anticancer and antimetastatic activities of Renieramycin M, a marine tetrahydroisoquinoline alkaloid, in human non-small cell lung cancer cells." Anticancer research **31**(1): 193.

Harris, D. C. (2016). Quantitative Chemical Analysis. United States of America, W. H. Freeman and Company.

Hoffmann, F., R. Radax, D. Woebken, M. Holtappels, G. Lavik, H. T. Rapp, M. L. Schläppy, C. Schleper and M. M. M. Kuypers (2009). "Complex nitrogen cycling in the sponge Geodia barretti." Environmental Microbiology **11**(9): 2228-2243.

Hågvar, E. B. (1998). Det zoologiske mangfoldet : dyregruppenes systematikk, bygning og levevis. Oslo, Universitetsforl.

Ibrahim, A. H., E. Z. Attia, D. Hajjar, M. A. Anany, S. Y. Desoukey, M. A. Fouad, M. S. Kamel, H. Wajant, T. A. M. Gulder and U. R. Abdelmohsen (2018). "New Cytotoxic Cyclic Peptide from the Marine Sponge-Associated Nocardiopsis sp. UR67." Mar Drugs **16**(9).

Jerry R. Mohrig, D. G. A., Gretchen E. Hofmeister, Paul F. Schatz and Christina Noring Hammond (2014). Laboratory Techniques in Organic Chemistry. United States of America, W. H. Freeman and Company.

Kober, K. M. and S. A. Nichols (2007). "On the phylogenetic relationships of hadromerid and poecilosclerid sponges." J. Mar. Biol. Ass. **87**(6): 1585-1598.

Koskinen, A. M. P. (2012). Alkaloids. Chichester, UK, Chichester, UK: John Wiley & Sons, Ltd**:** 257-287.

Lab, N. (2019). "Nitrogen NMR." from http://chem.ch.huji.ac.il/nmr/techniques/1d/row2/n.html.

Laport, M., O. C. S. Santos and G. Muricy (2009). "Marine Sponges: Potential Sources of New Antimicrobial Drugs." Current pharmaceutical biotechnology **10**: 86-105.

Liu, H., L. Ding, H. Zhang, D. Mellor, H. Wu, D. Zhao, C. Wu, Z. Lin, J. Yuan and D. Peng (2018). "The Metabolic Factor Kynurenic Acid of Kynurenine Pathway Predicts Major Depressive Disorder.(Report)." Frontiers in Psychiatry **9**.

Mehbub, M. F., J. Lei, C. Franco and W. Zhang (2014). "Marine sponge derived natural products between 2001 and 2010: trends and opportunities for discovery of bioactives." Mar Drugs **12**(8): 4539-4577.

Miller, J. M. (2005). Chromatography Concepts and Contrasts. Hoboken, New Jersey, John Wiley & Sons.

NationalCancerInstitute. (2009). "Success Story: Halichondrin B (NSC 609395) E7389 (NSC 707389)." Retrieved 14.09, 2018, from https://web.archive.org/web/20090710205200/http://dtp.nci.nih.gov/timeline/noflash/success_stories/S4_halichondrinB.htm.

Osinga, R., J. Tramper and R. Wijffels (1999). "Cultivation of Marine Sponges." Marine Biotechnology **1**: 509-532.

Paterson, I. and E. A. Anderson (2005). "Chemistry. The renaissance of natural products as drug candidates." Science (New York, N.Y.) **310**(5747): 451.

Paul, V. J., R. Ritson-williams and K. Sharp (2011). "Marine chemical ecology in benthic environments." Nat. Prod. Rep. **28**(2): 345-387.

Perdikaris, S., T. Vlachogianni and A. Valavanidis (2013). "Bioactive Natural Substances from Marine Sponges: New Developments and Prospects for Future Pharmaceuticals." Natural Products Chemistry & Research **1**.

Pérez-López, P., E. Ternon, S. González-García, G. Genta-Jouve, G. Feijoo, O. P. Thomas and M. T. Moreira (2014). "Environmental solutions for the sustainable production of bioactive natural products from the marine sponge Crambe crambe." Science of the Total Environment **475**: 71-82.

Pinsky, C., G. B. Giavim and R. Bose (1989). "Kynurenic acid protects against neurotoxicity and lethality of toxic extracts from contaminated atlantic coast mussels." Progress in Neuropsychopharmacology & Biological Psychiatry **13**(3-4): 595-598.

Plitman, E., Y. Iwata, F. Caravaggio, S. Nakajima, J. K. Chung, P. Gerretsen, J. Kim, H. Takeuchi, M. M. Chakravarty, G. Remington and A. Graff-Guerrero (2017). "Kynurenic Acid in Schizophrenia: A Systematic Review and Meta-analysis." Schizophrenia Bulletin **43**(4): 764-777.

Pogoda, D., J. Janczak, S. Pawlak, M. Zaworotko and V. Videnova - Adrabinska (2019). "Tautomeric polymorphism of the neuroactive inhibitor kynurenic acid." Acta Crystallographica Section C **75**(6): 793-805.

Proksch, P. (1994). "Defensive roles for secondary metabolites from marine sponges and sponge-feeding nudibranchs." Toxicon **32**(6): 639-655.

Ruppert, E. E., R. S. Fox and R. D. Barnes (2004). Invertebrate zoology : a functional evolutionary approach. Belmont, Calif, Thomson - Brooks/Cole.

Sagar, S., M. Kaur and K. Minneman (2010). "Antiviral Lead Compounds from Marine Sponges." Marine Drugs **8**(10): 2619-2638.

Shen, S., D. Liu, C. Wei, P. Proksch and W. Lin (2012). "Purpuroines A–J, halogenated alkaloids from the sponge Iotrochota purpurea with antibiotic activity and regulation of tyrosine kinases." Bioorganic & Medicinal Chemistry **20**(24): 6924-6928.

Singleton, W. (2018). Invertebrate Reproduction and Development, EDTECH.

Sipkema, D., M. Franssen, R. Osinga, J. Tramper and R. Wijffels (2005). "Marine Sponges as Pharmacy." Marine Biotechnology **7**(3): 142-162.

Smith, R. M. (2005). Understanding Mass Spectra: A Basic Approach. Hoboken, NJ, USA, Hoboken, NJ, USA: John Wiley & Sons, Inc.

Suleiman Al-Khalil, A. A., Dawud El-Eisawi and Asfar Al-Shibib (1998). "Transtorine: A new quinoline alkaloid from Ephedra transitoria." Journal of Natural Products **61**(2): 262-263.

Suwannarach, N., J. Kumla, K. Sujarit, T. Pattananandecha and S. Lumyong (2020). "Natural Bioactive Compounds from Fungi as Potential Candidates for Protease Inhibitors and Immunomodulators to Apply for Coronaviruses." Molecules **25**(8): 1800.

Sømme, L. S. (2018). "Svamper." Retrieved 22.05, 2019, from https://snl.no/svamper.

Tan, P., F. W. Luscinskas and S. Homer-Vanniasinkam (1999). "Cellular and Molecular Mechanisms of Inflammation and Thrombosis." European Journal of Vascular & Endovascular Surgery **17**(5): 373-389.

Taylor, M. W., R. Radax, D. Steger and M. Wagner (2007). "Sponge-Associated Microorganisms: Evolution, Ecology, and Biotechnological Potential." Microbiology and Molecular Biology Reviews **71**(2): 295.

Thompson, J., R. Walker and D. Faulkner (1985). "Screening and bioassays for biologically-active substances from forty marine sponge species from San Diego, California, USA." International Journal on Life in Oceans and Coastal Waters **88**(1): 11-21.

Thoms, C. and P. Schupp (2007). "Chemical defense strategies in sponges: A review." Porifera Research: Biodiversity, Innovation and Sustainability: 627-637.

Uria, A. and J. Piel (2009). "Cultivation-independent approaches to investigate the chemistry of marine symbiotic bacteria." Fundamentals and Perspectives of Natural Products Research **8**(2): 401-414.

Voultsiadou, E. (2007). "Sponges: an historical survey of their knowledge in Greek antiquity." J. Mar. Biol. Ass. **87**(6): 1757-1763.

Warabi, K., W. T. Zimmerman, J. Shen, A. Gauthier, M. Robertson, B. B. Finlay, R. v. Soest and R. J. Andersen (2004). "Pachymoside A − A novel glycolipid isolated from the marine sponge Pachymatisma johnstonia." Canadian Journal of Chemistry **82**(2): 102-112.

Yong-Cheng, L., C. Sheng-Ping, Z. Xun, W. Jue-Heng, L. Xiu-Jian, S. Zhi-Gang, S. Li, Y. Jie and H. Gu-Ping (2011). "Statistical Research on Marine Natural Products Based on Data Obtained between 1985 and 2008." Marine Drugs **9**(4): 514-525.

Yoo Kyung Lee, J.-H. L., and Hong Kum Lee (2001). "Microbial Symbiosis in Marine Sponges." The Journal of Microbiology **Vol. 39, No. 4**(December): 254-264.

Zelentsova, E. A., P. S. Sherin, O. A. Snytnikova, R. Kaptein, E. Vauthey and Y. P. Tsentalovich (2013). "Photochemistry of aqueous solutions of kynurenic acid and kynurenine yellow." Photochem. Photobiol. Sci. **12**(3): 546-558.

Appendix A - Acquisition parameters of NMR experiments

^{1}H- 600 MHz

Current Data Parameters
NAME   Nov15-2019-larsh
EXPNO   10
PROCNO   1

F2 - Acquisition Parameters
Date_   20191115
Time   14.12 h
INSTRUM CAB AV4 600 MHZ BASIC
PROBHD Z151284_0002 (
PULPROG   zg30
TD   65536
SOLVENT   DMSO
NS   64
DS   2
SWH   11904.762 Hz
FIDRES   0.363304 Hz
AQ   2.7525120 sec
RG   101
DW   42.000 usec
DE   43.01 usec
TE   298.0 K
D1   1.00000000 sec
TD0   1
SFO1   600.1337058 MHz
NUC1   1H
P0   2.63 usec
P1   7.88 usec
PLW1   6.40450001 W

F2 - Processing parameters
SI   65536
SF   600.1300048 MHz
WDW   EM
SSB   0
LB   0.30 Hz
GB   0
PC   1.00

COSY 600 MHz

Current Data Parameters
NAME   Nov15-2019-larsh
EXPNO   11
PROCNO   1

F2 - Acquisition Parameters
Date_   20191115
Time   14.51 h
INSTRUM CAB AV4 600 MHZ BASIC
PROBHD Z151284_0002 (
PULPROG   cosygpmfphpp
TD   2048
SOLVENT   DMSO
NS   4
DS   16
SWH   7812.500 Hz
FIDRES   7.629395 Hz
AQ   0.1310720 sec
RG   101
DW   64.000 usec
DE   40.00 usec
TE   298.0 K
D0   0.00005397 sec
D1   2.00000000 sec
D11   0.03000000 sec
D12   0.00002000 sec
D16   0.00020000 sec
IN0   0.00012800 sec
TDav   1
SFO1   600.1333007 MHz
NUC1   1H
P1   7.88 usec
P2   15.76 usec
P17   2500.00 usec
PLW1   6.40450001 W
PLW10   0.63655001 W
GPNAM[1]   SMSQ10.100
GPZ1   10.00 %
GPNAM[2]   SMSQ10.100
GPZ2   20.00 %
P16   1000.00 usec

F1 - Acquisition parameters
TD   256
SFO1   600.1333 MHz
FIDRES   61.035156 Hz
SW   13.018 ppm
FnMODE   States-TPPI

Figure A1 – Acquisition parameters for ^{1}H (left) and COSY (right) experiments. Every fraction was recorded using the same parameters for the different experiments.

HSQC 600 MHz

Current Data Parameters
NAME   Nov15-2019-larsh
EXPNO   12
PROCNO   1

F2 - Acquisition Parameters
Date_   20191115
Time   15.21 h
INSTRUM CAB AV4 600 MHZ BASIC
PROBHD Z151284_0002 (
PULPROG hsqcedetgpsisp2.3
TD   2048
SOLVENT   DMSO
NS   4
DS   32
SWH   7812.500 Hz
FIDRES   7.629395 Hz
AQ   0.1310720 sec
RG   101
DW   64.000 usec
DE   40.00 usec
TE   298.0 K
CNST2   145.0000000
CNST17   -0.5000000
D0   0.00000300 sec
D1   1.50000000 sec
D4   0.00172414 sec
D11   0.03000000 sec
D16   0.00020000 sec
D21   0.00344800 sec
D24   0.00086200 sec
IN0   0.00002009 sec
TDav   1
SFO1   600.1328206 MHz
NUC1   1H
P1   7.89 usec
P2   15.78 usec
P28   0 usec
PLW1   6.40450001 W
SFO2   150.9141262 MHz
NUC2   13C
CPDPRG[2   garp4
P3   12.00 usec
P14   500.00 usec
P24   2000.00 usec
P31   1730.00 usec
PCPD2   60.00 usec
PLW0   0 W
PLW2   86.90000153 W
PLW12   3.47600007 W
SPNAM[3] Crp60,0.5,20.1
SPOAL3   0.500
SPOFFS3 0 Hz
SPW3   19.11899948 W
SPNAM[7] Crp60comp.4
SPOAL7   0.500
SPOFFS7 0 Hz
SPW7   19.11899948 W
SPNAM[18 Crp60_xfilt.2
SPOAL18   0.500
SPOFFS18 0 Hz
SPW18   5.52580023 W
GPNAM[1] SMSQ10.100
GPZ1   80.00 %
GPNAM[2] SMSQ10.100
GPZ2   20.10 %
GPNAM[3] SMSQ10.100
GPZ3   11.00 %
GPNAM[4] SMSQ10.100
GPZ4   -5.00 %
P16   1000.00 usec
P19   600.00 usec

F1 - Acquisition parameters
TD   256
SFO1   150.9141 MHz
FIDRES   194.522247 Hz
SW   164.987 ppm
FnMODE Echo-Antiecho

HMBC 600 MHz

Current Data Parameters
NAME   Nov15-2019-larsh
EXPNO   13
PROCNO   1

F2 - Acquisition Parameters
Date_   20191116
Time   2.47 h
INSTRUM CAB AV4 600 MHZ BASIC
PROBHD Z151284_0002 (
PULPROG hmbcetgpl3nd
TD   4096
SOLVENT   DMSO
NS   64
DS   16
SWH   7812.500 Hz
FIDRES   3.814697 Hz
AQ   0.2621440 sec
RG   101
DW   64.000 usec
DE   40.00 usec
TE   298.0 K
CNST6   120.0000000
CNST7   170.0000000
CNST13   8.0000000
D0   0.00000300 sec
D1   2.00000000 sec
D6   0.06250000 sec
D16   0.00020000 sec
IN0   0.00001506 sec
TDav   1
SFO1   600.1333007 MHz
NUC1   1H
P1   7.89 usec
P2   15.78 usec
PLW1   6.40450001 W
SFO2   150.9178988 MHz
NUC2   13C
P3   12.00 usec
P24   2000.00 usec
PLW2   86.90000153 W
SPNAM[7] Crp60comp.4
SPOAL7   0.500
SPOFFS7 0 Hz
SPW7   19.11899948 W
GPNAM[1] SMSQ10.100
GPZ1   80.00 %
GPNAM[3] SMSQ10.100
GPZ3   14.00 %
GPNAM[4] SMSQ10.100
GPZ4   -8.00 %
GPNAM[5] SMSQ10.100
GPZ5   -4.00 %
GPNAM[6] SMSQ10.100
GPZ6   -2.00 %
P16   1000.00 usec
CNST30   0.598116

F1 - Acquisition parameters
TD   256
SFO1   150.9179 MHz
FIDRES   259.443756 Hz
SW   220.045 ppm
FnMODE Echo-Antiecho

^{15}N HSQC 600 MHz

Current Data Parameters
NAME   Nov15-2019-larsh
EXPNO   17
PROCNO   1

F2 - Acquisition Parameters
Date_   20191128
Time   11.10 h
INSTRUM CAB AV4 600 MHZ BASIC
PROBHD Z151284_0002 (
PULPROG   hsqcetgpsi2
TD   2048
SOLVENT   DMSO
NS   64
DS   16
SWH   8196.722 Hz
FIDRES   8.004611 Hz
AQ   0.1249280 sec
RG   101
DW   61.000 usec
DE   40.00 usec
TE   298.0 K
CNST2   90.0000000
D0   0.00000300 sec
D1   2.00000000 sec
D4   0.00277778 sec
D11   0.03000000 sec
D16   0.00020000 sec
D24   0.00138889 sec
IN0   0.00002055 sec
TDav   1
ZGOPTNS
SFO1   600.1339008 MHz
NUC1   1H
P1   7.93 usec
P2   15.86 usec
P28   0 usec
PLW1   6.40450001 W
SFO2   60.8197664 MHz
NUC2   15N
CPDPRG[2   garp
P3   35.00 usec
P4   70.00 usec
PCPD2   220.00 usec
PLW2   77.24199677 W
PLW12   1.95500004 W
GPNAM[1]   SMSQ10.100
GPZ1   80.00 %
GPNAM[2]   SMSQ10.100
GPZ2   8.10 %
GPNAM[3]   SMSQ10.100
GPZ3   11.00 %
GPNAM[4]   SMSQ10.100
GPZ4   -5.00 %
P16   1000.00 usec
P19   600.00 usec

F1 - Acquisition parameters
TD   32
SFO1   60.81977 MHz
FIDRES   1520.681274 Hz
SW   400.049 ppm
FnMODE Echo-Antiecho

Figure A2 – Acquisition parameters for HSQC (left), HMBC (middle) and ^{15}N HSQC (right) experiments. Every fraction was recorded using the same parameters for the different experiments.
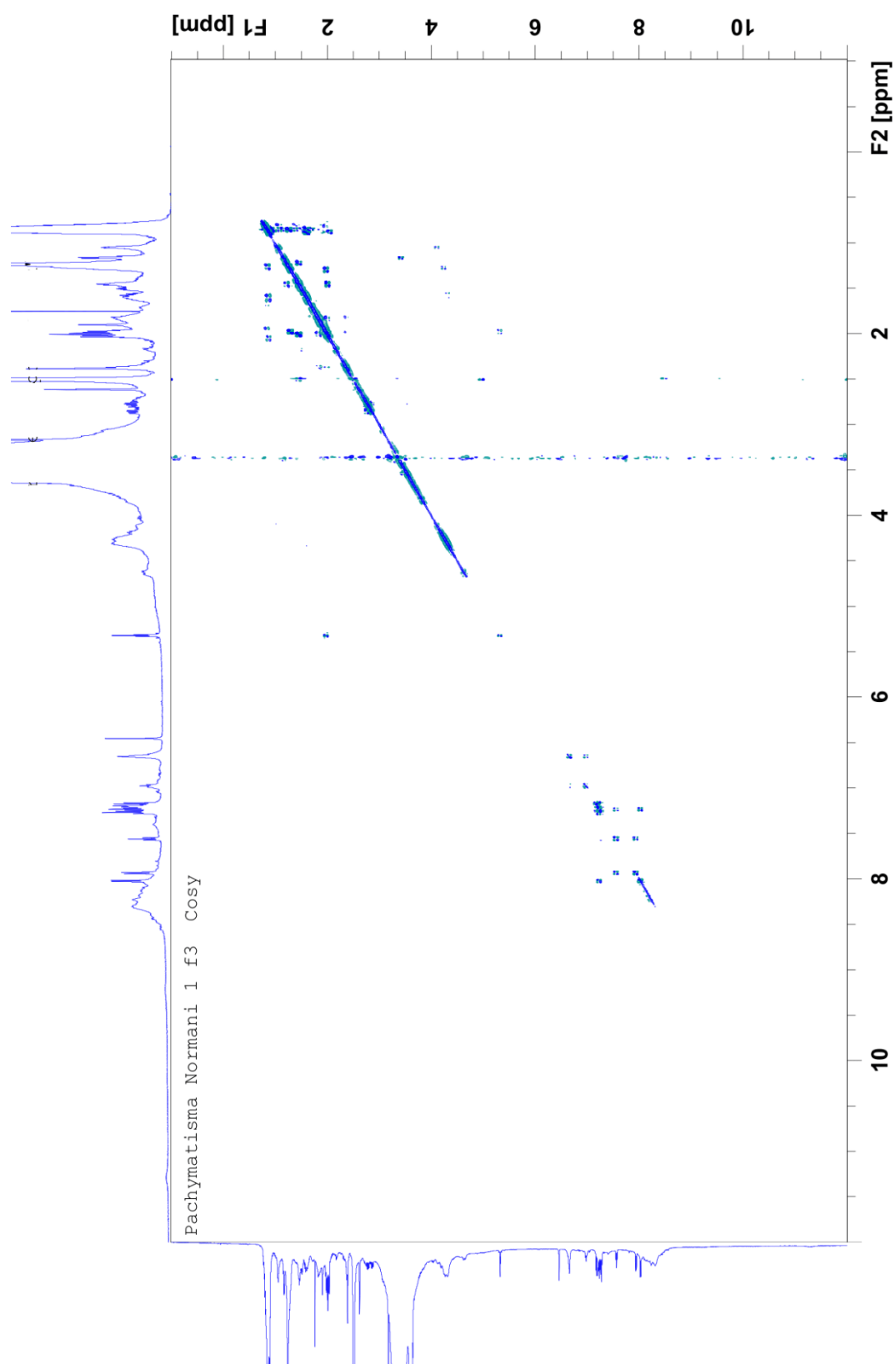
Appendix B – NMR spectra of F3-1

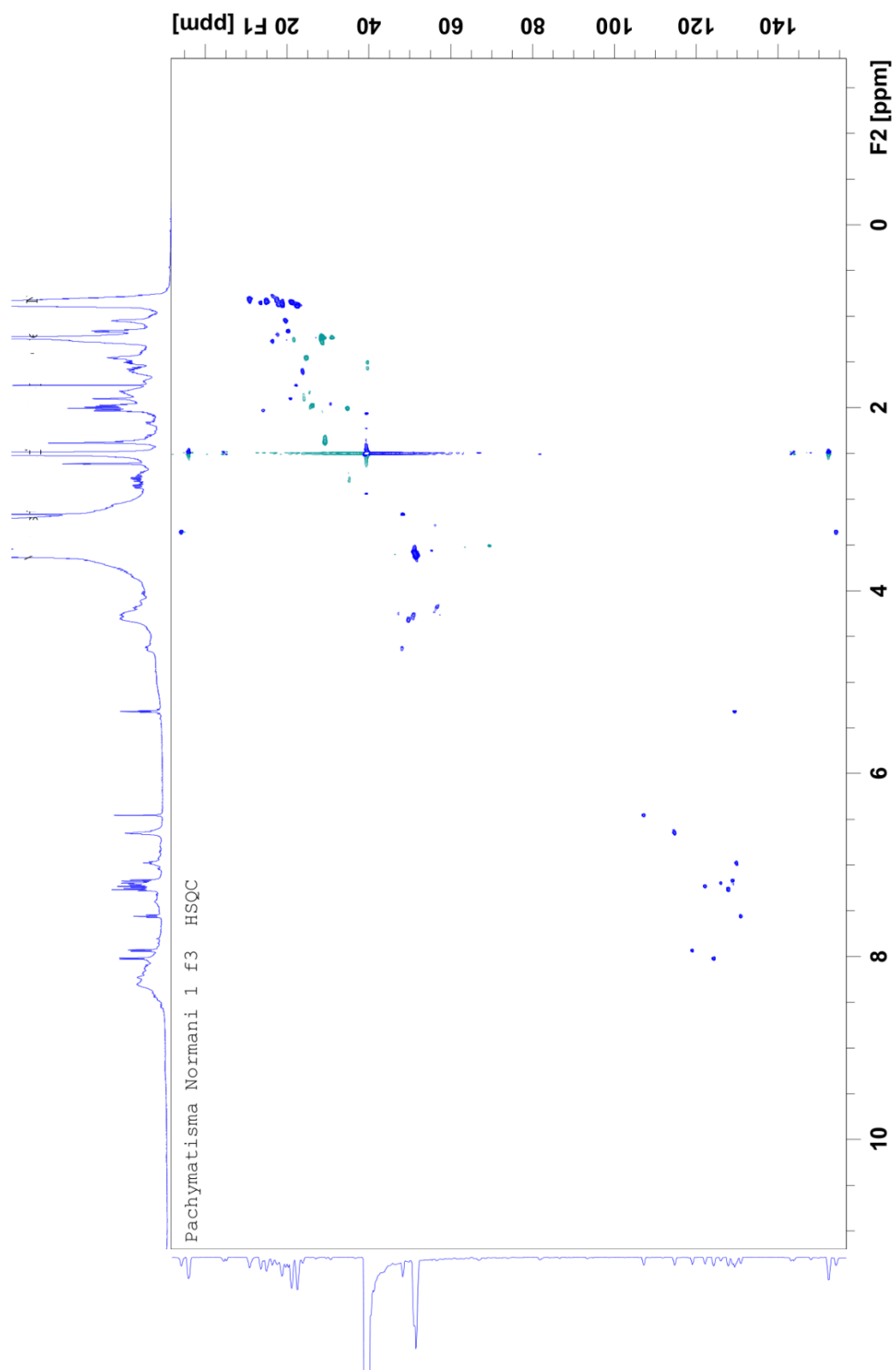Figure B1 – COSY spectrum of **F3-1**, recorded at 600 MHz and dissolved in d$_6$-DMSO at 25°C.

Figure B2 – HSQC spectrum of **F3-1**, recorded at 600 MHz and dissolved in d$_6$-DMSO at 25°C.
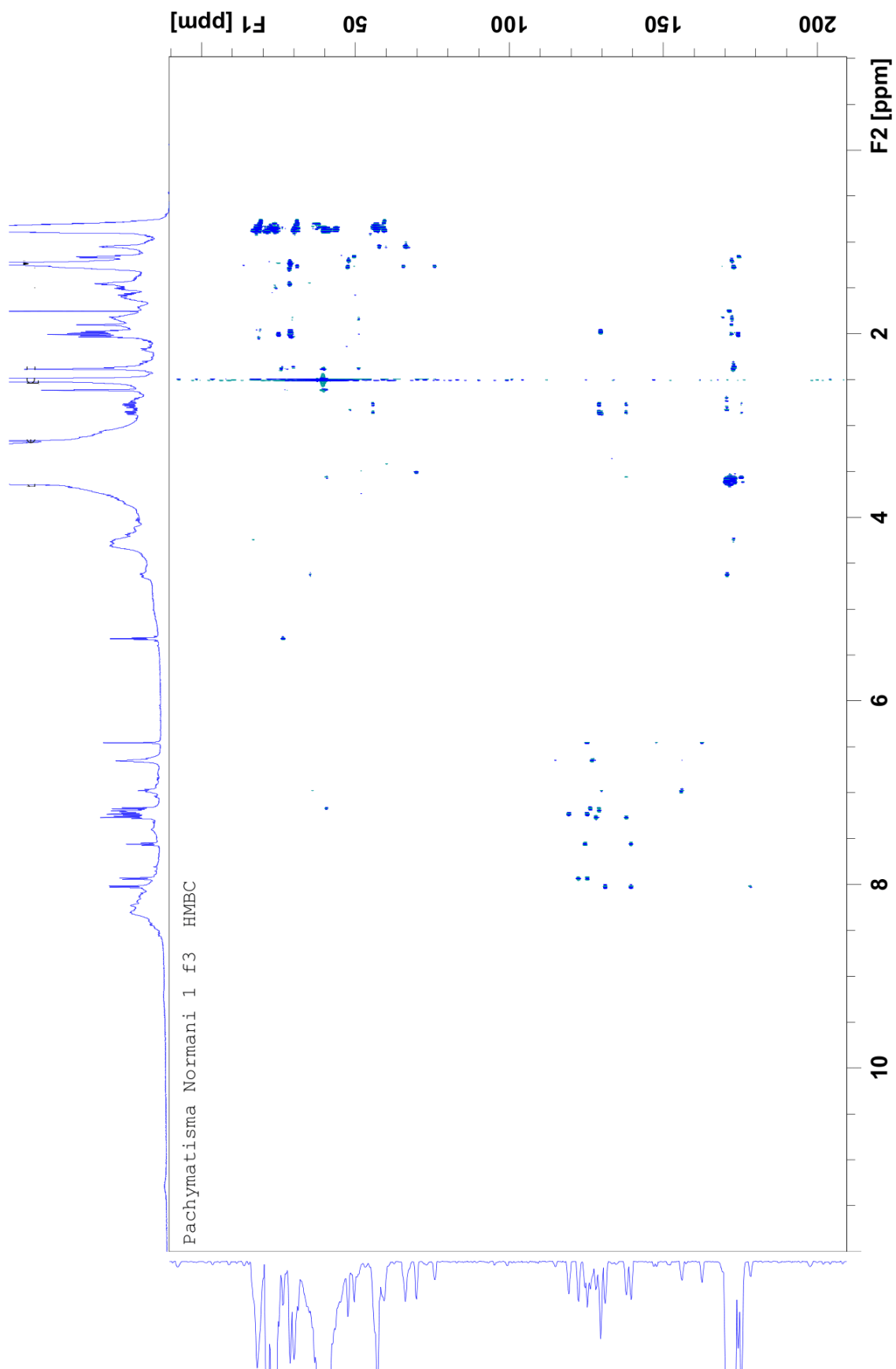
Figure B3 – HMBC spectrum of **F3-1**, recorded at 600 MHz and dissolved in d$_6$-DMSO at 25°C.
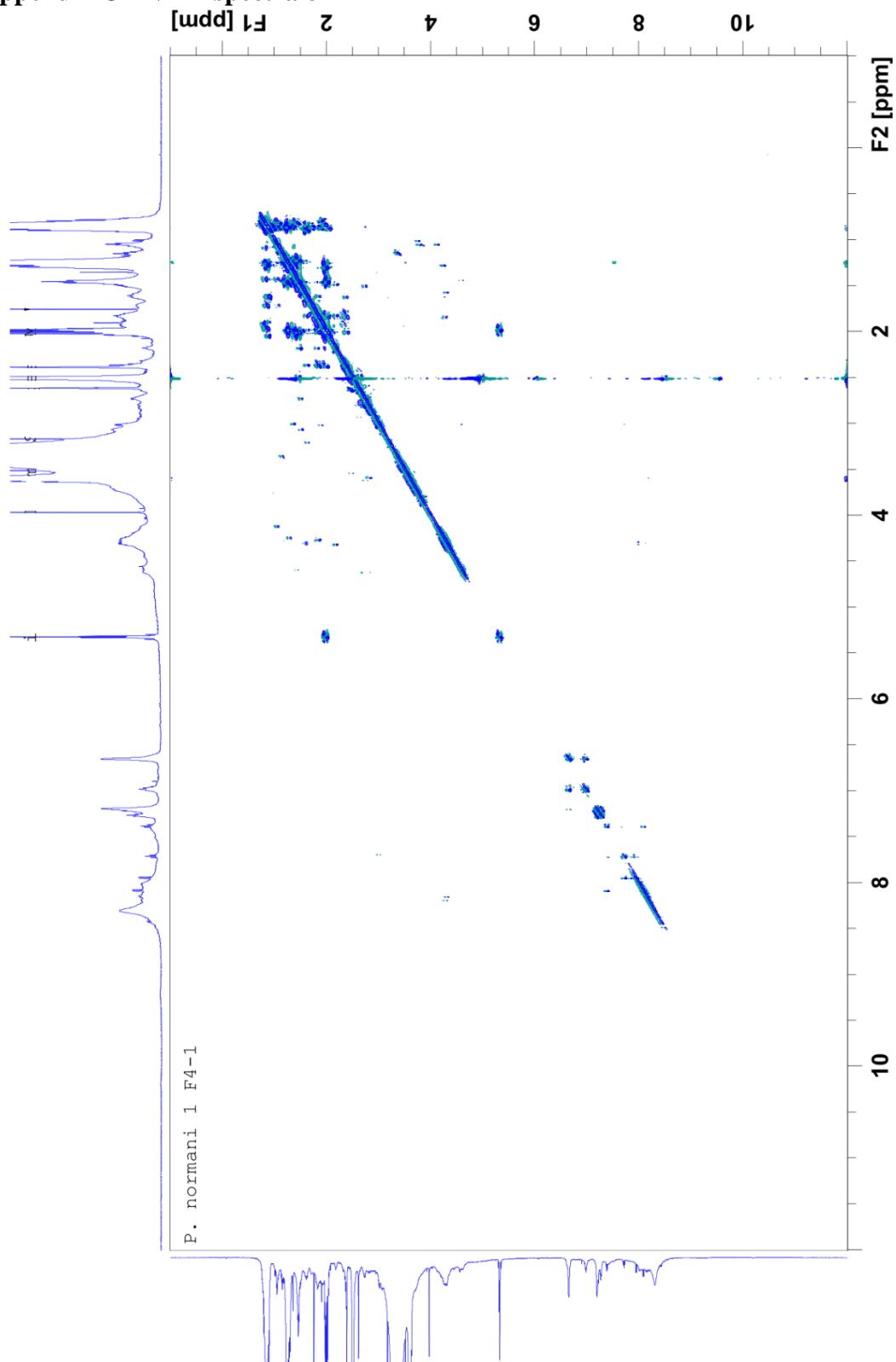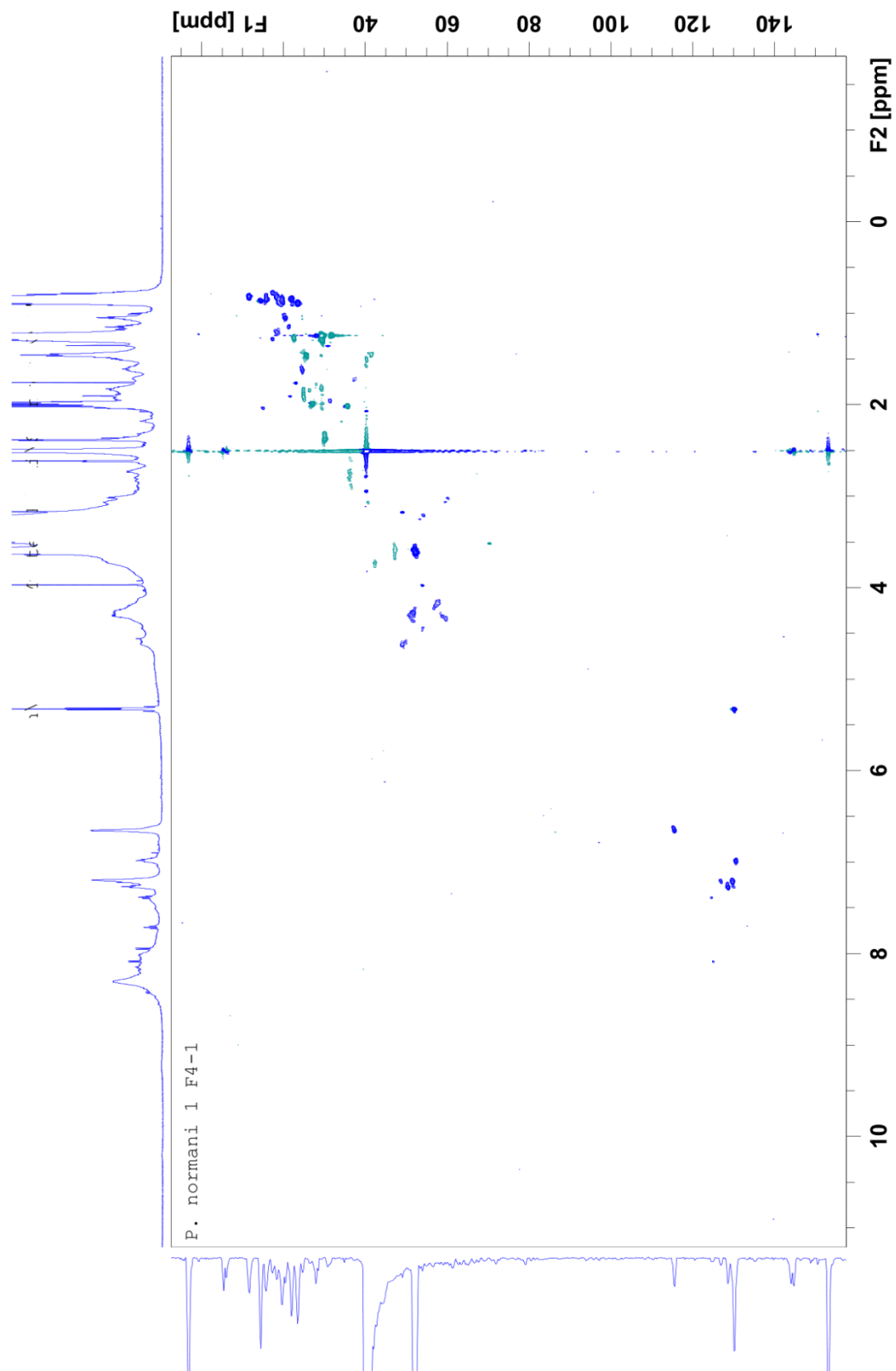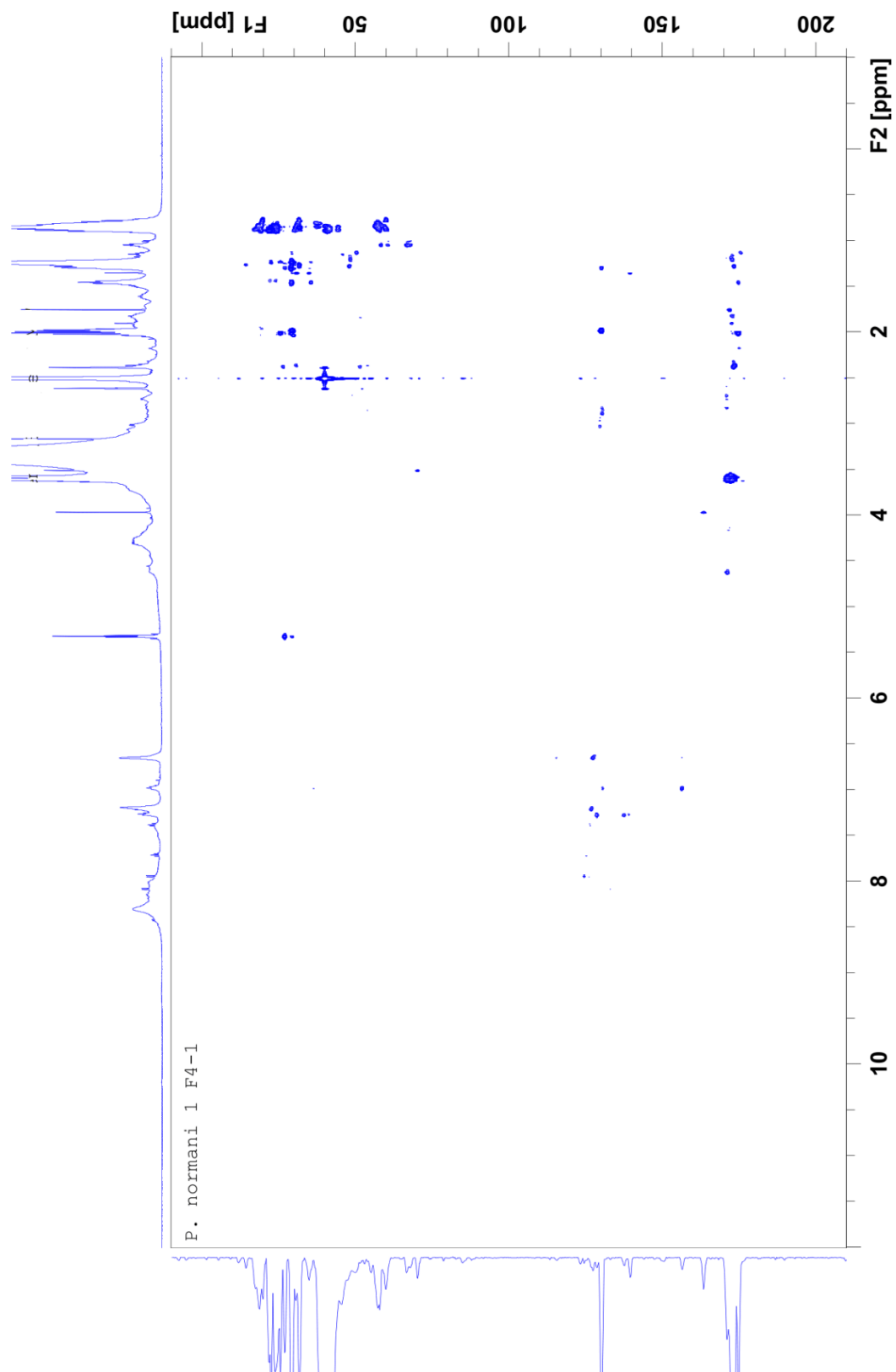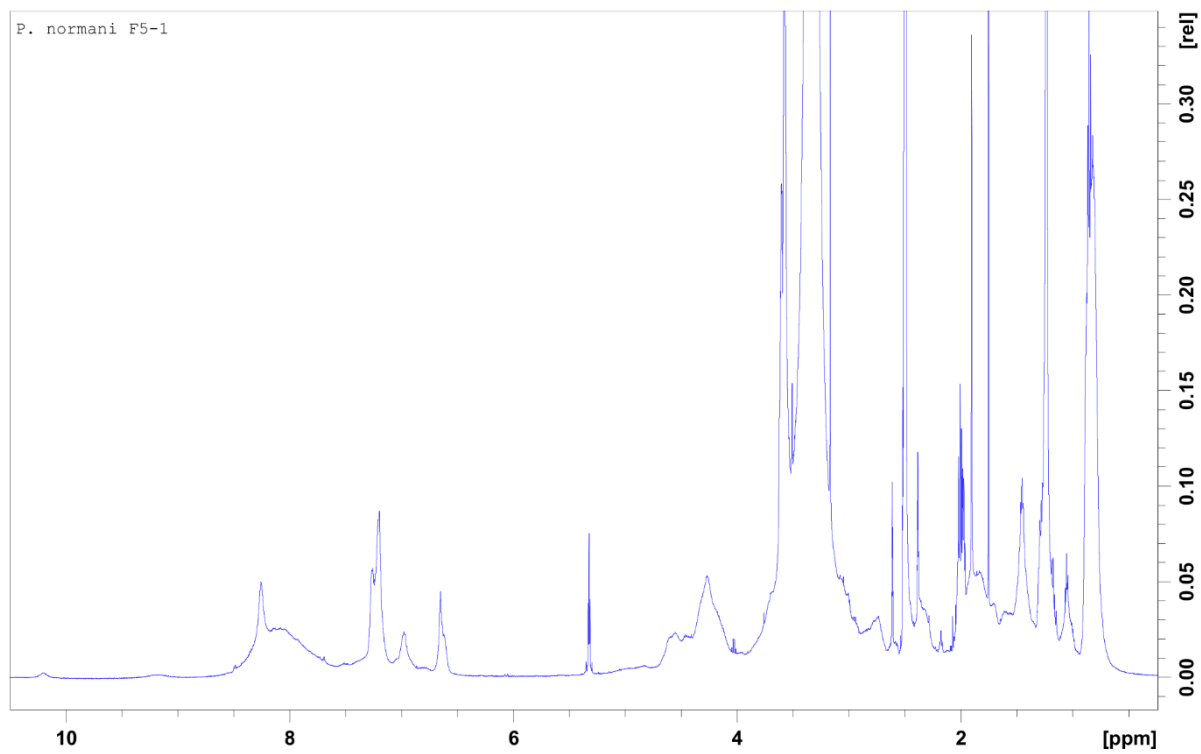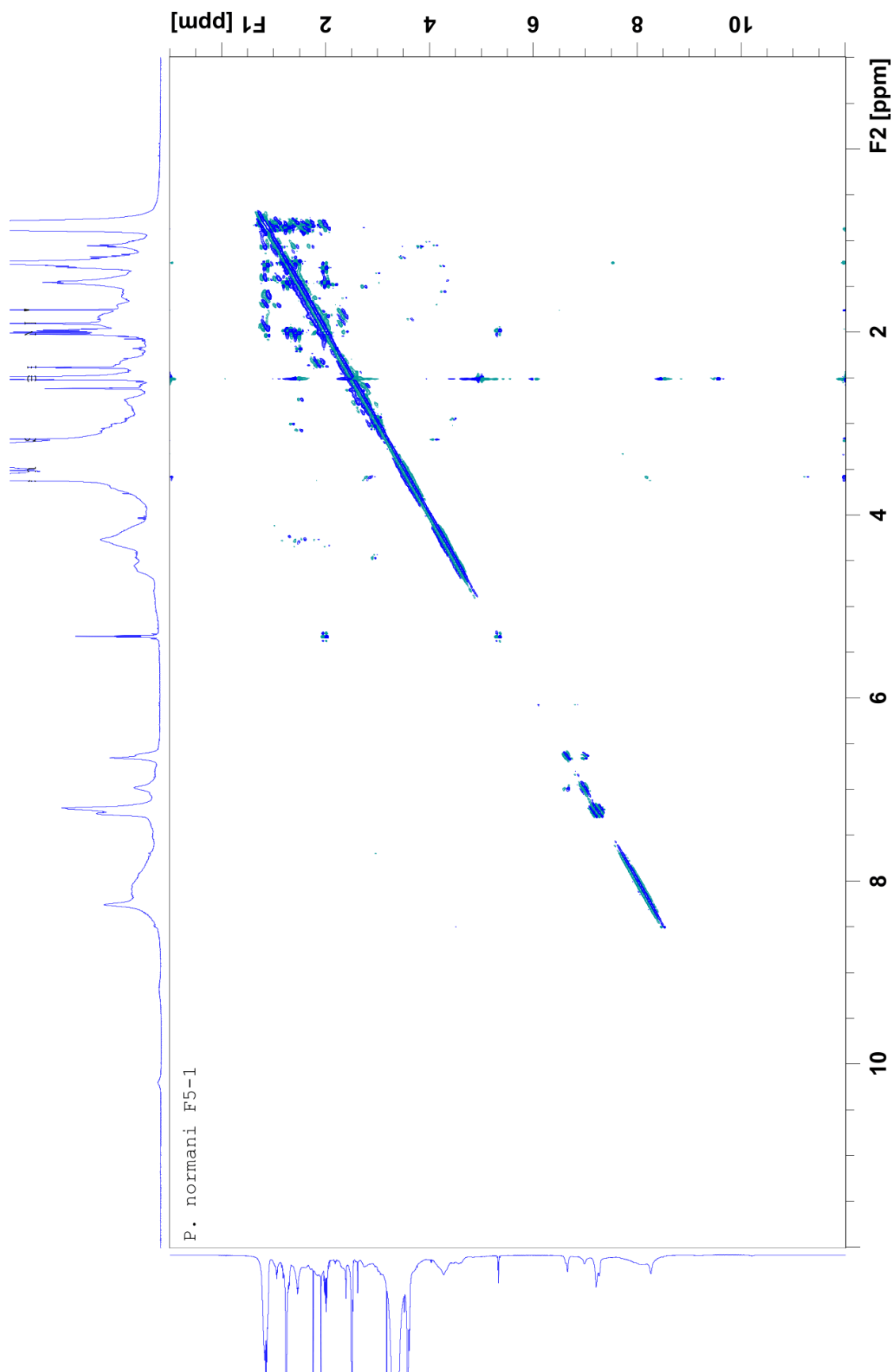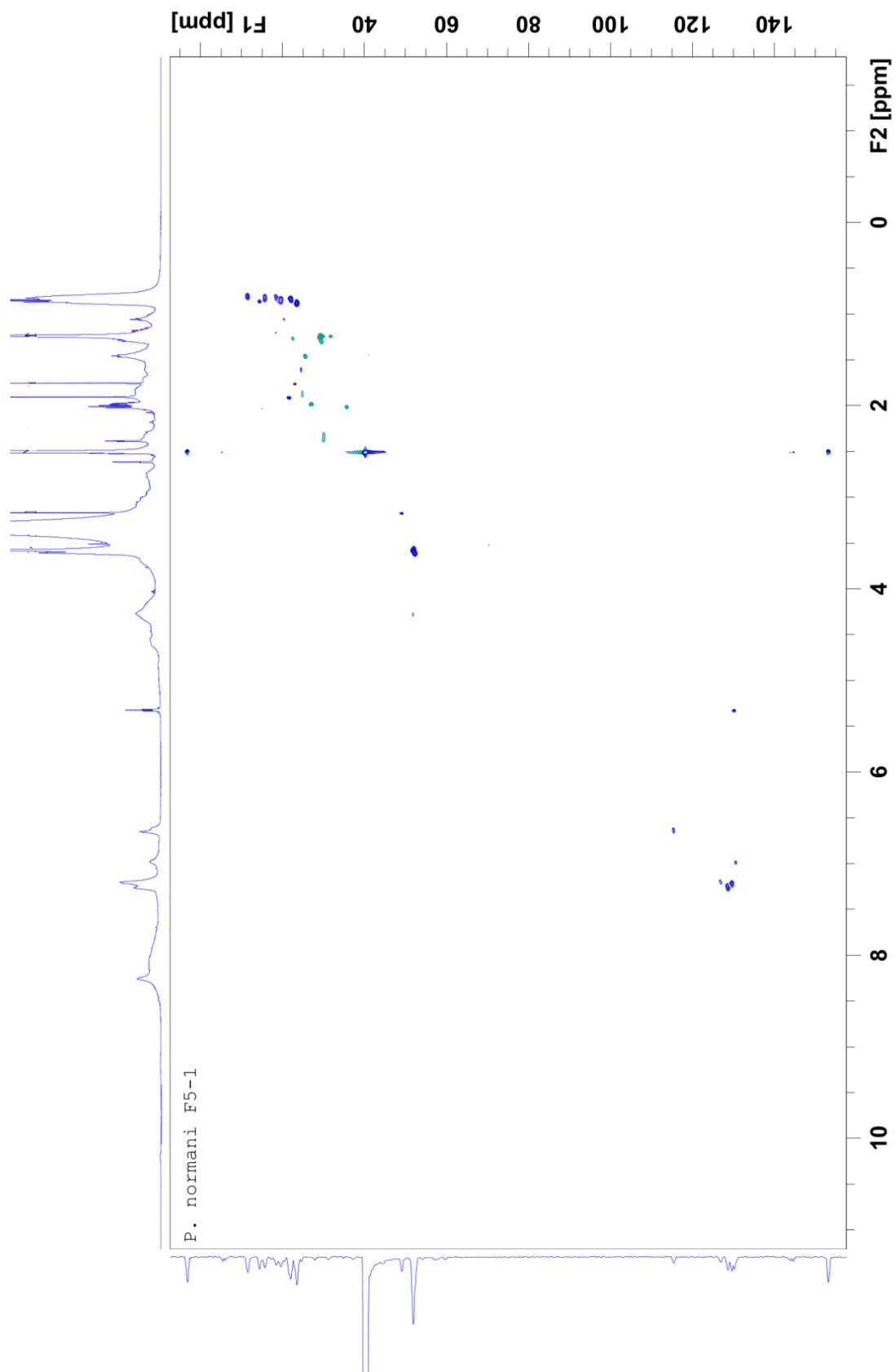
Appendix C - NMR spectra of F4-1

Figure C1 – COSY spectrum of **F4-1**, recorded at 600 MHz and dissolved in d$_6$-DMSO at 25°C.

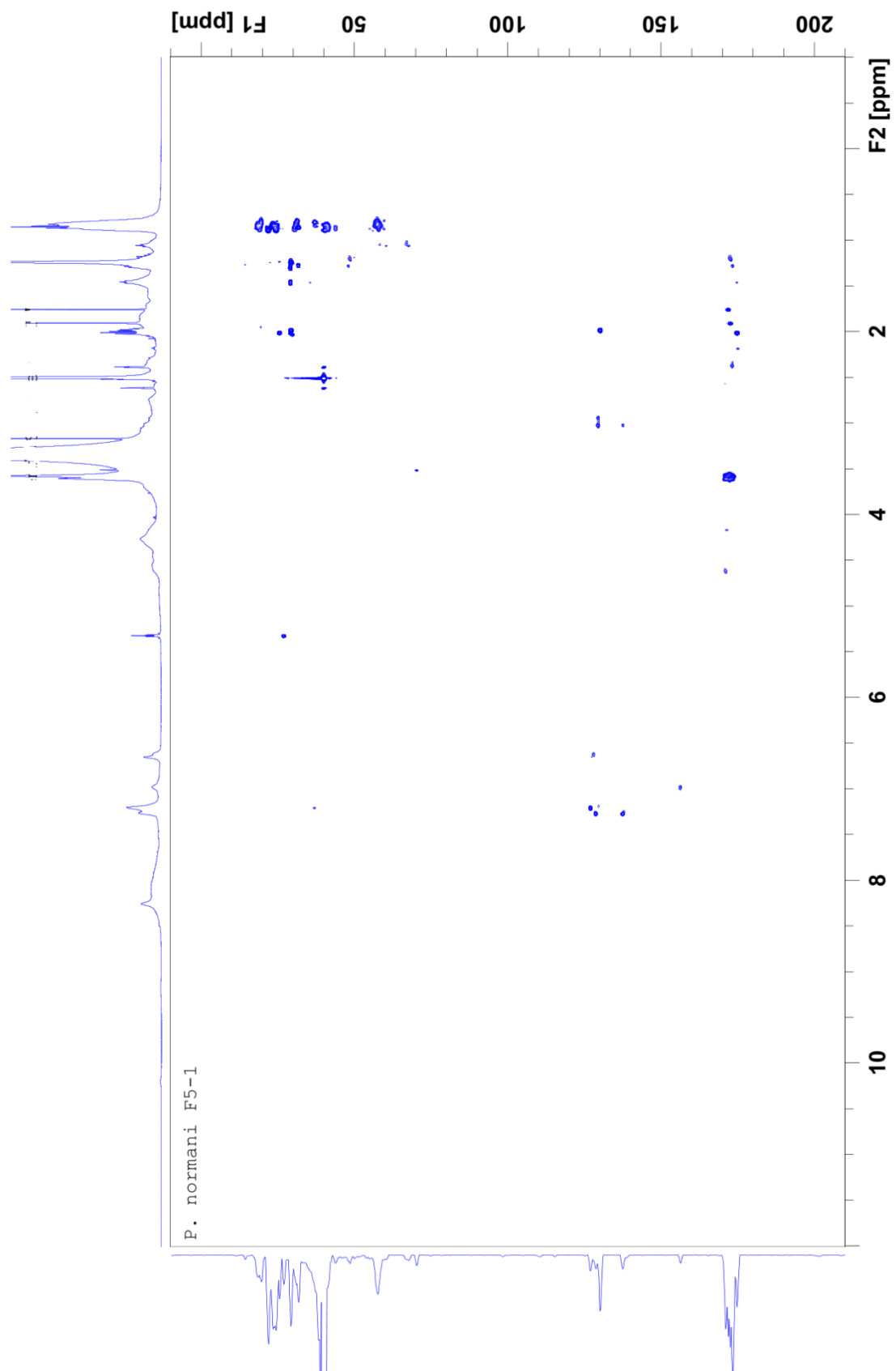Figure C2 – HSQC spectrum of **F4-1**, recorded at 600 MHz and dissolved in d$_6$-DMSO at 25°C.

Figure C1 – HMBC spectrum of **F4-1**, recorded at 600 MHz and dissolved in d$_6$-DMSO at 25°C.
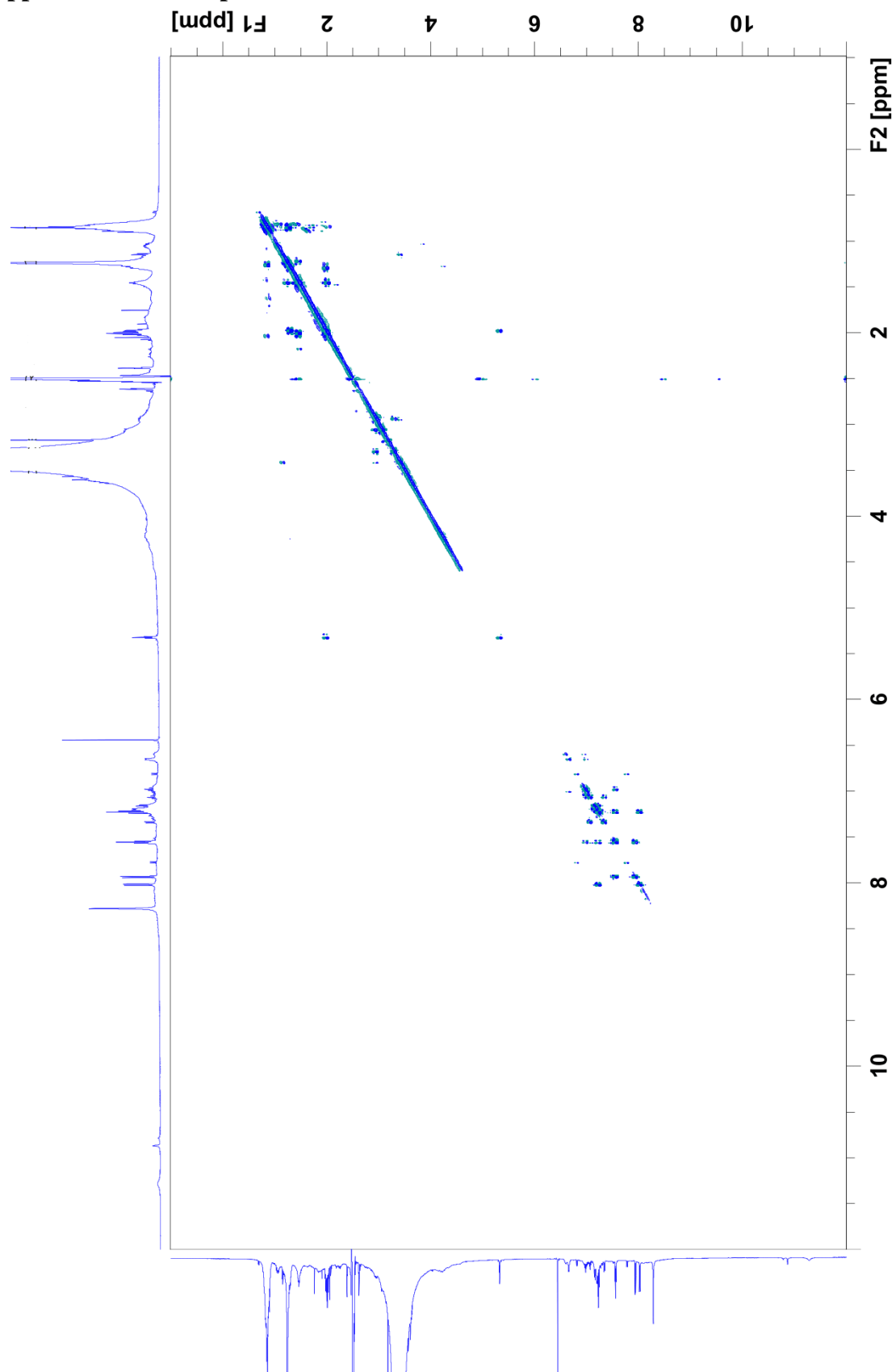
Appendix D - NMR spectra of F5-1

Figure D1 – ^{1}H NMR spectrum of **F5-1**, recorded at 600 MHz and dissolved in d$_6$-DMSO at 25°C.

Figure D2 – COSY spectrum of **F5-1**, recorded at 600 MHz and dissolved in d$_6$-DMSO at 25°C.

Figure D3 – HSQC spectrum of **F5-1**, recorded at 600 MHz and dissolved in d_6-DMSO at 25°C.

Figure D4 – HMBC spectrum of **F5-1,** recorded at 600 MHz and dissolved in d$_6$-DMSO at 25°C.

Appendix E - NMR spectra of F3-2

Figure E1 – COSY spectrum of **F3-2**, recorded at 600 MHz and dissolved in d₆-DMSO at 25°C.
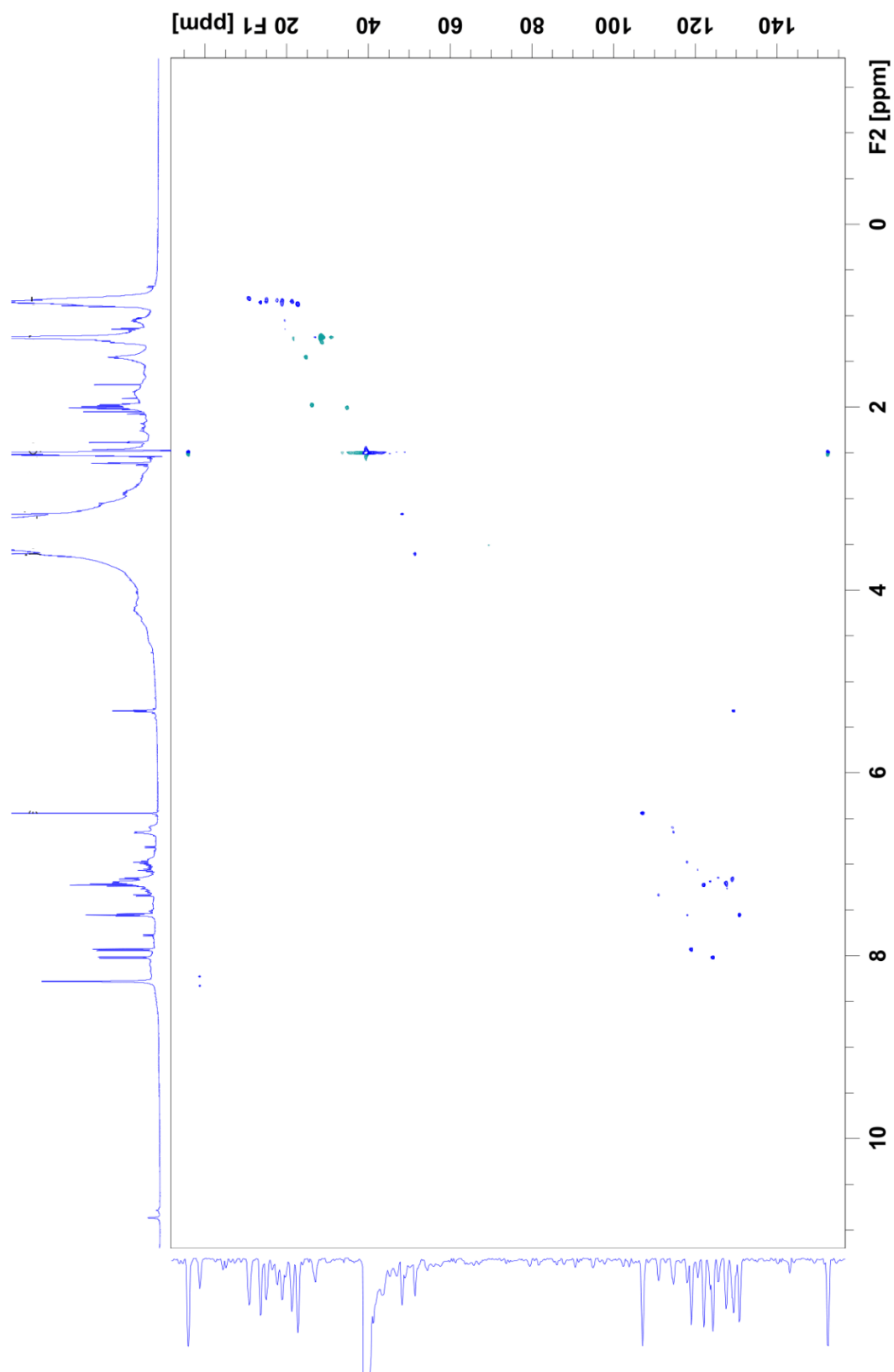
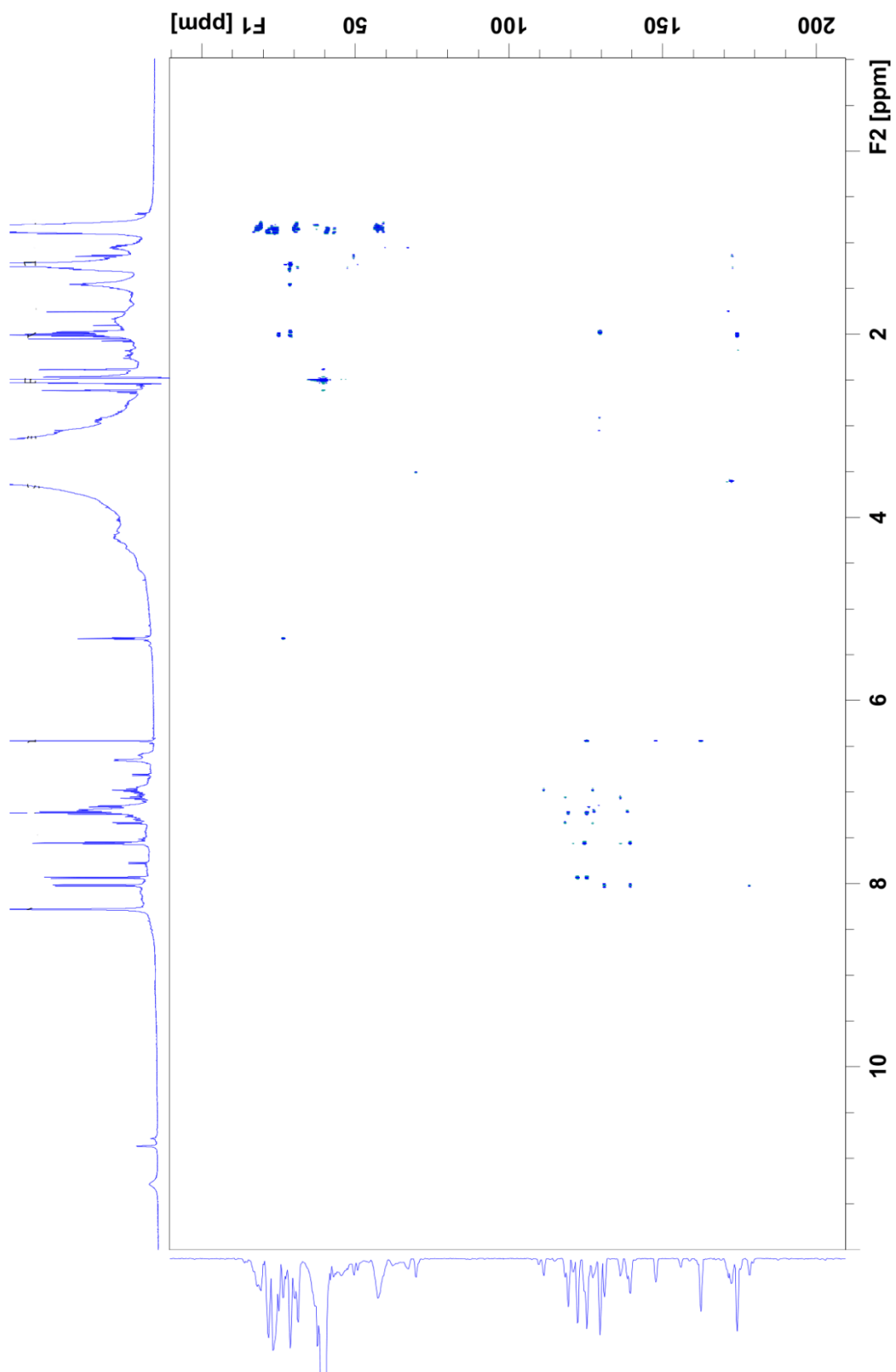Figure E2 – HSQC spectrum of **F3-2**, recorded at 600 MHz and dissolved in d$_6$-DMSO at 25°C.

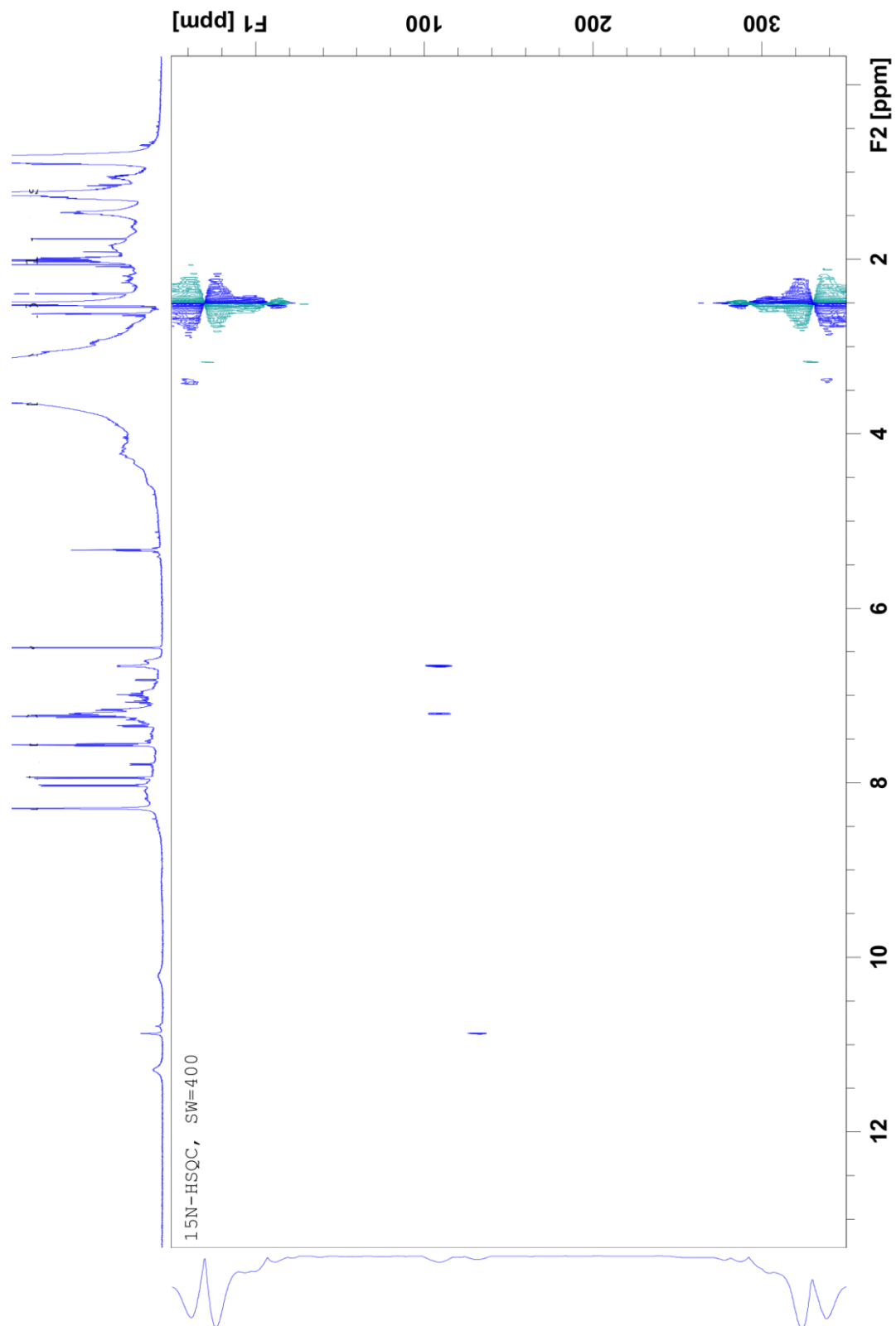Figure E3 – HMBC spectrum of **F3-2**, recorded at 600 MHz and dissolved in d$_6$-DMSO at 25°C.

Figure E4 – ^{15}N HSQC spectrum of **F3-2**, recorded at 600 MHz and dissolved in d$_6$-DMSO at 25°C.